CHALMERS

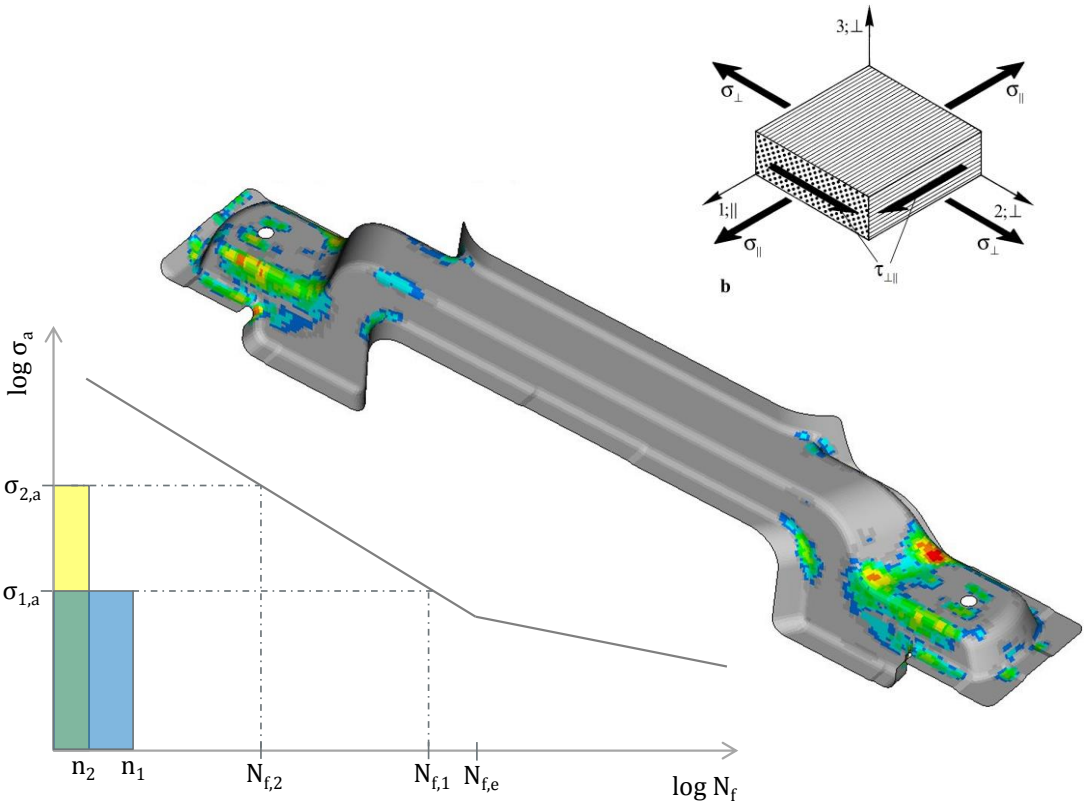

Multi-axial Fatigue Models for Composite Lightweight Structures

Master's Thesis in Applied Mechanics

HARTWIG PÖRTNER

Department of Applied Mechanics
Division of Material and Computational Mechanics
CHALMERS UNIVERSITY OF TECHNOLOGY
Göteborg, Sweden 2013

Master's Thesis 2013:79

MASTER'S THESIS IN APPLIED MECHANICS

Multi-axial Fatigue Models for Composite Lightweight Structures

HARTWIG PÖRTNER

Department of Applied Mechanics
Division of Material and Computational Mechanics
CHALMERS UNIVERSITY OF TECHNOLOGY
Göteborg, Sweden 2013

Multi-axial Fatigue Models for Composite Lightweight Structures
HARTWIG PÖRTNER

Master's Thesis 2013:79
ISSN 1652-8557
Department of Applied Mechanics
Division of Material and Computational Mechanics
Chalmers University of Technology
SE-412 96 Göteborg
Sweden
Telephone: + 46 (0)31-772 1000

Cover:
Damage plot of a cross member, S-N curve and stress components of a unidirectional.

Chalmers Reproservice
Göteborg, Sweden 2013

Multi-axial Fatigue Models for Composite Lightweight Structures
Master's Thesis in Applied Mechanics

HARTWIG PÖRTNER
Department of Applied Mechanics
Division of Material and Computational Mechanics
Chalmers University of Technology

ABSTRACT

Due to the challenging restrictions regarding the exhaust emissions of cars, more and more metal components are replaced by composites due to their high strength to weight ratio. The components need to sustain complex loadings during a life-time of a vehicle. In the early development phase, fatigue simulations are carried out to predict the fatigue behaviour of components. This can be done fairly accurate for metals but the simulation tools and research are limited when it comes to composite material.

Therefore, this thesis deals with the fatigue simulation of composites subjected to variable amplitude loadings under plane stress conditions and it is concerned in particular with models to account for multi-axial stress states. Focus lies on the interaction between transverse stress and shear stress. Three methods to account for stress interaction are presented and applied to a case study of a carbon fibre reinforced polymer (CRFP) cross member in an AUDI car body subjected to complex load histories. Two methods reduce the complex loading to constant amplitude loadings in transverse and shear direction, respectively, one is based on the static failure criteria of composites proposed by Puck [4] and the other uses Hashin's fatigue failure criterion [5] to account for multi-axiality. A third method computes an equivalent stress at each time step by using Puck's static failure criterion to obtain an equivalent stress history which is then used for fatigue assessment.

In this case study of the CFRP cross member subjected to complex loading under plane stress conditions fatigue analysis was carried out by analysing each stress component $(\sigma_1, \sigma_2, \tau_{12})$ separately. Mean stress effects were taken into account by constant life diagrams and linear damage accumulation according to the Palmgren-Miner rule was assumed. The three methods were applied to this analysis and the results showed that accounting for multi-axial stress states in fatigue analysis is of high importance. When accounting for multi-axial stress states the resulting damage was up to 20 times higher than the damage due to the single stress component. Furthermore the results of the two methods using the Puck criterion were surprisingly close. It is recommended to use the method of computing an equivalent stress according to Puck's theory, since it is the physically most reasonable approach. Biaxial fatigue testing to validate the methods is needed.

Key words: Fibre-reinforced composites, failure criterion, Hashin, Multi-axial fatigue, Puck, Variable amplitude loading

Contents

Preface

This Master's Thesis has been carried out at the development department at AUDI AG in Ingolstadt, Germany, from April 2013 to September 2013. First of all I would like to express my appreciation to my supervisor at AUDI, Dr.-Ing. Ulrich Knaust, for the support during this time and the valuable input during the weekly meetings. In addition, I would like to thank my colleagues at AUDI and in particular Clemens Hahne for the advices, the answers to my questions and all the small sketches on scrap of paper. Thanks a lot!

Furthermore, I would like to direct my sincerest gratitude to Lennart Joseffson, Professor at Chalmers University of Technology, for examining the Thesis and the highly appreciated remarks and advices. Studying at Chalmers was often challenging but it was always a pleasure and therefore I would like to thank my friends for a great time in Gothenburg. If it was working on assignment in the computer basements or taking a coffee break in Café Bulten, it was always a pleasure. Credits also go to the Apian-WG, who made life in Ingolstadt liveable. It was a great time.

Last but not least, I would like to thank Florian Mack, who did not directly contribute to this thesis, but he gave me the advice of studying at Chalmers, a decision I haven't regretted a single time. Florian, if you read this by any chance, thanks a lot!

Ingolstadt October 2013

Hartwig Pörtner

Notations

Roman upper case letters

$\mathbf{A}$	extensional stiffness matrix
$\mathbf{B}$	coupling matrix
$\mathbf{C}$	bending stiffness matrix
E	elasticity modulus
G	shear modulus
M	resultant moments
N	resultant forces or number of cycles
R	fracture strength or stress ratio
$\mathbf{Q}$	stiffness matrix in lamina coordinate system
$\overline{\mathbf{Q}}$	stiffness matrix in global coordinate system
$\mathbf{T}$	transformation matrix

Roman lower case letters

a_{bc}	Variable notation for something
f_E	stress exertion
h	laminate thickness
k	curvature or slope of S-N curve
p	pitch factor
u	displacement in x-direction
v	displacement in y-direction
w	displacement in z-direction
z	distance from mid-plane

Greek lower case letters

γ	shear angle
ε	strain
ν	Poisson's ratio
σ	normal stress
τ	shear stress

Greek upper case letters

Θ	fibre orientation angle

Abbreviations

APDI	A Posteriori Damage Interaction

CFRP	Carbon fibre reinforced polymer
FF	Fibre failure
FRP	Fibre reinforced polymer
IFF	Inter-fibre failure
LTS	Load over time signal
MBHA	Method based on Hashin's approach
RBE	Rigid Body Element
SSCM	Single Stress Component Method
UD	Unidirectional
WWFE	World-wide fibre exercise

Indices

1	orientation longitudinal to the fibre direction
2,3	orientation perpendicular to the fibre direction
e	endurance limit
f	regarding the fibre
FF	fibre failure
fr	fracture
IFF	inter-fibre failure
m	regarding the matrix
s	symmetric
u	ultimate
I	maximum principal stress
II	minimum principal stress
$\perp$	transverse direction
$\parallel$	longitudinal direction
$\perp\parallel$	transverse longitudinal direction

Superscripts

$+$	tension
$-$	compression
$\perp$	transverse direction
$\parallel$	longitudinal direction
$\perp\parallel$	transverse longitudinal

1 Introduction

This chapter shall give an overview about the background, objective and content of the Thesis, which was carried out at the development department at AUDI AG in Ingolstadt, Germany.

1.1 Background

The European commission adopted a law which stipulates a reduction of the fleet CO_2 emission to 130g CO_2/km until 2015 [1]. Furthermore, a current point of discussion is a further reduction to only 95g CO_2/km until 2020 [1]. These regulations force the car manufactures to decrease the exhaust emission significantly, which is in most cases only obtainable by reducing the car's fuel consumption. One way of achieving these goals is to reduce the weight of the car by replacing steel components by lighter materials, e.g. fibre reinforced polymers (FRP). Fibre reinforced polymers, and especially carbon fibre reinforced polymers (CFRP), have a low density but high strength and therefore a high lightweight potential.

Through the lifetime of a car complex loadings affect the strength of the structural parts of a car. Therefore, the components have to be designed such that they withstand certain loadings. To make full use of their lightweight potential and to reduce the number of expensive prototypes, the use of advanced simulation methods is essential.

The current solution for the evaluation of metal parts in AUDI processes is to predict its fatigue life with the help of linear finite element method (FEM) and linear damage accumulation theory. A concept for the evaluation of CFRP components has been worked out, which considers the anisotropic stiffness, strength and damage characteristics of the material [2], [3]. The concept evaluates each stress component separately, meaning that no interaction between stress components is taken into account, which does not agree with the failure mechanism of composites.

1.2 Objectives

The aim of this Master's Thesis is the improvement of the described fatigue simulation method in terms of consideration for multi-axial stress states. Three different methods, which account for multi-axial stressing, are applied to a fatigue analysis of a CFRP component. Hahne [2] proposed two of these methods, which are based on Puck's failure criteria for composites [4]. The third method is based on the fatigue failure criterion proposed by Hashin [5]. Based on the results of the fatigue analyses a recommendation for the application of these methods in standard processes is given and areas, where improvements in terms of method, processes and tools are necessary, are pointed out.

1.3 Outline of the Thesis

The Thesis contains six chapters. Chapter 2 deals with the basic principles in analysis of composites. Failure mechanisms as well as two failure criteria of composites are presented. Furthermore, the basic principles of fatigue analysis are explained.

Chapter 3 concerns with the fatigue assessment by using the commercial simulation tool FEMFAT. It consists of two subchapters. In the first one, the process of fatigue assessment of metal components by using FEMFAT is described. A work-around for the analysis of composites, which was developed by Hahne and Kloska, is outlined in the second subchapter.

This work around does not take stress interaction into account. The scope of the 4th chapter is therefore to present three models from literature, which enables the consideration of multi-axial stress states.

These three methods are applied to a fatigue analysis of a composite component in chapter 5. The results obtained from the different approaches are compared and discussed.

Finally, the conclusions, which are drawn from the results of the thesis, are presented in chapter 6 and also recommendations, how these methods can be used in the simulation process and where improvement needs to be carried out, are given.

2 Theory

As the title of the Master's Thesis already states, this work deals with the fatigue behaviour of composites. Therefore, the basic concept of analysing composites is described in the beginning of this chapter. Fatigue comes along with failure of the material and hence the failure mechanisms of composites are explained and how failure can be estimated by failure criteria. Hereafter follows a brief description of fatigue assessment in general, where at the end of the chapter the special characteristics of the fatigue behaviour of composites are pointed out.

2.1 Composite material - Basics

A *composite* is a material which is *composed* by two or more distinct materials. In engineering applications composites consist usually of two materials with different material properties. Well known composites are e.g. fibre reinforced polymers (FRP), which consist of a polymer matrix and embedded fibre material. The main purposes of the matrix material are to keep the fibres in position and to protect them from harsh environment. In addition, their purpose is the redistribution of loadings. Usually glass, aramid or carbon fibres are used. Carbon fibres are frequently used in the automotive industry due to their high strength-to-weight ratio and high stiffness.

In this Master's Thesis the analyses are limited to carbon fibre reinforced polymers (CFRP) in an epoxy polymer matrix. The composites are laminates. Their structure, material properties and also their failure behaviour are described in the following subsections.

2.1.1 Unidirectional laminate

A unidirectional laminate (UD laminate) consists of multiple UD laminae as shown in Figure 2.1. The fibres in one layer are oriented in the same direction. A composite is anisotropic. Due to the processing of lamina it is possible that material defects are present, but for analyses on the macroscopic scale the following assumptions are made [6]:

- Fibres are perfectly straight and parallel aligned
- Bonding between fibres and matrix is perfect
- Fibres are distributed equally over the cross-section

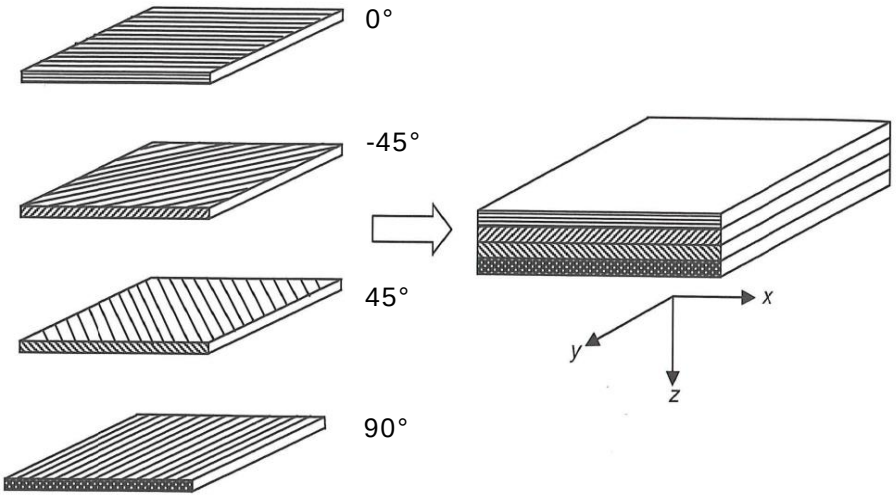

Figure 2.1: A four-ply laminate [6]

Figure 2.1 also depicts the laminate orientation code, a convention used to label laminates according to their fibre orientations. The main rules are listed below:

- Fibre angle is always referred to the x-axis
- Laminae are listed in sequence from the first lamina laid up
- Neighbouring laminae with same orientation angle are labelled by a numerical subscript, i.e.$[45/45] \equiv [45_2]$
- Symmetric laminates are labelled with the index s
- Non-repeated lamina in symmetric laminates are over lined $\bar{}$, i.e. $[90/45/90] \equiv \left[90/\overline{45}\right]_s$

Using this orientation code, the four ply laminate in Figure 2.1 would be labelled as [0/-45/45/90]. Before the analysis of such a laminate is described, the analysis of one single layer, a UD lamina, is explained.

2.1.2 Analysis of an UD lamina

Considering a 3-dimensional stress state the UD lamina is subjected to six stresses, as shown in Figure 2.2. These stresses are namely:

- Normal stresses: σ_1, σ_2 and σ_3
- Shear stresses: τ_{21}, τ_{23} and τ_{31}

The index 1 is referred to the direction of the fibre, whereas indices 2 and 3 are referred to the direction transverse to the fibre direction. Since the material properties are identically with respect to the material axes 2 and 3, a unidirectional composite can be considered to be transverse isotropic. That means the plane normal to the fibre

direction can be considered as the isotropic plane and the mechanical properties in all planes normal to this isotropic plane are identical (see Figure 2.2 right)

In that case the use of the word stressing instead of stress is preferable. Therefore, only four unique stressings are acting on a UD lamina. These are normal stressing longitudinal to the fibre direction, $\sigma_{\parallel}$ (σ_1), normal stressing transverse to the fibre direction, $\sigma_{\perp}$ $(\sigma_2; \sigma_3)$ and the transverse-longitudinal shear stressings $\tau_{\perp\parallel}(\tau_{21}; \tau_{31})$ and transverse-transverse shear stressings $\tau_{\perp\perp}(\tau_{23})$, respectively. In order to distinguish between compressive stressings and tensile stressings a superscript for tension (+) and for compression (-) is used. [7]

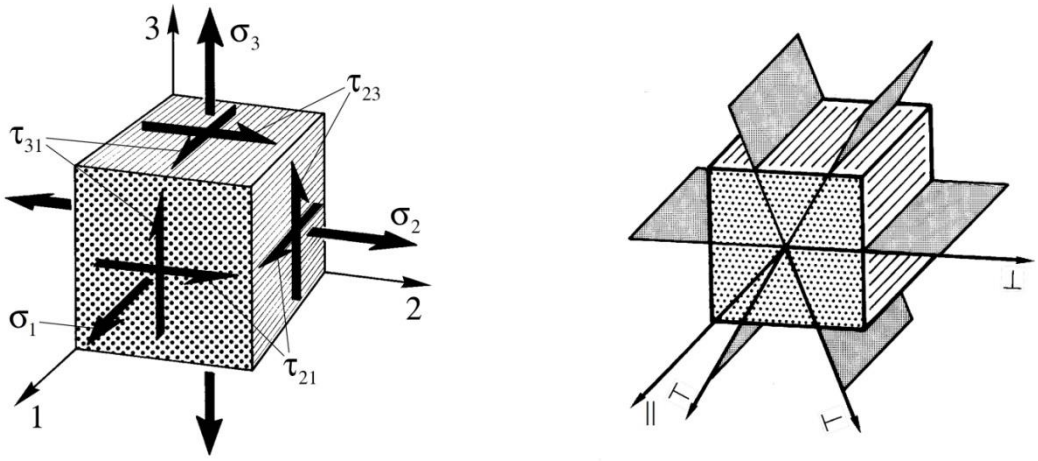

Figure 2.2: Left: Stresses acting on an element of a UD-lamina [8]) Right: Transverse isotropy - The plane 2-3 in the right Figure is a plane of isotropy. The material properties are the same in all planes perpendicular to the plane of isotropy [8]

Composites are often used in applications where the assumption of plane-stress conditions $(\sigma_3 = \tau_{13} = \tau_{23} = 0)$ is valid. Based on the transverse isotropy the relation between the stresses in the material coordinate system under plane stress conditions can be related to the strains according to equation (2.1).

$$\begin{Bmatrix} \sigma_1 \\ \sigma_2 \\ \tau_{12} \end{Bmatrix} = \underbrace{\begin{bmatrix} \frac{E_{\parallel}}{1-\upsilon_{\parallel\perp}\upsilon_{\perp\parallel}} & \frac{\upsilon_{\parallel\perp}E_{\parallel}}{1-\upsilon_{\parallel\perp}\upsilon_{\perp\parallel}} & 0 \\ \frac{\upsilon_{\parallel\perp}E_{\parallel}}{1-\upsilon_{\parallel\perp}\upsilon_{\perp\parallel}} & \frac{E_{\perp}}{1-\upsilon_{\parallel\perp}\upsilon_{\perp\parallel}} & 0 \\ 0 & 0 & G_{\parallel\perp} \end{bmatrix}}_{\boldsymbol{Stiffness\ matrix\ Q}} \begin{Bmatrix} \varepsilon_1 \\ \varepsilon_2 \\ \gamma_{12} \end{Bmatrix} = \begin{bmatrix} \mathrm{Q}_{11} & \mathrm{Q}_{12} & 0 \\ \mathrm{Q}_{12} & \mathrm{Q}_{22} & 0 \\ 0 & 0 & \mathrm{Q}_{66} \end{bmatrix} \begin{Bmatrix} \varepsilon_1 \\ \varepsilon_2 \\ \gamma_{12} \end{Bmatrix} \qquad (2.1)$$

where $E_{\parallel}$ is the Young's modulus longitudinal to the fibre direction, $E_{\perp}$ is the Young's modulus transverse to the fibre direction and $G_{\parallel\perp}$ is the in-plane shear modulus of the lamina. $\upsilon_{\parallel\perp}$ and $\upsilon_{\perp\parallel}$ are the major and minor Poisson's ratios. These material properties are determined by the mechanical properties of the fibre and matrix material and also by their volume fraction, i.e. how much fibres and how much matrix material does the lamina consist of. How to determine these material parameters is well described in Chapter 3 in [6].

A laminate is usually stacked with layers of different fibre orientation angles, which means the local material coordinate system changes with respect to a fixed reference coordinate system when the fibre orientation changes, as depicted in Figure 2.1. Therefore, it is useful to express the stresses and strains in fixed reference coordinate systems. The stresses and strains can be transformed from the local material coordinate system into the global reference coordinate system by the following relations:

$$\begin{Bmatrix} \sigma_1 \\ \sigma_2 \\ \tau_{12} \end{Bmatrix} = \mathbf{T}_1 \begin{Bmatrix} \sigma_x \\ \sigma_y \\ \tau_{xy} \end{Bmatrix} \tag{2.2}$$

$$\begin{Bmatrix} \varepsilon_1 \\ \varepsilon_2 \\ \gamma_{12} \end{Bmatrix} = \mathbf{T}_2 \begin{Bmatrix} \varepsilon_x \\ \varepsilon_y \\ \gamma_{xy} \end{Bmatrix} \tag{2.3}$$

where $\mathbf{T}_1$ is the stress-transformation matrix given as:

$$\mathbf{T}_1 = \begin{bmatrix} \cos^2\theta & \sin^2\theta & 2\sin\theta\cos\theta \\ \sin^2\theta & \cos^2\theta & -2\sin\theta\cos\theta \\ -\sin\theta\cos\theta & \sin\theta\cos\theta & \cos^2\theta - \sin^2\theta \end{bmatrix} \tag{2.4}$$

and $\mathbf{T}_2$ is the strain-transformation matrix given as:

$$\mathbf{T}_2 = \begin{bmatrix} \cos^2\theta & \sin^2\theta & \sin\theta\cos\theta \\ \sin^2\theta & \cos^2\theta & -\sin\theta\cos\theta \\ -2\sin\theta\cos\theta & 2\sin\theta\cos\theta & \cos^2\theta - \sin^2\theta \end{bmatrix} \tag{2.5}$$

The angle θ describes the rotational angle between the global x-axis and the local axis longitudinal to the fibre direction. Substituting equation (2.2) and (2.3) into equation (2.1) one obtains the stress-strain relation for an orthotropic lamina in global coordinates as follows:

$$\begin{Bmatrix} \sigma_x \\ \sigma_y \\ \tau_{xy} \end{Bmatrix} = \mathbf{T}_1^{-1} \begin{bmatrix} Q_{11} & Q_{12} & 0 \\ Q_{12} & Q_{22} & 0 \\ 0 & 0 & Q_{66} \end{bmatrix} \mathbf{T}_2 \begin{Bmatrix} \varepsilon_x \\ \varepsilon_y \\ \gamma_{xy} \end{Bmatrix} \tag{2.6}$$

For simplicity a $\bar{\boldsymbol{Q}}$ matrix can be defined similar to the $\boldsymbol{Q}$ matrix, which relates the global strains to the global stresses as shown in equation (2.7)

$$\begin{Bmatrix} \sigma_x \\ \sigma_y \\ \tau_{xy} \end{Bmatrix} = \begin{bmatrix} \bar{Q}_{11} & \bar{Q}_{12} & 0 \\ \bar{Q}_{12} & \bar{Q}_{22} & 0 \\ 0 & 0 & \bar{Q}_{66} \end{bmatrix} \begin{Bmatrix} \varepsilon_x \\ \varepsilon_y \\ \gamma_{xy} \end{Bmatrix} \tag{2.7}$$

As already mentioned a laminate consists usually of more than one ply with different fibre orientation. The analysis for such a laminate is described in the following paragraph.

2.1.3 Analysis of laminated composites [6]

The evaluation of composites regarding stress analysis can be carried out by using the classical laminate theory (CLT). It is used to establish the elasticity equations of the multi-layer composite (MLC) from the elastic properties of each UD lamina. In order to determine the deformations of a single lamina the elasticity equation of the MLC is used. Having obtained the deformations, one can determine the stresses within the lamina.

When using this concept, several assumptions are made. It is assumed that the bond between two laminae is perfect and infinitesimally thin, which means that the displacements remain continuous and the two laminae cannot slip relatively to each other. Furthermore it is assumed that the laminate is loaded under plane stress, i.e. stress components along the thickness of the laminae are zero. In addition it is assumed that Kirchhoff's theory is valid when the laminate is subjected to bending loads.

Resultant forces and moments

For a laminate consisting of n layers and a total thickness h as shown in Figure 2.3 the resultant forces $\boldsymbol{N}$ acting on the mid-plane of the laminate can be obtained by integrating the corresponding stress over the laminate thickness h. Due to the fact that the laminate may consist of plies with different fibre orientation and therefore different stiffness matrices with respect to the reference coordinate system, the integration is split into a summation of the resultant forces in each layer.

$$\begin{Bmatrix} N_x \\ N_y \\ N_{xy} \end{Bmatrix} = \int_{-\frac{h}{2}}^{\frac{h}{2}} \begin{Bmatrix} \sigma_x \\ \sigma_y \\ \tau_{xy} \end{Bmatrix} dz = \sum_{k=1}^{n} \int_{h_{k-1}}^{h_k} \begin{Bmatrix} \sigma_x \\ \sigma_y \\ \tau_{xy} \end{Bmatrix}_k dz \tag{2.8}$$

The same procedure can be carried out for the resultant moments $\boldsymbol{M}$, which can be computed according to equation (2.9):

$$\begin{Bmatrix} M_x \\ M_y \\ M_{xy} \end{Bmatrix} = \int_{-\frac{h}{2}}^{\frac{h}{2}} \begin{Bmatrix} \sigma_x \\ \sigma_y \\ \tau_{xy} \end{Bmatrix} z\, dz = \sum_{k=1}^{n} \int_{h_{k-1}}^{h_k} \begin{Bmatrix} \sigma_x \\ \sigma_y \\ \tau_{xy} \end{Bmatrix}_k z\, dz \tag{2.9}$$

where z is the distance from the mid-plane of the laminate.

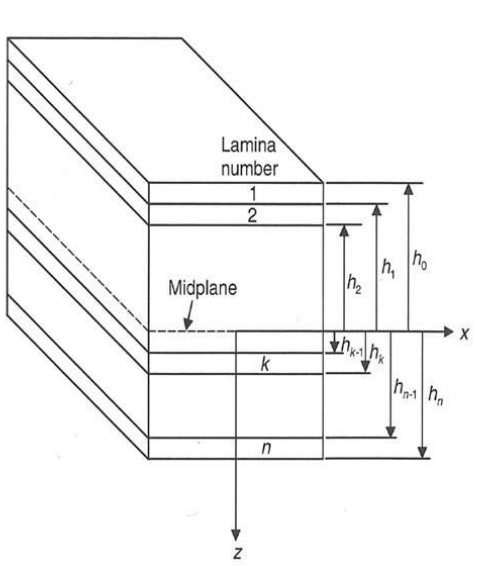

Figure 2.3: Geometry of a multi-layered laminate [6]

Kinematics

The strains at any point in the deformed laminate can be related to the displacements $(u_0,\ v_0\ and\ w_0)$ and to the curvature $(k_x, k_y\ and\ k_{xy})$.

$$\begin{Bmatrix} \varepsilon_x \\ \varepsilon_y \\ \gamma_{xy} \end{Bmatrix} = \begin{Bmatrix} \varepsilon_x^0 \\ \varepsilon_y^0 \\ \gamma_{xy}^0 \end{Bmatrix} + z \begin{Bmatrix} k_x \\ k_y \\ k_{xy} \end{Bmatrix} \tag{2.10}$$

where the mid-plane strains are derived from membrane theory and the curvatures are derived from Kirchhoff's plate theory as follows:

$$\begin{Bmatrix} \varepsilon_x^0 \\ \varepsilon_y^0 \\ \gamma_{xy}^0 \end{Bmatrix} = \begin{Bmatrix} \frac{\partial u_0}{\partial x} \\ \frac{\partial v_0}{\partial y} \\ \frac{\partial u_0}{\partial y} + \frac{\partial v_0}{\partial x} \end{Bmatrix} \wedge \begin{Bmatrix} k_x \\ k_y \\ k_{xy} \end{Bmatrix} = \begin{Bmatrix} \frac{\partial^2 w_0}{\partial x^2} \\ \frac{\partial^2 w_0}{\partial y^2} \\ 2\frac{\partial^2 w_0}{\partial x\,\partial y} \end{Bmatrix} \tag{2.11}$$

The stress in the k-th lamina can be computed from the stiffness matrix of layer k, $\bar{\boldsymbol{Q}}_k$, and the mid-plane strains and curvature as:

$$\{\boldsymbol{\sigma}\}_k = \bar{\boldsymbol{Q}}_k \boldsymbol{\varepsilon} = \bar{\boldsymbol{Q}}_k \{\boldsymbol{\varepsilon}^0 + z\boldsymbol{k}\} \tag{2.12}$$

where the subscript k refers to the ply number, z is the distance from the mid-plane and the vectors $\boldsymbol{\varepsilon}^0$ and $\boldsymbol{k}$ are the mid-plane strains and the curvature as given in equation (2.11). The lamina stiffness matrix $\bar{Q}$ is constant for each lamina and therefore equation (2.12) gives a linear variation of stress for each lamina. Depending on the fibre orientation the stiffness matrix with respect to global coordinates varies for each lamina. This leads to a discontinuous variation of stress within the laminate as shown in Figure 2.4.

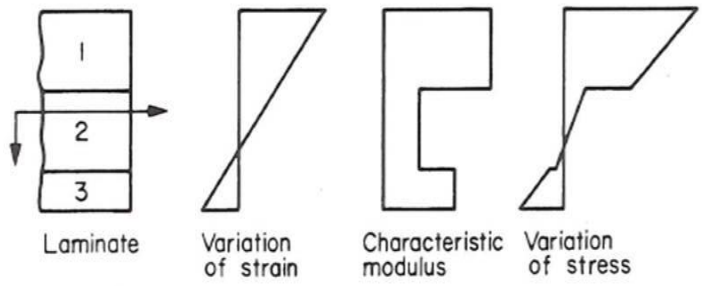

Figure 2.4: Variation of strain and stress in a three plies laminate with different fibre orientation angles [6]

Having obtained the stresses as function of mid-plane strain and curvature the resultant forces and resultant moments given in equation (2.8) and (2.9) can be expressed as:

$$\begin{Bmatrix} \boldsymbol{N} \\ \boldsymbol{M} \end{Bmatrix} = \begin{bmatrix} \boldsymbol{A} & \boldsymbol{B} \\ \boldsymbol{B} & \boldsymbol{D} \end{bmatrix} \begin{Bmatrix} \boldsymbol{\varepsilon}^0 \\ \boldsymbol{k} \end{Bmatrix} \tag{2.13}$$

where $\boldsymbol{A}, \boldsymbol{B}$ and $\boldsymbol{D}$ are 3x3 matrices, which elements are computed according to equation (2.14), (2.15) and (2.16), respectively.

$$A_{ij} = \sum_{k=1}^{n} \left(\bar{Q}_{ij}\right)_k (h_k - h_{k-1}) \tag{2.14}$$

$$B_{ij} = \frac{1}{2} \sum_{k=1}^{n} \left(\bar{Q}_{ij}\right)_k (h_k^2 - h_{k-1}^2) \tag{2.15}$$

$$D_{ij} = \frac{1}{3} \sum_{k=1}^{n} \left(\bar{Q}_{ij}\right)_k (h_k^3 - h_{k-1}^3) \tag{2.16}$$

The matrix $\boldsymbol{A}$ is called the extensional stiffness matrix. It relates the resultant forces to the mid-plane strains. In a similar way the bending stiffness matrix $\boldsymbol{D}$ relates the resultant moments to the plate curvatures. The matrix $\boldsymbol{B}$ gives information about the coupling between bending and extension. In case of non-zero coupling matrix $\boldsymbol{B}$, normal and shear forces acting on the mid-plane result not only into mid-plane strains but also into bending and twisting of the laminate plate.

For given resultant forces and resultant moments, inverting equation (2.13) gives the mid-plane strains $\boldsymbol{\varepsilon}^0$ and curvature $\boldsymbol{k}$ in the laminate. These can then be used to determine the stresses in each lamina according to equation (2.12). To summarize the CLT one could say that based on the elasticity parameters of each homogenised UD lamina which form the multi-layered composite, the CLT is used to compute the stresses and deformations of each individual lamina. These stresses should of course be withstood by the lamina. Hereby an advantage of composites is the fact, that the designer has the possibility to change fibre orientations, layups and laminae thicknesses to design the laminate in such a way that it suits its application best. Nevertheless when the stresses in a laminate are too high failure might occur. The physical appearance of failure and how the failure may be predicted through failure criteria is described in the following paragraph "Failure of composites".

2.1.4 Failure of composites

UD-laminates can fail in two ways, namely fibre failure and inter-fibre failure. Figure 2.5 gives an overview of the two different kind of failures. Fibre failure (FF) is caused by the stress longitudinal to the fibre direction, $\sigma_{\parallel}$, whereas inter-fibre failure (IFF) is caused by the transverse stress $\sigma_{\perp}$ and the shear stresses $\tau_{\perp\parallel}$ and $\tau_{\perp\perp}$.

In case of FF not only one, but a bunch of fibres break whether due to high tensile stresses or due to high compressive stress. A broken fibre cannot bear any loading, which leads to a stress redistribution to the remaining fibres. This usually leads to complete failure of the lamina and might also lead to a complete failure of the laminate.

In case of IFF a crack runs through the matrix material or the matrix-fibre interface. The crack propagates parallel to the fibre direction through the thickness of the lamina. It is stopped only by fibres of the neighbouring layers with different fibre orientation. IFF may be tolerated in multi-layered composites with different fibre orientations, since the stresses are redistributed to adjacent layers. The fibre strength is much higher than the matrix strength and therefore IFF does not lead directly to failure in that case. On the downside IFF usually comes along with a degradation of the composite material in terms of stiffness. Furthermore, cracks stopped at neighbouring layers, can lead on the one hand to delamination (two neighbouring layers separate from each other) and on the other hand to a notch effect at the fibres, which can decrease their fatigue resistance. In general a composite should always be designed against IFF. [8]

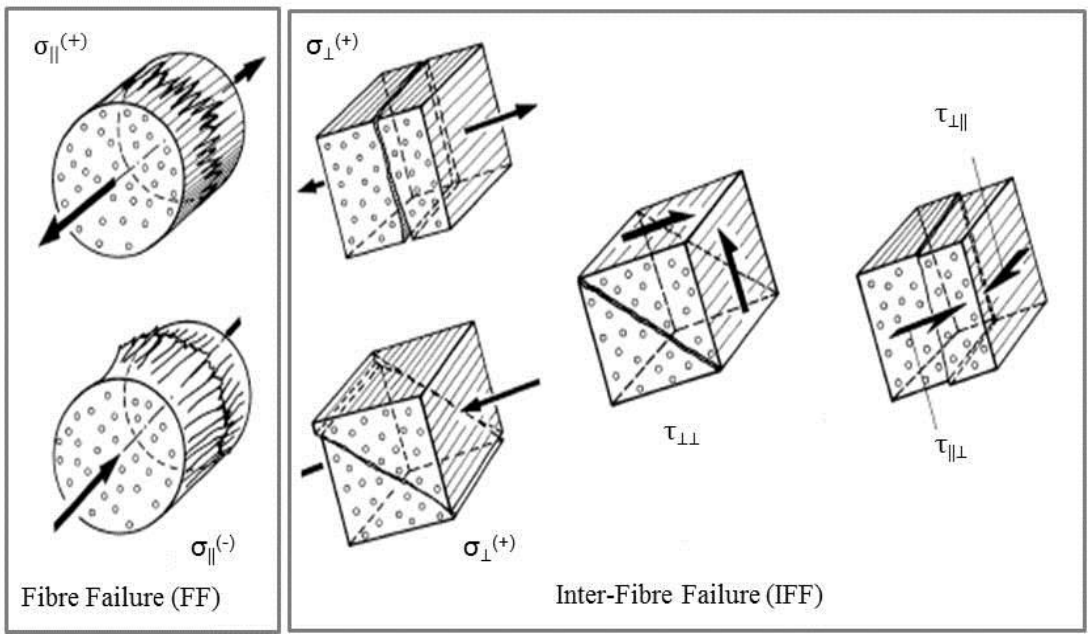

Figure 2.5: Failure modes of a UD laminate [4]

Failure criteria

Failure criteria are used to determine whether a given stress state leads to failure in the lamina and, depending on the criterion, what kind of failure mode will occur when it comes to failure. Many failure criteria were developed within the history of composite. A rather simple theory, the so called "Maximum stress theory" was proposed by Jenkin [9] in the 1920s, which is described further below. The probably most well-known failure theory of composites was developed by Tsai and Azzi and is based on the theory for anisotropic plasticity according to Hill. It is also known as the Tsai-Hill criterion [10]. Another well-known criterion is the so called Tsai-Wu criterion [11], which is implemented in many commercial software. A point of criticism is the fact that although both criteria take combined stresses into account, it is done without any physical motivation for the interaction. Instead they are mathematically easy to use criterion

One of the first failure criterion for composites which took stress interaction under plane stress conditions based on a physical approach into account was proposed by Hashin and Rotem in 1973 [5]. It was extended to three dimensional stress states by Hashin in 1980 [12]. Based on Hashin's proposal of applying the idea of Mohr's circle for metals to UD laminae, Puck proposed a criterion, which assumes failure in the plane with the lowest fracture resistance. It is based on a physical approach unlike the Tsai-Wu criterion and it differentiates between fibre failure and inter-fibre failure.

Hinton, Kaddour and Soden asked the leading experts in failure analysis of composites to apply their failure models to several test cases within the so called "World-wide Failure Exercise (WWFE)" [13]. They compared the results and came to the conclusion that Puck's failure theory gives, among others, very good results and it differentiates between different failure modes. Therefore, the Puck criterion is used in this Thesis. But before illuminating Puck's failure criterion, the maximum stress theory, which plays also a role in this thesis, shall be briefly explained.

Maximum stress theory [6]

The maximum stress theory, which is commonly attributed to Jenkin [9], predicts failure when the stresses in the principal material axes exceed the corresponding material strength. In order to avoid failure it has to be ensured that the stress limits are not exceeded:

$$-R_{\parallel}^{-} < \sigma_{\parallel} < R_{\parallel}^{+} \tag{2.17}$$

$$-R_{\perp}^{-} < \sigma_{\perp} < R_{\perp}^{+} \tag{2.18}$$

$$\left|\tau_{\perp\parallel}\right| < R_{\perp\parallel} \tag{2.19}$$

where R is the strength of the material and its index denotes the direction. As soon as one of the inequalities above is violated the material fails by a failure mode which is associated with the allowable stress. No interaction of stress components is taken into account and therefore certain loading conditions, e.g. superposition of tensile and shear stresses, lead to non-conservative results.

As already mentioned a failure criterion which takes stress interaction into account and which is based on a physical approach is the Puck criterion. It is described in the following.

Puck's failure criterion [4]

Puck proposed the criterion in 1996 [4] (see also [7]). An important quantity is the stress exertion f_E, sometimes also called stress exposure or effort. It can be understood as a degree of utilization of the material. If the stress exposure is $f_E \geq 1$ failure occurs, when it is smaller than one, the lamina can withstand the stressing. The Puck criterion distinguishes between fibre and inter-fibre failure.

Fibre failure criterion

Fibre failure depends only on the longitudinal stress but it has to be distinguished between tension and compression due to the different material strength. Therefore, the failure criterion can be written as the ratio between the stress and the associated strength:

$$f_{E,FF} = \frac{\sigma_1}{R_{\parallel}^{+}} \quad \text{for } \sigma_1 > 0 \tag{2.20}$$

$$f_{E,FF} = \frac{|\sigma_1|}{R_{\parallel}^{-}} \quad \text{for } \sigma_1 < 0 \tag{2.21}$$

Since the strength is per definition positive, the absolute value of the longitudinal stress has to be taken into account when it comes to compression (negative normal stress).

Inter-fibre failure criterion

In case of IFF one can distinguish between three different fracture modes, which are shown in Figure 2.6, where a lamina is subjected to transverse normal stress and a shear stress. Fracture mode A and B have the same fracture plane, which is normal to the transverse stress. The fracture plane is different for fracture mode C, where fracture occurs under a certain angle. For plane-stress conditions the IFF criterion can be expressed in the form of three failure conditions.

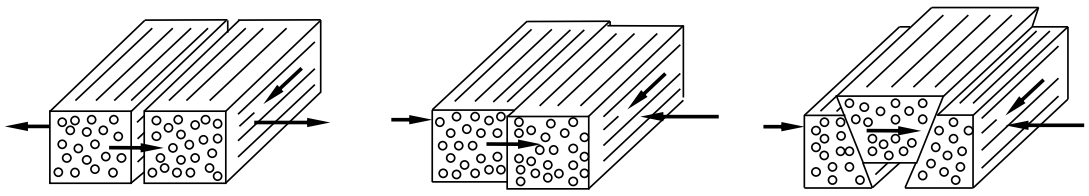

Figure 2.6: Failure modes under plane stress condition

Fracture mode A for $\sigma_2 \geq 0$

In case of fracture mode A failure can occur due to pure tensile transverse stress σ_2, pure transverse-longitudinal shear stress τ_{21} and a combination of both stresses. The exertion is calculated according to:

$$f_{E,IFF} = \sqrt{\left(1 - p_{\perp\parallel}^{+} \frac{R_{\perp}^{+}}{R_{\perp\parallel}}\right)^2 \left(\frac{\sigma_2}{R_{\perp}^{+}}\right)^2 + \left(\frac{\tau_{21}}{R_{\perp\parallel}}\right)^2} + p_{\perp\parallel}^{+} \frac{\sigma_2}{R_{\perp\parallel}} \tag{2.22}$$

The cracks are propagating along the thickness of the lamina, which means per definition that the angle of the fracture plane is $\Theta_{fp} = 0°$.

Fracture mode B for $\sigma_2 < 0$ and $0 < \left|\frac{\sigma_2}{\tau_{12}}\right| < \left|\frac{R_{\perp\perp}^{A}}{\tau_{12,c}}\right|$

Fracture mode B occurs when a compressive stress σ_2 is superimposed by shear stress τ_{21}. The compressive stress closes the cracks and increases the friction along the fracture plane. Therefore, the material can sustain a higher shear stress than the actual shear strength $R_{\perp\parallel}$. In case of fracture mode B the exertion for IFF is computed as:

$$f_{E,IFF} = \sqrt{\left(\frac{\tau_{21}}{R_{\perp\parallel}}\right)^2 + \left(\frac{p_{\perp\parallel}^{-}}{R_{\perp\parallel}} \sigma_2\right)^2} + p_{\perp\parallel}^{-} \frac{\sigma_2}{R_{\perp\parallel}} \tag{2.23}$$

Fracture mode C for $\sigma_2 < 0$ and $0 \leq \left|\frac{\tau_{12}}{\sigma_2}\right| \leq \left|\frac{\tau_{12,c}}{R_{\perp\perp}^{A}}\right|$

When the compressive stress is increased the fracture mode changes to mode C. The angle of the fracture plane is in that case $\Theta_{fp} \neq 0°$. A so called "wedge effect" occurs, where the compressive stress disperse a part (wedge) out of the lamina (see Figure 2.5). It might happen that this wedge effect is so strong that it burst the whole laminate and leads to complete failure. Therefore, this fracture mode should be strictly avoided. The exertion for IFF in fracture mode C is computed as:

$$f_{E,IFF} = \left[\left(\frac{\tau_{21}}{2\left(1+p_{\perp\perp}^{-}\right)R_{\perp\parallel}}\right)^2 + \left(\frac{\sigma_2}{R_{\perp}^{-}}\right)^2\right] \frac{R_{\perp}^{-}}{(-\sigma_2)} \tag{2.24}$$

The three equations for IFF given above contain some parameters which were not yet explained. These are $R_{\perp\perp}^{A}$, $\tau_{12,c}$, and the so called pitch factors $\left(p_{\perp\parallel}^{+}, p_{\perp\parallel}^{-} \text{ and } p_{\perp\perp}^{-}\right)$. The two material properties $R_{\perp\perp}^{A}$ and $\tau_{12,c}$ define basically the point when the fracture mode changes from fracture mode B to fracture mode C, this is when the ratio $\left|\frac{\sigma_2}{\tau_{12}}\right|$ becomes larger than the ratio $\left|\frac{R_{\perp\perp}^{A}}{\tau_{12,c}}\right|$. Both parameters can be computed as follows:

$$R_{\perp\perp}^{A} = \frac{\mathrm{R}_{\perp}^{-}}{2\left(1+p_{\perp\perp}^{-}\right)} \tag{2.25}$$

$$\tau_{12,c} = R_{\perp\parallel}\sqrt{1 + 2p_{\perp\perp}^{-}} \tag{2.26}$$

The pitch factors can be determined experimentally. In case no test data is available Puck et al. [14] suggest the following parameters for CFRP.

Table 2.1: Suggestion of pitch factors for CFRP [14]

$p^{+}_{\perp\parallel}$ [-]	$p^{-}_{\perp\parallel}$ [-]	$p^{+}_{\perp\perp}$ [-]	$p^{-}_{\perp\perp}$ [-]
0.35	0.30	0.25 – 0.30	0.25 – 0.30

Failure occurs when the stress exertion is equal to one. Using the three equations for IFF (equation (2.22), (2.23), (2.24)) and setting $f_{E,IFF} = 1$ one obtains the fracture curve as depicted in Figure 2.7. If a stress state in the lamina exists with transverse stress σ_2 and a shear stress τ_{12} such that the position vector touches or exceeds the fracture curve, IFF takes place. It illustrates also which fracture mode will occurs depending on the stress state, σ_2, τ_{21}.When subjected to pure transverse stress σ_2 the fracture curve is bounded by its compressive and tensile material strength, respectively. One can also see the effect that the material can withstand higher shear stresses when it is subjected to compressive transverse loads due to higher friction at the crack surfaces.

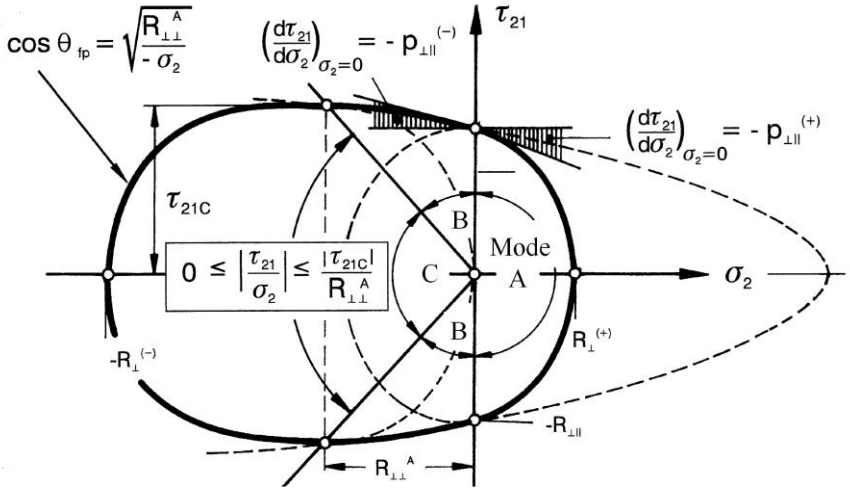

Figure 2.7: Fracture curve for inter-fibre failure under plane stress [4]

For the sake of completeness it should be mentioned that the fracture curve for inter-fibre failure, as shown in Figure 2.7, is influenced by the longitudinal stress σ_1. For increasing σ_1, the fracture curve shrinks. The fracture curve is plotted for different longitudinal stresses in Figure 2.8. The envelope for the fracture curves forms a body, which is bounded by the plane for fibre failure for high longitudinal stress. Due to its shape it is sometimes referred to "Puck's fracture cigar". The effect of decreasing resistance against inter-fibre failure for increasing longitudinal stress is only significant for high longitudinal stresses and is therefore not taken into account in this Thesis work.

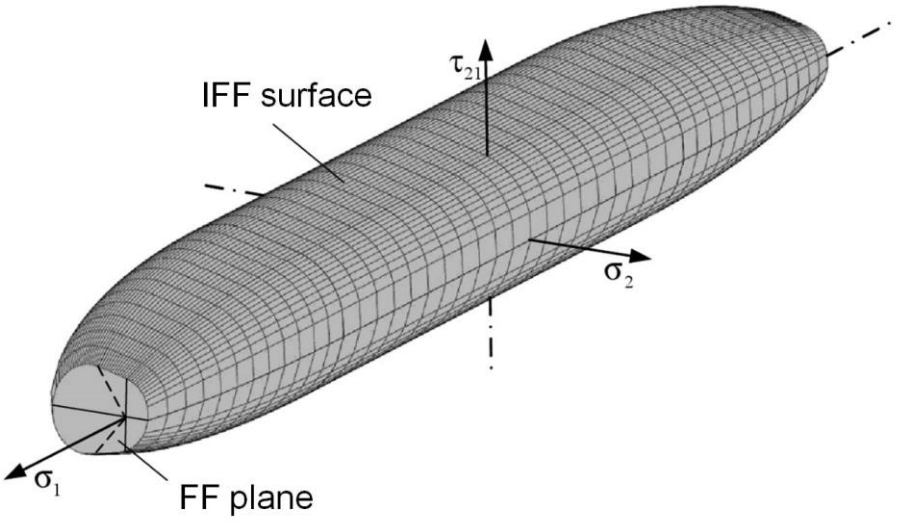

Figure 2.8: Fracture body for IFF and FF under plane stress condition [8]

The failure modes of composites and two failure criteria were explained. In the next section the fatigue behaviour of composite material is explained, but before that is done, the general concept of fatigue analysis is illustrated and effects that come into play are briefly explained.

2.2 Fatigue behaviour of materials

Components in vehicles are subjected to repeated loadings during their service life. The resulting stresses can lead to microscopic damage in the material, which can accumulate to a macroscopic damage under cyclic stress and lead to failure of the component even though the stresses are below the materials ultimate strength. This process of failure under cyclic loading is called *fatigue*.

When it comes to fatigue analyses, three major approaches exist. These are namely the stress based approach, the strain based approach and the fracture mechanics approach. The strain based approach is used, when the interest is in the local yielding at stress raiser. The fracture mechanics approach is used, when the interest is in the propagation of cracks. In this Master's Thesis the stress based approach is used, which is based on the averaged stress in an affected region. Especially when it comes to fatigue analysis of large systems using the finite element method (FEM), the stress based approach is usually applied.

In the following paragraphs the basic concept in fatigue analysis is briefly explained and effects, which come into play, are described. At the end of the chapter the fatigue behaviour of composites is depicted and the main differences with respect to the fatigue behaviour of metals are pointed out.

2.2.1 Definitions and basic concepts [15]

A load cycle can be described by its characteristic quantities, which are listed below:

- Maximum stress, σ_{max}
- Minimum stress, σ_{min}
- Mean stress, σ_m
- Amplitude stress, σ_a, and stress range, $\Delta\sigma$

When the minimum and maximum stress levels remain constant over time, the loading is called constant amplitude stressing and is shown in Figure 2.9. The stress range, $\Delta\sigma$, is defined as the difference of the maximum stress and the minimum stress.

$$\Delta\sigma = \sigma_{max} - \sigma_{min} \tag{2.27)}$$

Half the stress range is the stress amplitude, $\sigma_a = \Delta\sigma/2$.

$$\sigma_a = \frac{\Delta\sigma}{2} = \frac{\sigma_{max} - \sigma_{min}}{2} \tag{2.28}$$

The mean stress, σ_m, is the average of the maximum and minimum stress. It can be computed as:

$$\sigma_m = \frac{\sigma_{max} + \sigma_{min}}{2} \tag{2.29}$$

The ratio between the minimum stress σ_{min} and the maximum stress σ_{max} is called the stress ratio R:

$$R = \frac{\sigma_{min}}{\sigma_{max}} \tag{2.30}$$

Figure 2.9 shows different loadings. In case of an alternating load with $\sigma_m = 0$, as shown in Figure (2.9 a), the stress ratio becomes $R = -1$. For a zero-to-tension load, see Figure (2.9 c), the stress ratio is $R = 0$. Sometimes a zero-to-tension load is referred to a R-value of $R = 0.1$. This is often done when it comes to testing of specimens. In order to ensure that the specimen is not unloaded at a certain point of time, the minimum stress is bounded to $\sigma_{min} = R \cdot \sigma_{max} = 0.1 \cdot \sigma_{max}$.

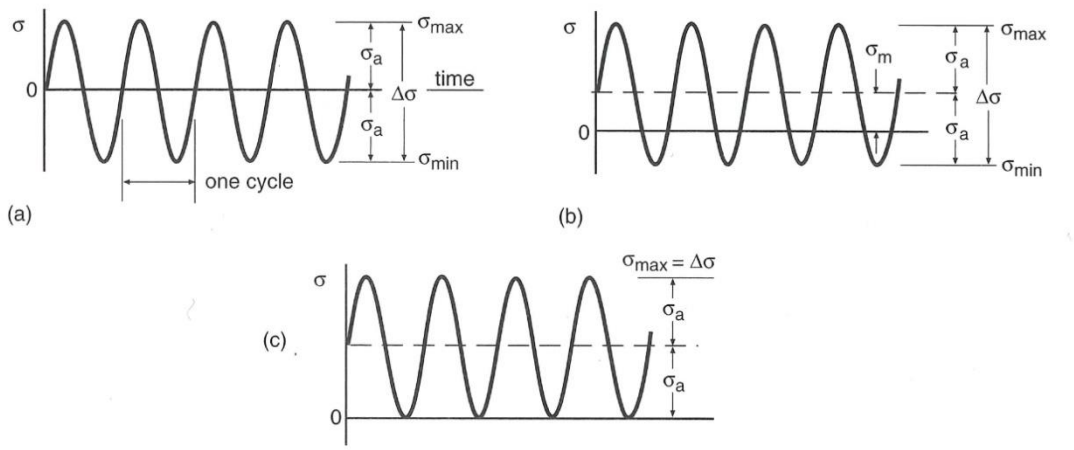

Figure 2.9: Constant amplitude cycling. Case (a) is completely reversed or alternating stressing, $\sigma_m = 0$; (b) has a nonzero mean stress σ_m; and (c) is zero-to-tension stressing, $\sigma_{min} = 0$. [15]

In general a test specimen will fail after a certain number of cycles when subjected to cyclic stress. Carrying out the same test at a higher stress amplitude will lead to a lower number of cycles to failure. The results of these tests can be plotted in a diagram to obtain the so called S-N curve. The nominal stress, S, is plotted over the number of cycles to failure N_f. The tests to obtain such S-N curves are usually carried out at a constant mean stress or for a constant R-value. The numbers of cycle to failure are plotted on a logarithmic scale. If the S-N data can be approximate by a straight line in a log-log plot, the corresponding equation can be written as:

$$\sigma = \sigma_o \left(\frac{N_f}{N_0}\right)^{\frac{-1}{k}} \tag{2.31}$$

where σ_0 and N_0 is an arbitrary fulcrum of the S-N curve and the parameter k describes its inclination. A small value of k means a steep inclination, whereas a large value of k corresponds to a flat inclination, as shown in Figure 2.10, with fulcrum $\sigma_0 = 100$ and $N_0 = 10^0$ for both curves.

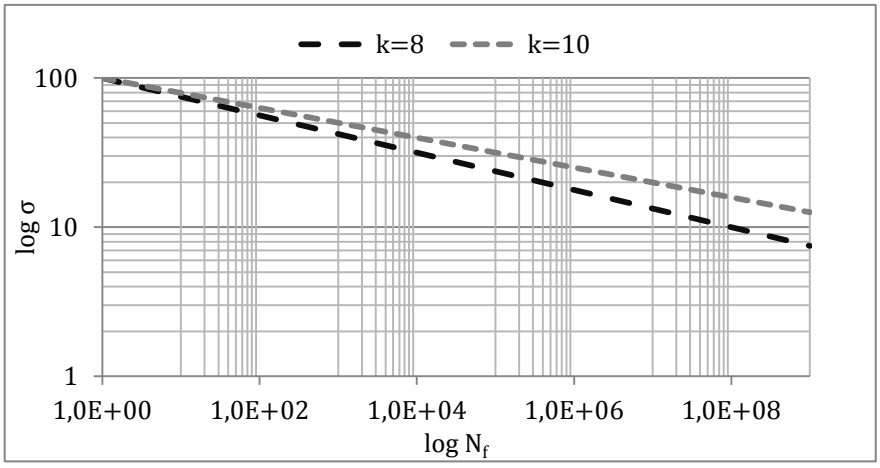

Figure 2.10: S-N curve for two different values of k

2.2.2 Linear damage accumulation according to Palmgren-Miner

Components in cars are usually not subjected to a loading with constant amplitude but to loadings with variable amplitudes, meaning that the load-time signal is not just a simple trigonometric function with constant stress amplitude but consists of cycles with varying amplitudes and different mean stresses. In order to analyse such a time signal cycle counting methods are applied. A popular method is the so called rainflow cycle counting method. It is used to count cycles of same stress amplitude and mean stress of an arbitrary time signal.

As an example: A rainflow cycle counting of a stress over time signal gives the information that the signal consists of three different stress amplitude levels $\sigma_{a,1}$, $\sigma_{a,2}$, $\sigma_{a,3}$ and each block of same stress amplitude is repeated n_1, n_2, n_3 times (see Figure 2.11). The partial damage D_i for each level can be computed as $D_i = \frac{n_i}{N_i}$. Where n_i is the number of cycles at a certain stress amplitude $\sigma_{a,i}$ and N_i is the number of cycles to failure obtained from the S-N curve for $\sigma_{a,i}$. The Palmgren-Miner rule states that the total damage D of the material arises from the sum of the partial damages $\frac{n_i}{N_i}$ according to equation (2.32):

$$D = \sum_{i=1}^{m} \frac{n_i}{N_i} \tag{2.32}$$

Per definition failure occurs when the total damage D is equal to one. If a safety factor against failure is considered, the maximum allowable total damage is set to values smaller than one. One drawback, which occurs when using the Palmgren-Miner rule, is that sequence effects of the stress-time signal are not taken into account.

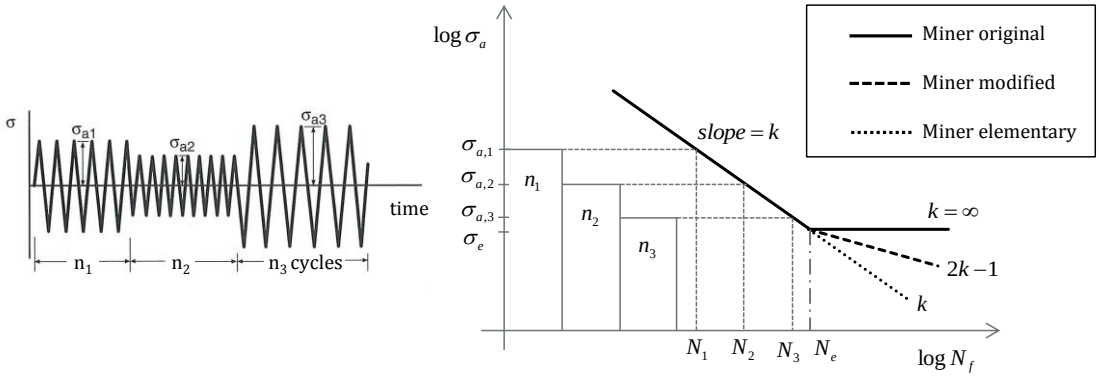

Figure 2.11: S-N curve: Linear damage accumulation according to Palmgren-Miner

Below a certain stress amplitude the continuation of the S-N curve changes. This stress limit is called the endurance limit, fatigue limit, or the knee point of the S-N curve, σ_e. It is related to a number of cycles to failure of N_e, which is for metals usually of magnitude $2 \cdot 10^6$ or 10^7. It can be distinguished between three different approaches. These are namely: Miner original, Miner elementary and Miner modified, respectively.

According to Miner original it is assumed that load cycles below the endurance limit do not contribute to the damage of the component at all. At that specific point the S-N curve becomes horizontal and the slope parameter k of the S-N curve is in that case infinite high, due to the definition of the slope. The assumption that load cycles below the endurance stress limit do not contribute to any damage of the structure may sometimes not be true.

The idea behind Miner elementary is that no endurance limit exists and the S-N curve proceeds with same slope in that region. That means that damage due to low stress amplitudes is equally taken into account as damage due to high stress amplitudes.

Haibach [16] states that both Miner original and Miner elementary contain some simplification. While the Miner original assumes that low stress amplitudes do not contribute to the total damage, which does not agree with experiments. On the other hand Miner elementary assumes that low stress amplitudes contribute in the same way as large amplitudes, which leads to an overestimation of the damage. Therefore, he proposes to use the method of Miner modified, a compromise between the two other methods. The slope of the S-N curve is altered to $2k - 1$ for fatigue life above the fatigue limit N_e. This assumption is often valid for metals but the fatigue behaviour of composite materials differs in some points, which is described in the following subsection.

2.2.3 Mean stress effects

The mean stress has an influence on the fatigue life of a specimen. For a given stress amplitude, a tensile mean stress would in general lead to shorter fatigue lives than a zero mean stress. One way of illustrating the influence of mean stress effects is a *constant life diagram (CLD;* also known as linear Goodman diagram), which is shown in Figure 2.12. The diagram can be derived from S-N curves for different mean stresses, which is the case in Figure 2.12, or from S-N curves for different R-values. Mean stresses were in that case 0, 140, 275 and 410 MPa, respectively. The lines in the Figure represent constant life. If the mean stress increases, the stress amplitude has to be decreased in order to obtain the same number of cycles to failure. For the special case when the mean stress is equal to the ultimate strength of the material, $\sigma_m = \sigma_u$, the allowable stress amplitude, σ_a, becomes zero.

If the fatigue life is evaluated by using stress amplitudes, one way of accounting for mean stresses is to compute an equivalent completely reversed stress amplitude and use an S-N curve for completely reversed loading, i.e. $R = -1$, to evaluate fatigue. Well known methods are e.g. Goodman or the approach by Smith Watson Topper (SWT approach). They both give an equation at hand to compute a completely reversed stress amplitude [15].

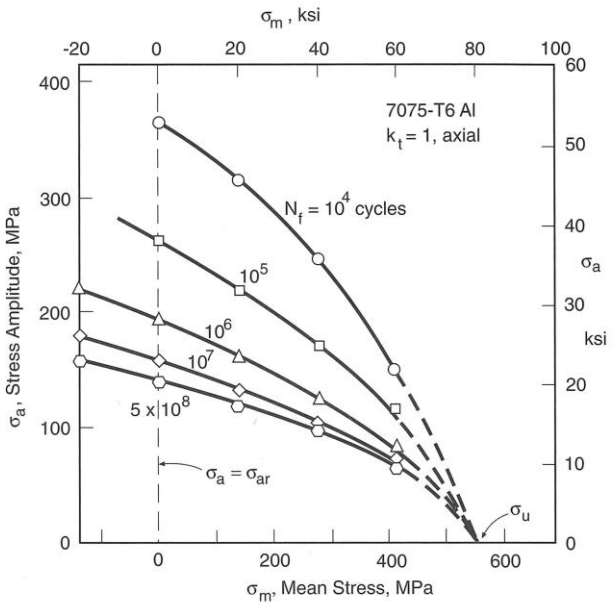

Figure 2.12: Constant life diagram derived from S-N curves at different mean stresses σ_m [15]

Another approach, which might be more suitable for composite material, is the computation of individual S-N curves for specific stress ratios by using a constant life diagram, which is briefly explained in the following. The computation of the slope of an S-N curve requires two points. It shall be assumed, that the S-N curves are defined for constant stress ratios and expressed in terms of stress amplitudes, σ_a, as functions of number of cycles to failure, N_f. For a given stress ratio, the first point of the S-N curve may be chosen as the point of static failure, i.e. number of cycles to failure $N_{f,1} = 10^0$. In case of tensional failure the sum of the corresponding stress amplitude and mean stress is equal to the material strength, R^+:

$$\sigma_a + \sigma_m = R^+ \tag{2.33}$$

Since the stress ratio, R, is known, the mean stress in equation (2.33) can be eliminated by an expression solely based on the stress amplitude, σ_a, and the stress ratio, R, by using the relations given in equations (2.28) –(2.30).

$$\sigma_a = R^+ \frac{(1-R)}{2} \tag{2.33}$$

The second fulcrum is the stress amplitude for the same stress ratio but a different number of cycles to failure, e.g. $N_{f,2} = 10^7$. It can be determined from a constant life diagram, which is exemplarily shown in Figure 2.13. The dashed line represents failure for $N_f = 10^7$ cycles. The curve is determined through fatigue test for different stress ratios (R_1, R_2, etc.) and usually it is only described for a couple of different stress ratios.

In case the stress ratio is not covered by the diagram at hand, one has to determine the stress amplitude and mean stress by using for example linear interpolation method, which is described in [17]. Having determined two points of the S-N curve, its slope parameter, k, can be determined according to equation (2.34):

$$k = \frac{\log(N_{f,2})/\log(N_{f,1})}{\log(\sigma_{a,2})/\log(\sigma_{a,1})} \tag{2.34}$$

Thus, the S-N curve is defined and can be used for the fatigue assessment.

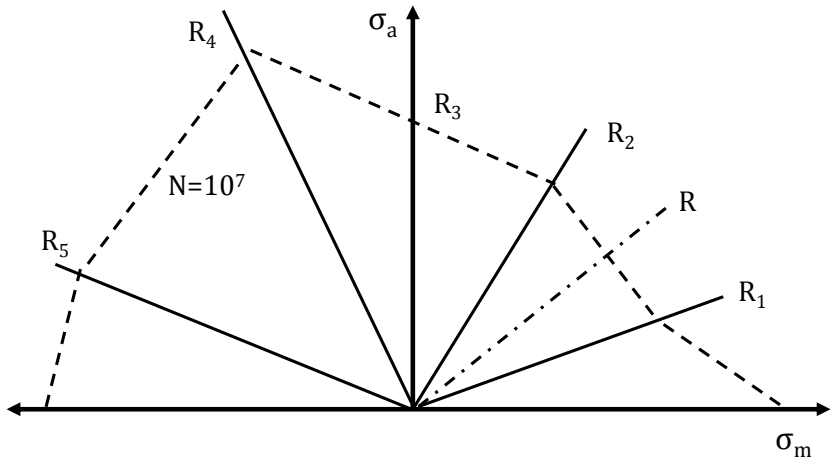

Figure 2.13: Example of a constant life diagram obtained from data at specific R-values

2.2.4 Fatigue behaviour of composites

Extensive research has been carried out about the fatigue behaviour of metals and it is understood very well so far. When it comes to fatigue behaviour of composites the research is less complete than for metals, especially when it comes to multi-axial fatigue. The main difference between metals and composites is the fact that composite material is inhomogeneous on a microscopic scale and anisotropic and therefore, the fatigue behaviour of composites differs from the fatigue behaviour of metals.

Metal fatigue failure is characterized by propagation of macroscopic cracks and the damage is often localised. Composites accumulate damage in a rather general fashion. Fatigue failure is influenced by several effects, i.e. fibre breakage, matrix cracking, delamination and debonding [18].

The slope of S-N curves, which can be regarded as a descriptor of the fatigue resistance, is very low for CFRP. That means that sensitivity to fatigue loads drops significantly as the stress amplitude drops, which can be considered as good. On the other hand a small increase in stress amplitude means a substantial shortening in fatigue life. In addition, the scatter in fatigue life is higher for composites than for metals. [19] This can be explained by the fact that the chance of including small errors through the manufacturing process is higher for composites compared to metals. Small material defects can lead to an initial damage in the material.

[20] carried out tests, where CFRP specimens were subjected to variable amplitude loadings. It was suggested that the Palmgren-Miner rule can also be applied to fatigue analysis of composites, but instead of assuming failure for $D = 1$, they suggested that an effective damage sum of $D_{eff} = 0.1$ should be used in case no value from experience is at hand. But since the scope of this Thesis is to apply different methods to account for multi-axial stress states, and simulation results are used for comparison, instead of predicting failure, it is assumed that failure occurs for a damage of $D = 1$.

3 Fatigue Simulation Process using commercial software FEMFAT

By using computational simulation techniques in the early product development phase different model variants can be easily compared against each other and the numbers of expensive prototypes can be reduced significantly in this way. A simulation tool for fatigue assessment is FEMFAT, developed by the Austrian company Magna Steyr. It is a well-established software used by various companies in the automotive and engineering industry. It carries out fatigue assessment based on the results of finite element analyses. The software consists of different modules. The FEMFAT MAX module is used for analysing components subjected to multi-axial loadings and it allows a superposition of multiple stress states.

All analyses within this Thesis were carried out with *FEMFAT MAX version 5.0* and whenever it is written FEMFAT in this report, it is referred to the software tool FEMFAT MAX. In the following section the simulation process for fatigue assessment of metal components is outlined. Hahne [2] and Kolska [3] adapted this process to fatigue simulation of composites, which is described in section 3.2.

3.1 Fatigue simulation process for metals

Figure 3.1 shows the basic workflow when using FEMFAT. An FE-model is subjected to a number of load cases in linear finite element analyses. Each load case results into a stress plot, which is scaled by a load time signal. These time signals can usually be obtained in two ways. They can be measured on a testing track or they can be simulated by using multi body dynamics (MBD) simulation techniques. The stress states over time are superposed to a single stress state at each time step, which represent the stress state due to the total loading. Based on this stress state as a function of time the fatigue assessment is carried out. The final output result is an analysis report and the damage distribution plot. The fatigue simulation process is explained more detailed in the following by using a complete vehicle as an example.

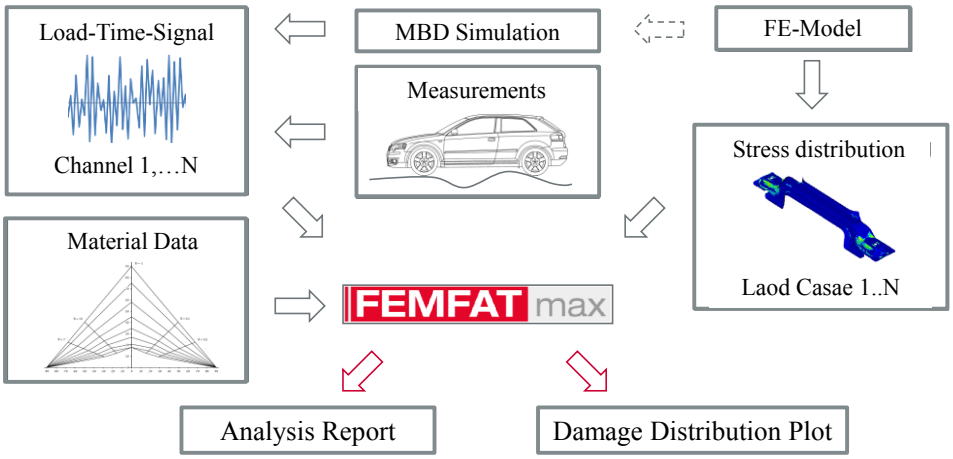

Figure 3.1: Process for fatigue assessment with FEMFAT MAX [3]

3.1.1 Geometry data

As a first step the geometry data, i.e. the FE-model, has to be imported into FEMFAT. Various input files types of different FE programmes are supported. It is possible to evaluate 2D and 3D elements but in this Thesis the analyses are limited to 2D elements. The geometry data allows FEMFAT to compute the distances between nodes. This information may be used to compute for example stress gradients, which are necessary for analysing the influence of notch effects.

The model of the car is a so called trimmed body model, as shown in Figure 3.2. A trimmed body is a model of a complete car where the suspension and engine are not included. Interior and exterior components, e.g. seats or doors, are represented by point masses, which are coupled to the car via rigid body elements.

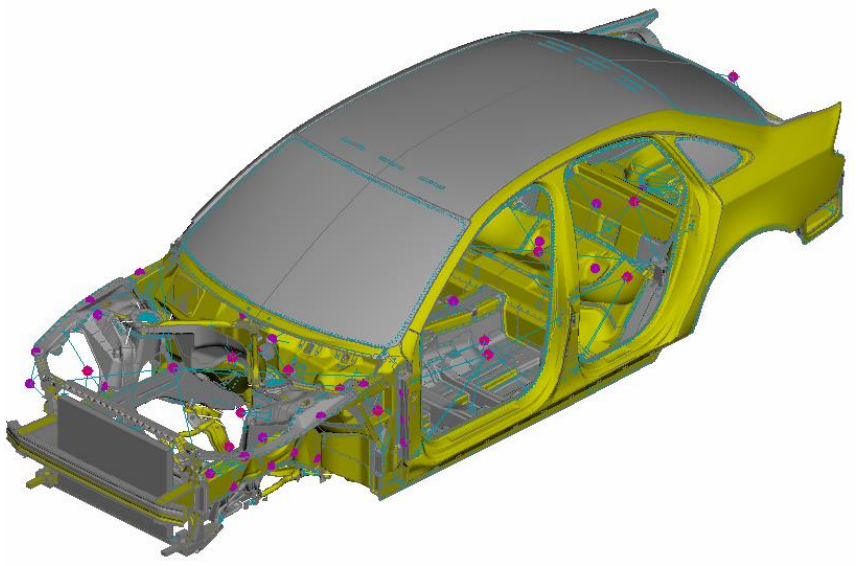

Figure 3.2: "Trimmed-body" model [3]

3.1.2 Stress data and load signals

The trimmed body is loaded by forces and moments in 22 points. Three forces and three moments are acting on each point in the direction of the three global coordinate axes, respectively. Figure 3.3 shows the locations of the 22 load application points. They represent the locations where the suspension is attached to the car body. In the linear static finite element analysis each load represents a single load case, i.e. the total number of load cases is 132 (22x6), where forces and moments are set to $F = 1000N$ and $M = 1000Nm$. The resulting stress plots can then be scaled by a load over time signal. These time signals can be obtained in two ways: Whether by using multi body dynamics simulations, where driving manoeuvres are simulated and the resulting forces and moments over time at the specific points are determined numerically, or by measuring the forces during driving tests, where several force and moment transducer are attached to the car body at the particular locations.

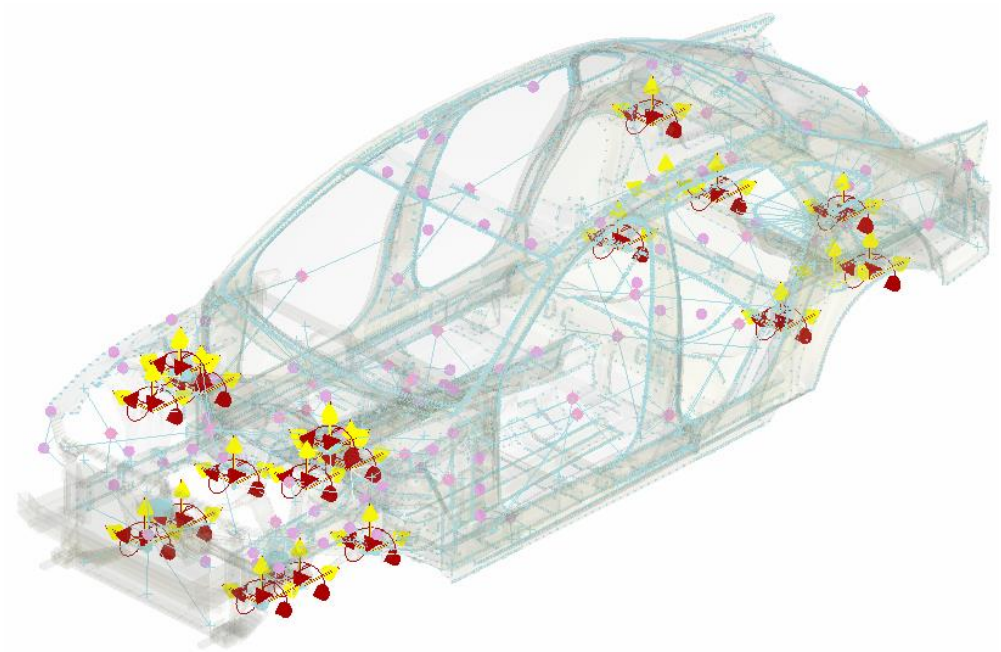

Figure 3.3: Load introduction points of the trimmed body model. Three forces, represented by yellow arrows, and three moments (red curved arrows) are acting on each point. [3]

FEMFAT evaluates stress data always at the nodes of the finite element. In case the result file contains stress data at the elements, the data is averaged at the nodes. In the analysis of the complete vehicle, the car body is subjected to 132 loads, forces are acting in 66 load cases and moments are acting in 66 load cases on the trimmed body. In order to reduce the computational effort not only for the static FEA but also for the fatigue simulation, only the force load cases are taken into account. All 66 moment load cases are neglected. The influence of the moments is rather small on the results of the fatigue analysis and therefore the simplification can be tolerated.

The load over time signals for the analysis are based on measurement data. The data is collected through different driving manoeuvres on the EVP testing track (*Ehra verschärfter Kurs für PKW – Ehra aggravated testing track for passenger cars*). As shown in Figure 3.4 the track consists of two symmetrical tracks, east and west, which are driven by turns four times in total during one driving cycle. The loops can be divided into different parts with different loading scenarios, e.g. different road surfaces, special steering manoeuvres or braking.

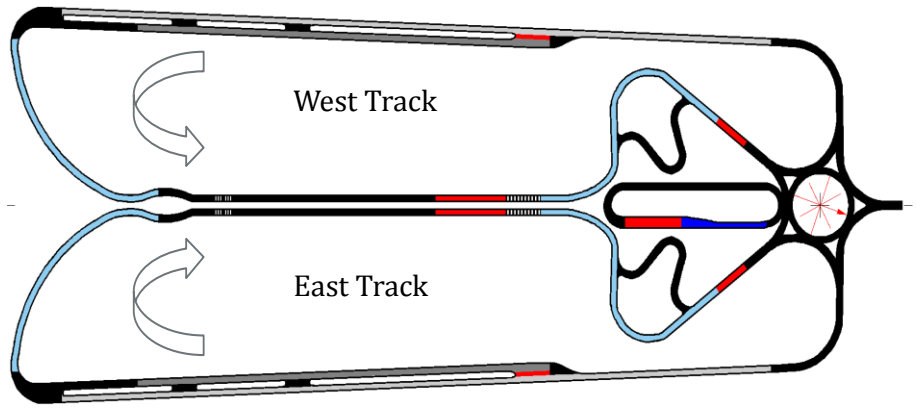

Figure 3.4: EVP testing track [21]

The resulting load time histories at the 22 attachment points are then used to multiply the corresponding FE stress plots over time. In addition, FEMFAT offers a feature that each stress plot can be scaled separately by a constant factor. This is useful if the units of a measured load over time signal differ from the units used in the FEA, e.g. a load of $F = 1kN$ was applied to a structure in a static FEA, but the measured load over time signal is in Newton. The stress plot can then be scaled by a factor of $f = 0.001$, such that both the stress plot and the load over time signal have the same units, i.e. Newton.

In order to carry out a fatigue assessment it is necessary to know the amplitude and mean stress of a stress over time signal. The stress state under plane stress conditions is defined by the three stress components σ_1, σ_2 and τ_{12}. These three stress components are usually not proportional with respect to each other but altering in a different way over time, which is exemplarily shown in Figure 3.5. One way of counting the number of cycles is the rainflow counting method. It can only be applied to a single time signal and not to three different stress over time signals. Therefore, an equivalent stress has to be computed which expresses the stress state as a single stress for each time step.

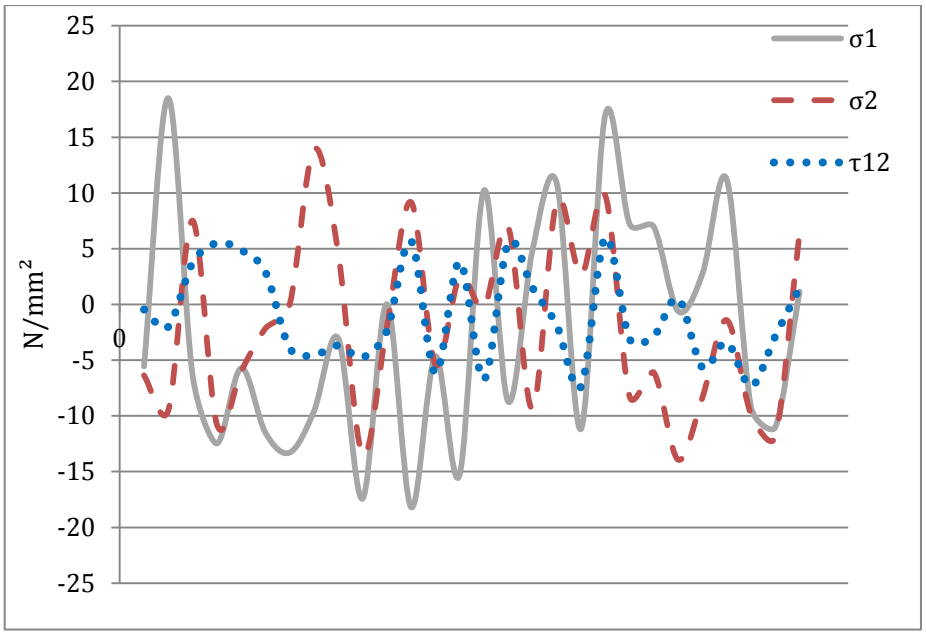

Figure 3.5: Plane stress state (σ_1, σ_2 and τ_{12}) varying over time

FEMFAT offers various methods for computing an equivalent stress. The methods can be distinguished between methods based on the critical plane approach or general methods. Methods based on the critical plane approach require a high computational effort. The method *normal stress in the critical plane* for example is seeking for the plane of a stress state with highest normal stress. Based on this normal stress the fatigue assessment is carried out. The computational effort is high for these methods but on the other hand they deliver more accurate results than general methods. General methods compute an equivalent stress based on the stress state by using for example the von Mises stress. Some methods which are available in FEMFAT are listed below:

- Normal stress in critical plane
- Material characteristic shear stress
- Signed von Mises stress
- Signed min/max principal stress

Since critical plane methods require high computational resources and the FE model has a high number of elements, these methods are not applied in the fatigue simulation process for metals. Instead the method of signed min/max principal stress is used. It computes the principal stress of a stress state. For a plane stress state the principal stresses can be computed according to equation (3.1) which reads:

$$\sigma_{I,II} = \frac{\sigma_x + \sigma_y}{2} \pm \sqrt{\left(\frac{\sigma_x - \sigma_y}{2}\right)^2 + \left(\tau_{xy}\right)^2} \tag{3.1}$$

where σ_I is the maximum principal stress and σ_{II} is the minimum principal stress. The principal stress with highest absolute value determines the equivalent stress

where its sign is also taken into account. According to the FEMFAT MAX user manual [22] this method shall be used when the interest is in a fast computation, which shows the critical region of the component and not in an accurate result in terms of fatigue life. The method of signed min/max principal stress is applied to the stress state in Figure 3.4 and the resulting equivalent stress is shown in Figure 3.5. The maximum stress in Figure 3.4 is less than 20 N/mm², whereas the maximum of the equivalent stress is slightly higher than 20 N/mm². Based on this equivalent stress history the rainflow counting method is carried out in order to determine the number of cycles together with the amplitude and mean stresses of each cycle, which define the rainflow class. This information is then used to carry out the fatigue assessment. The maximum number of rainflow classes is limited to 64 in FEMFAT.

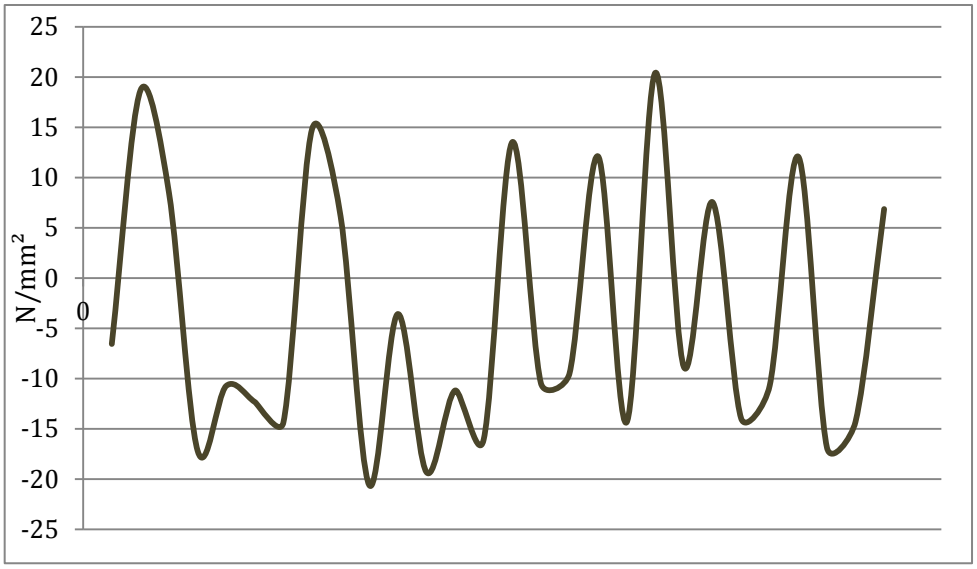

Figure 3.6: Resulting equivalent stress based on the stress over time signals as shown in Figure 3.5. Equivalent stress was determined by the signed min/max principal stress method.

3.1.3 Influence factors

Fatigue behaviour of materials can be influenced by several factors and FEMAT offers the possibility of taking most of them into account. One of these factors is the effect of surface finish. Smooth surfaces increase the resistance to fatigue, whereas a rough surface introduces small cracks at the surface, which facilitate the crack propagation and decrease the fatigue resistance [15]. Furthermore, surface treatments like shot peening or nitriding of steel may also be considered.

Two other important influence factors are the stress gradient and the mean stress effect. The stress gradients are obtained from the stress data and the finite element model, which is used to compute the distances between the nodes. High stress gradients usually appear at notches. A high stress peak is decreasing rapidly over the distance from the notch. The material is not sensitive to the peak stress, but rather to the average stress that acts over a small region [15]. That means that the fatigue life would be shorter when the stress peak is used for fatigue analysis instead of an

average stress value over a small region. Therefore, FEMFAT suggests that the influence of stress gradients should be activated to obtain more realistic results [23].

Having deactivated the influence of mean stress, means that only stress amplitudes are considered in the fatigue life evaluation and mean stresses are neglected. As shown in chapter 2.2.3 the mean stress plays an important role when it comes to fatigue assessment and therefore needs to be considered. FEMFAT offers multiple ways for mean stress accounting, e.g. Goodman or by using constant life diagrams, which is the case in this Thesis.

3.1.4 Output data

The main output of the fatigue analysis is the resulting damage, *D*. It can be written into output files of the same format as output files of various FE programmes. In case the stress analysis was carried out in NASTRAN the FEMFAT results can be written in an output file of NASTRAN type. The damage plot can then be visualised in a post processor, e.g. METAPOST. A detailed protocol file is also output by FEMFAT. It contains a summary of the fatigue analysis including material data, analysis parameters and damage results.

Furthermore, it is possible to display the equivalent stress over time signal for the critical node or for any selected node, when it is defined in a detailed result group. The fatigue analysis is based on this equivalent stress history, on which the rainflow counting method is applied to. The rainflow counting method, which is implemented in FEMFAT, differentiates between a closed load cycle and a residuum. A residuum is a hysteresis loop which is not closed (see [16] for more information). It is often weighted as half a cycle, which means that two residua with same mean and amplitude stress are counted only as one cycle, instead of two. The weighting of residua can be defined in FEMFAT and the rainflow matrices can be output in the form of text files and as figures. The weighting factor for residua is defined as $f = 0.5$ in this Thesis. The result of the rainflow counting method is available as an output and is used in this Thesis. It gives information not only about the number of cycles of each rainflow class but also about the partial damage of each rainflow class.

3.2 Fatigue simulation process for composites

FEMFAT was designed for the fatigue analysis of metal structures. It offers an option to analyse fibre reinforced polymers but this is limited to short fibre reinforced polymers. In order to use FEMFAT for analysing composite materials Hahne [2] and Kloska [3] suggested a method where, due to the orthotropic behaviour of FRP and the different material strengths in transverse and longitudinal fibre direction, the stress components are analysed separately. In order to verify the feasibility of the method, they applied it to an existing fatigue analysis of the trimmed body model, which is shown in Figure 3.2. Since the car did not contain any FRP component, the cross member was replaced by a CFRP cross member, which is highlighted in yellow in Figure 3.7. The composite layup was set to $[0°/90°/45°/\text{-}45°]_s$, which gives a quasi-isotopic material behaviour. The thickness of the cross member was increased such

that the stiffness did not change significantly between the steel cross member and the CFRP cross member.

Kloska adapted the process for fatigue assessment of metal components in two parts, where the handling of stress data and the handling of material data is treated differently compared to the metal process. The motivation behind these changes and their implementation are described in the following two subsections.

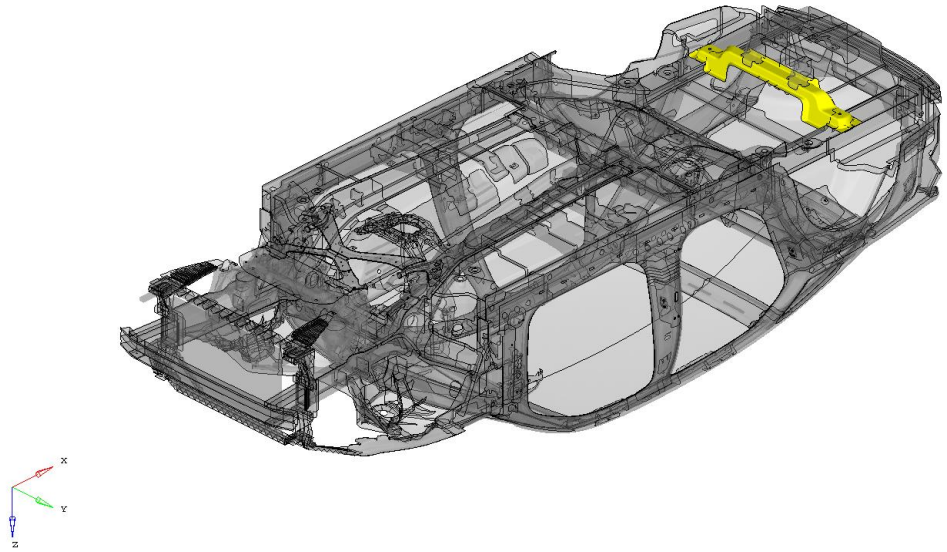

Figure 3.7: The Cross member whose material was changed from steel to CFRP is highlighted in yellow.

3.2.1 Stress data modification

As already mentioned, each stress component is analysed separately. FEFMAT offers no appropriate function such that only one stress component of a stress tensor is taken into account for the fatigue analysis. Therefore, the resulting stress data of the FEA is written into a text file by NASTRAN, a so called punch file. This text file can then be manipulated in a way that it suits the application. The element property for composite material (PCOMPG) is not supported by FEMFAT and has to be changed to a PSHELL property, which is the property for standard shell-elements. Since a standard shell-element contains only one "layer", the stress data of each layer has to be written into single stress input files. This means that an analysis of a composite, which consist of eight layers under plane stress conditions (three stress components) leads to 24 (8x3) stress data files. Since the stress components are analysed separately this method is referred to the *single stress component method* in this Thesis. It is similar to the maximum stress theory, which was described in chapter 2.1.4 as a failure criterion for composite. It states that each stress component is analysed separately and no interaction between the stress components is taken into account.

By using the single stress component method an issue arises, which is described in the following. A single finite element, which consists of one layer, is analysed. Its stress state is given as:

$$\begin{bmatrix} \sigma_1 & \tau_{12} \\ \tau_{12} & \sigma_2 \end{bmatrix} = \begin{bmatrix} 0 & 20 \\ 20 & 20 \end{bmatrix} \rightarrow \begin{bmatrix} 0 & 0 \\ 0 & 0 \end{bmatrix}_{\sigma_1} \wedge \begin{bmatrix} 0 & 20 \\ 20 & 0 \end{bmatrix}_{\tau_{12}} \wedge \begin{bmatrix} 0 & 0 \\ 0 & 20 \end{bmatrix}_{\sigma_2} \tag{3.2}$$

where the shear stress component, τ_{12}, is equal to the normal stress component, σ_2. Furthermore, it is subjected to an altering load over time signal, which is of simple triangle form and shown in Figure 3.8.

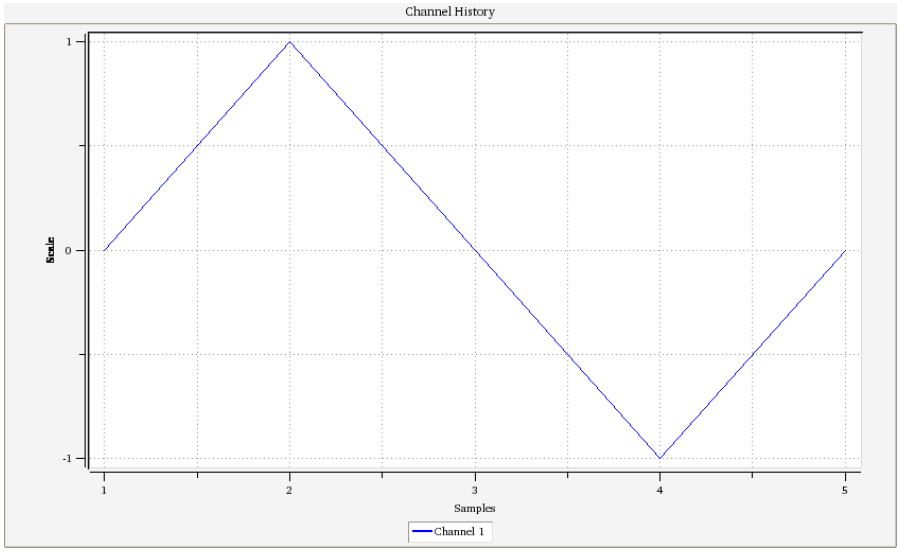

Figure 3.8: Load over time signal

By applying the method of single stress component, the stress data is split into three files (cf. equation 3.2). Three fatigue analysis in FEFMAT are carried out, but since $\sigma_1 = 0$, only two analyses need to be run. FEMAT computes an equivalent stress according to the method of min/max principal stress (cf. 3.1.2). In case of pure shear stressing the resulting principal stresses are computed as:

$$\sigma_{I,II} = \frac{\sigma_1 + \sigma_2}{2} \pm \sqrt{\left(\frac{\sigma_1 - \sigma_2}{2}\right)^2 + (\tau_{12})^2} \rightarrow \sigma_{I,II} = \pm|\tau_{12}| \tag{3.3}$$

The first and second principal stress are of same magnitude and an equivalent stress according to min/max principal stress is not unique anymore, which is also shown by using the concept of Mohr's circle in Figure 3.11 for this particular case. In the case that the maximum absolute value is not unique, FEMFAT chooses always the positive principal stress as the equivalent stress, i.e. $\sigma_{eq} = \tau_{12}$, since tensional stress is usually more critical than compressive. The equivalent stress over time signal for this particular case is shown in Figure 3.9. It is only positive and has a maximum value of $\sigma_{max} = 20MPa$ and a minimum value of $\sigma_{min} = 0MPa$. This leads to two load cycles with mean stress of $\sigma_m = 10MPa$ and an amplitude stress of $\sigma_a = 10MPa$.

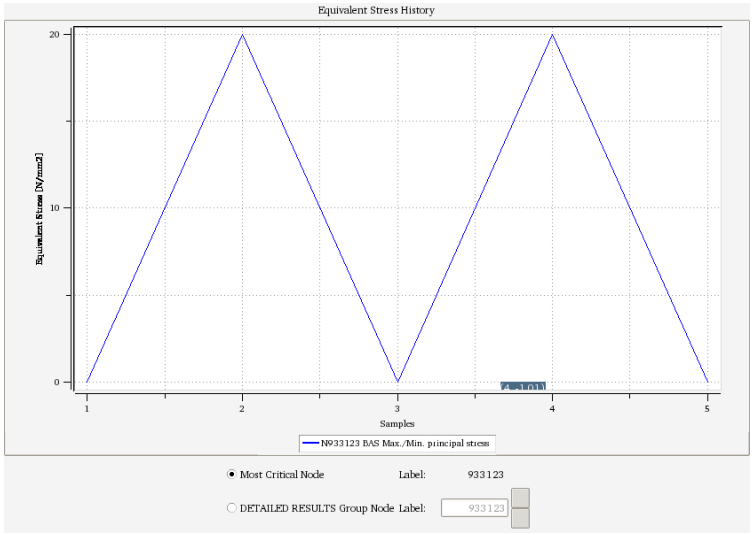

Figure 3.9: Equivalent stress for pure shear stressing. The equivalent stress is only positive defined.

In case of analysing the transverse stress, where all stress components are zero except the σ_2-component, the min/max principal stress method leads to equivalent stresses as:

$$\sigma_{I,II} = \frac{\sigma_1 + \sigma_2}{2} \pm \sqrt{\left(\frac{\sigma_1 - \sigma_2}{2}\right)^2 + (\tau_{12})^2} \rightarrow \sigma_I = \sigma_2 \wedge \sigma_{II} = 0 \tag{3.1}$$

In this case the equivalent stress according to the min/max principal method is unique, and equal to $\sigma_{eq} = \sigma_2$, which is visualized by a Mohr's circle in Figure 3.11. The equivalent stress over time signal is shown in Figure 3.10. It is varying in the same way as the load over time signal.

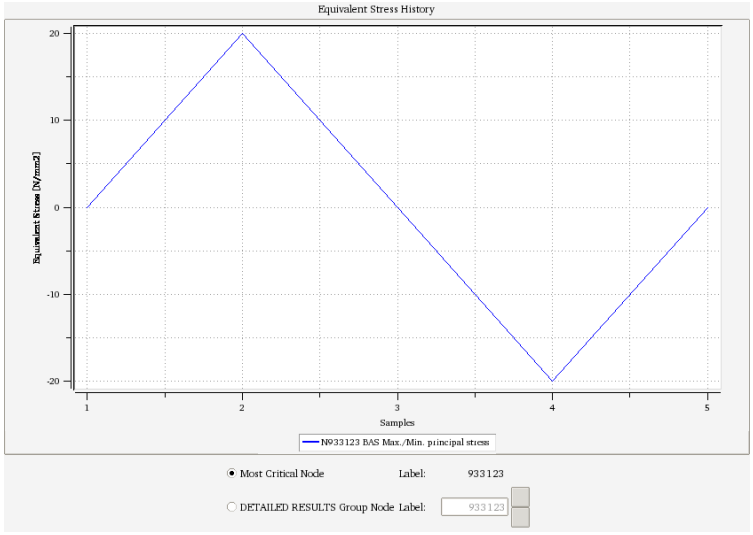

Figure 3.10: Equivalent stress for pure transverse stressing. The equivalent stress is altering according to the load over time signal shown in Figure 3.8.

This equivalent stress can be expressed as one cycle, which has a mean stress of $\sigma_m = 0MPa$ and a stress amplitude of $\sigma_a = 20MPa$. Table 3.1 compares the resulting damages for the two stressings. The damage due to pure transverse stressing is much higher than the damage due to pure shear stressing, eventhough the stress components σ_2 and τ_{12} were of same magnitude. The difference is due to the equivalent stress, where the stress amplitude is twice as high for the case of pure transverse loading compared to the pure shear loading case. The fact that the number of load cycles is twice as high for the shear stress has only a minor influence.

Table 3.1: Resulting damage for the two simple loading cases (based on same material properties)

Pure shear stressing	Pure transverse stressing
$D_{\perp\parallel} = 3.8 \cdot 10^{-12}$	$D_{\perp} = 1.3 \cdot 10^{-7}$

Therefore, it is proposed to change the procedure of carrying out the single stress component method slightly, such that the shear stress component, τ_{12}, is written to the position of the transverse stress, σ_2. Thereby, the case where the minimum and maximum principal stress are of the same magnitude is avoided.

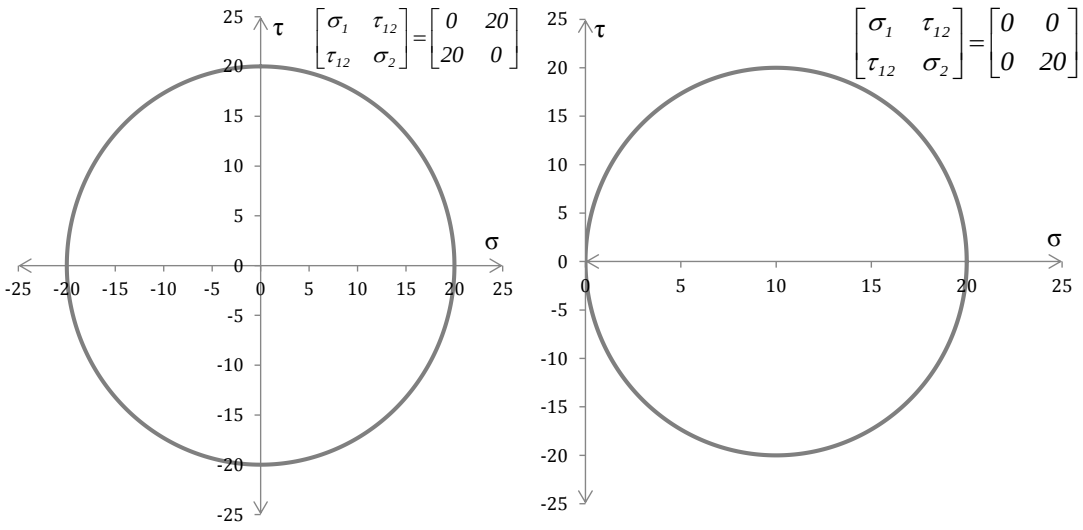

Figure 3.11: Mohr's circle for pure shear stress state (left) and pure normal stress state (right). For pure shear stressing the minimum and maximum principal stresses have same absolute value, which is not the case for pure normal stressing.

The reason for analysing each stress component separately, is based on the fact that the composite material is orthotropic and the material properties differ especially for transverse and longitudinal fibre direction. The material properties are described in a more detailed fashion in the next section.

3.2.2 Material modelling

Typical materials are already predefined in FEMFAT, but these materials are metals and not composite materials. Thus it is required to define the material properties of the composite material. Each stress component is analysed separately and therefore Kloska [3] defined three materials, one material for each direction (transverse, shear and longitudinal), where the material data was taken from Hahne [2]. The materials are defined by the static strengths, a constant life diagram (CLD) and an S-N curve.

Figure 3.12 shows the CLD for transverse stressing. The solid lines indicate lines of constant fatigue life, whereas the dashed lines are lines of constant stress ratios, *R*. The material strength in tension is significantly lower compared to the material strength in compression. The critical stress ratio, R_{crit}, is the ratio between the static material strength in compression (-180 N/mm²) and the material strength in tension (39 N/mm²). Stressing which lies to the left of the critical stress ratio results into compressive failure of the material, while tensional failure occurs when the loading is to the right of the critical R-value. The highest stress amplitude can be sustained for a mean stress of approximately $\sigma_{\perp,m} \approx -60 - (-70\ ) N/mm^2$.

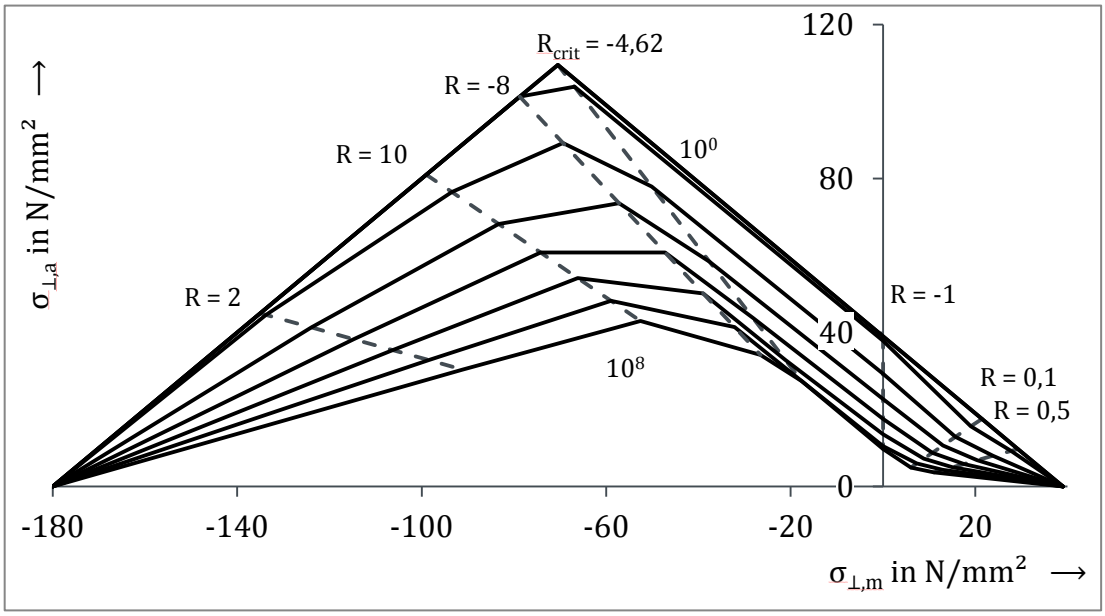

Figure 3.12: Constant life diagram of CFRP unidirectional material under transverse stressing taken from [3] based on [2]

The CLD for shear stressing is symmetric with respect to the $\tau_{\perp\parallel,a}$-axis as shown in Figure 3.13 and therefore the critical stress ratio is $R_{crit} = -1$. It implies that a negative shear stress causes the same damage as a positive shear stress. In other words, if a torsional moment is applied to a tube, which results into shear stress, failure does not depend whether the tube is twisted clockwise or counter clockwise.

The material strength of a unidirectional lamina is largest in fibre direction, which is $R_{\parallel}^{+} = 1500 N/mm^2$ in tension and $R_{\parallel}^{-} = 1000 N/mm^2$ and depict in the CLD as shown in Figure 3.14. That means that the critical R-value is $R_{crit} = -2/3$.

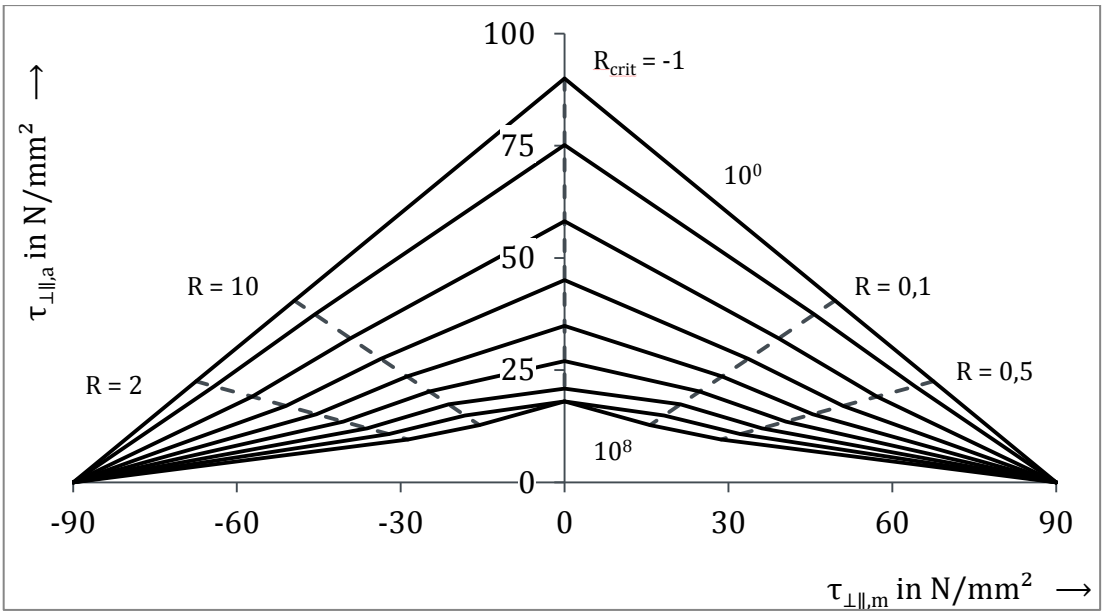

Figure 3.13: Constant life diagram of a CFRP unidirectional material under shear stressing taken from [3] based on [2]

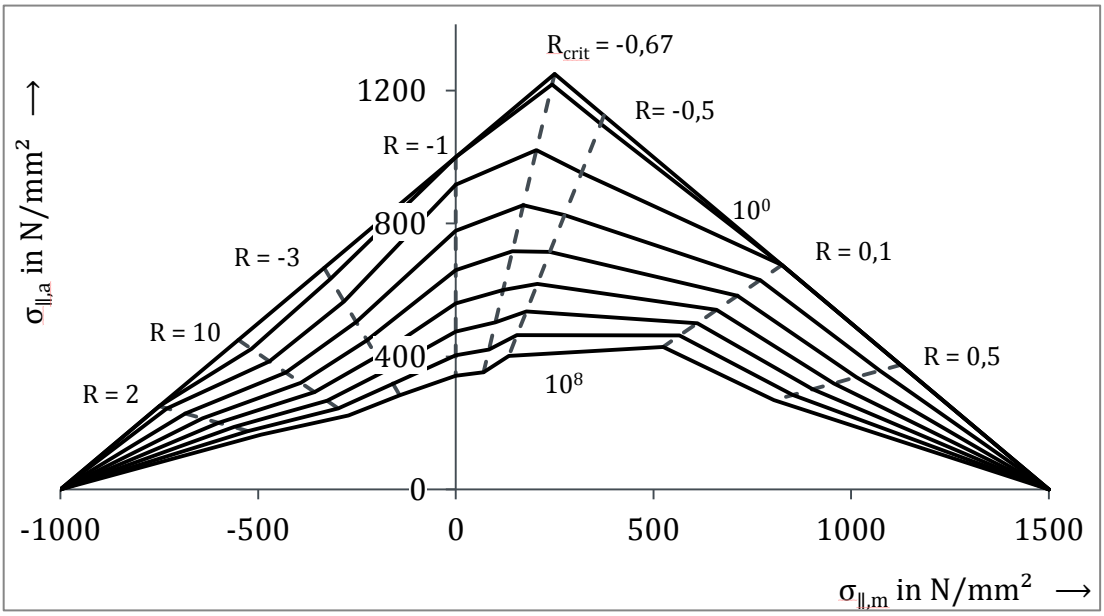

Figure 3.14: Constant life diagram of a CFRP unidirectional material under longitudinal stressing taken from [3] based on [2]

In order to account for the mean stress effect, FEMFAT requires only the constant life diagram for a specific number of cycles. Furthermore it requires the slope of the S-N curve for alternating stressing $(R = -1)$ and the endurance limit in terms of stress and number of cycles to failure as an input. The slopes for the three different loading types are given in Table 3.2. The trend of the S-N curve may change at the endurance, as described in chapter 2.2.2, and it is distinguished between three different formulation, namely Miner original, Miner modified and Miner elementary. In this case the method of Miner modified is applied, since no exact information about the material behaviour in the region of fatigue life higher than the endurance limit is

available and the Miner modified approach is a compromise between the other two formulations. The endurance limit is set to $N_e = 10^7$ cycles.

Table 3.2: Slope, k, of the S-N curve for longitudinal, transverse and shear stressing, respectively

longitudinal, $k_{\parallel}$	transverse, $k_{\perp}$	shear, $k_{\perp\parallel}$
14.0	9.25	9.0

The fatigue analysis according to the concept of single stress component is applied to the cross member in Chapter 5. By using this concept each stress component is analysed separately and no stress interaction is taken into account. It is similar to the *maximum stress theory*, which is a static failure criterion for composites and was described in Chapter 2.1.4. Not taking stress interaction into account leads to non-conservative results and does not correspond to the failure criteria proposed by Puck. Therefore, stress interaction needs to be utilised. Three models to account for multi-axial stress states are described in the next chapter. They are applied to the fatigue analysis of the cross member in Chapter 5.

4 Multi-axial Fatigue Models for Composites

In chapter 2.1.4 the failure modes of composites were described and Puck's failure theory was outlined. It was pointed out that under plane stress conditions there is no interaction of stress components when it comes to fibre failure, but in case of inter-fibre failure an interaction between the transverse normal stress component, σ_2, and the shear stress component, τ_{12}, exists. This interaction is currently not taken into account in the fatigue analysis of composite components as described in chapter 3.2.

In order to improve the validity of fatigue analysis of composites stress interaction needs to be taken into account. Three methods which account for multi-axial stress states are explained in the following. They are applied to the fatigue analysis of a complete vehicle simulation in chapter 5. The first method was proposed by Hahne [2]. It is based on Puck's failure theory and uses the stress exertion to compute an equivalent stress. The second method, an a posteriori damage interaction method, which was also proposed by Hahne [2], is in its principals based on a suggestion by the society of German engineers (VDI – Verein Deutscher Ingenieure) [24]. It is claimed, that Puck's static failure theory may be adopted to fatigue analyses as well. Its procedure is described in section 4.2. The third method to account for stress interaction, which is originally used for welded metal structures suggested by the International Institute for Welding [6], is described in section 4.3. It is slightly modified in a way, such that it fits the fatigue behaviour of composites.

4.1 Stress interaction according to Puck's theory

The Puck failure criterion states that failure occurs when the stress exertion, f_E, which, in case of IFF, is a function of the stress components σ_2 and τ_{12}, is equal to one. Based on this fact it may be assumed that different stress states cause the same damage when their stress exertion is the same. Therefore, it is plausible to use the stress exertion for the computation of an equivalent stress.

Figure 4.1 illustrates this concept for the case that a stress state *P* lies in the region of fracture mode *A*. The stress exertion, $f_{E,IFF}$, for point *P* is computed by using equation (2.22) for inter-fibre failure under plane stress conditions. In order to compute an equivalent transverse stress the point *P* is projected onto the σ_2-axis such that the stress exertion remains constant. That means that if the stress state σ_2, τ_{12} possesses a stress exertion of $f_{E,IFF}$, one can "translate" this stress state into an equivalent transverse stress $\sigma_{2,eq} = f_{E,IFF} \cdot R_\perp$, where $R_\perp$ is the material strength in transverse direction. It can be seen that $\sigma_{2,eq}$ is larger than the sole σ_2-component. The change in magnitude is due to the shear stress part which is now taken into account.

Instead of computing an equivalent transverse stress, one could also compute an equivalent shear stress, $\tau_{12,eq}$, by projecting the stress state *P* not onto the σ_2-axis but onto the τ_{12}-axis. The procedure is the same and the equivalent shear stress would be computed as $\tau_{12,eq} = f_{E,IFF} \cdot R_{\perp\parallel}$. Again one can see the difference in magnitude between the single shear stress component τ_{12} and the equivalent shear stress component $\tau_{12,eq}$ in Figure 4.1.

The procedure is summarized in the equation (4.1) to (4.4). Depending on the sign of σ_2, the equivalent transverse stress, $\sigma_{2,eq}$, is computed as:

$$\sigma_{2,eq} = f_{E,IFF} \cdot R_{\perp}^{+} \qquad \text{for} \quad \sigma_2 \geq 0 \tag{4.1}$$

$$\sigma_{2,eq} = -f_{E,IFF} \cdot R_{\perp}^{-} \qquad \text{for} \quad \sigma_2 < 0 \tag{4.2}$$

Since the material strength and the stress exertion are always positive defined, the equation for equivalent transverse stress in compression has to be written with a minus sign. The equivalent shear stress, $\tau_{2,eq}$, is computed as:

$$\tau_{12,eq} = f_{E,IFF} \cdot R_{\perp\parallel} \qquad \text{for} \quad \tau_{12} \geq 0 \tag{4.3}$$

$$\tau_{12,eq} = -f_{E,IFF} \cdot R_{\perp\parallel} \qquad \text{for} \quad \tau_{12} < 0 \tag{4.4}$$

It has to be kept in mind that the stress exertion is determined differently depending on the fracture mode (see equations (2.22), (2.23) and (2.24)).

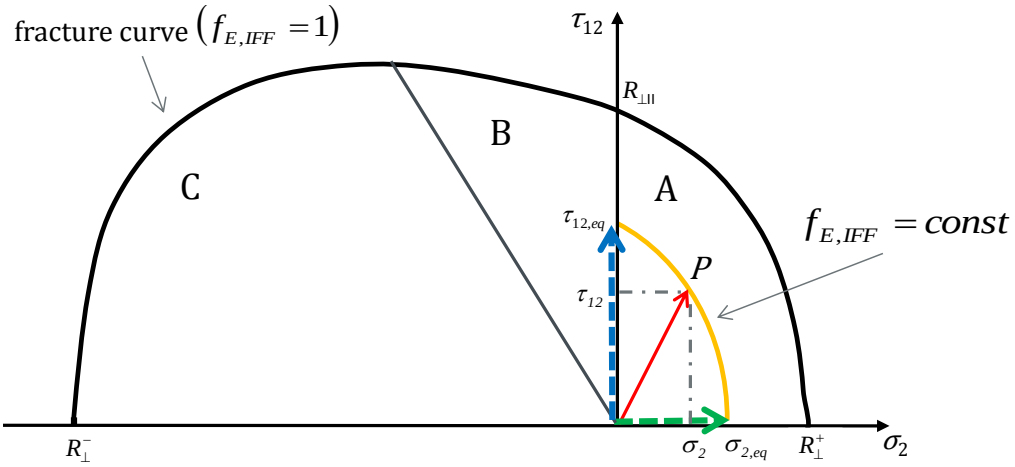

Figure 4.1: Equivalent transverse (green) and equivalent shear stress (blue) using the principal of constant stress exertion, $f_{E,IIF}$

Why determine both an equivalent shear stress and an equivalent transverse stress? This shall be briefly illustrated in the following loading case scenario:

A tubular specimen with fibre oriented in circumferential direction is subjected to a torsional moment, which leads to a mean shear stress, τ_m, and shear stress amplitude, τ_a. In addition to the torsional moment a minor, alternating transverse load is applied. The stress over time signal may look as shown in the left Figure in Figure 4.2. If the stress over time signal is plotted in the stress interaction diagram, that means that at each point of time there is a pair of stress values $(\sigma_2;\ \tau_{12})$, which is represented by a single dot in the stress interaction diagram, one would obtain the plot to the right in Figure 4.2. The Figure shows also the fracture curve for static failure and it marks the three regions of different fracture modes. The two lines between fracture mode B and fracture mode C represent the borders, where the fracture mode changes from mode B to mode C.

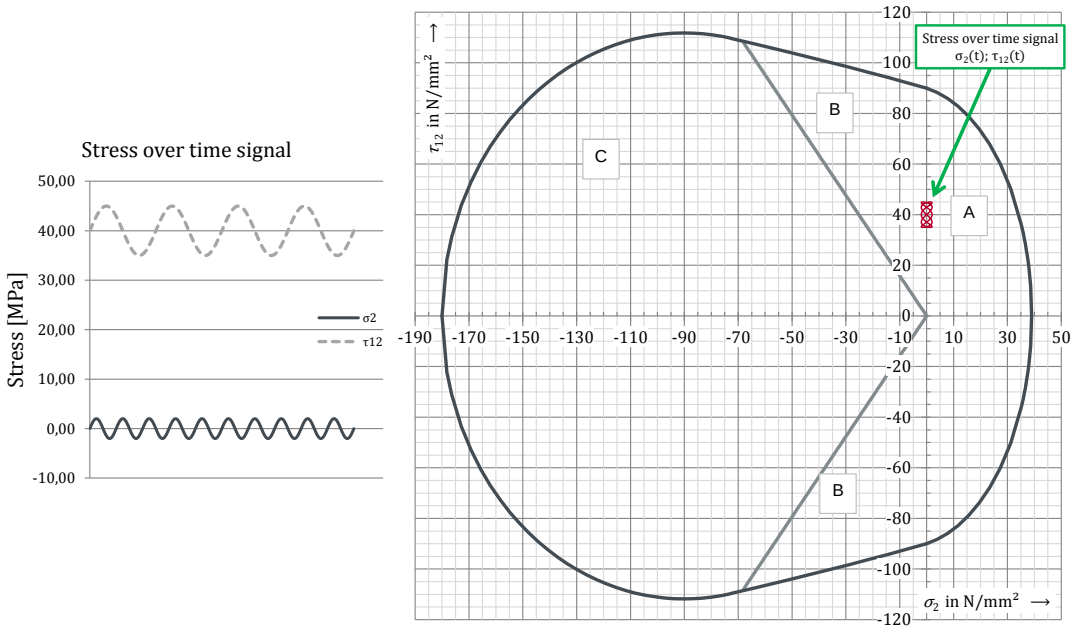

Figure 4.2: Loading scenario of a tubular specimen. Left: Stress-over-time-signal. Right: Interaction diagram with fracture curve for IFF. The red point cloud represents the stress over time signal.

The shear stress is dominating in this loading scenario and the stress exertion is altering between 0.4 and 0.5. When it comes to determination of equivalent stresses, an equivalent transverse stress, $\sigma_{2,eq}$, would result in an altering stress signal with minimum and maximum values of:

$$\sigma_{2,eq,min} = -f_{E,IFF} \cdot R_{\perp}^{-} \approx 0.5 \cdot 180MPa = -90MPa$$

$$\sigma_{2,eq,max} = f_{E,IFF} \cdot R_{\perp}^{+} \approx 0.5 \cdot 39MPa = 19.5MPa$$

This would lead to very large stress ranges, even though the actual stress ranges in the original time signal are rather small. Figure 4.3 shows the resulting equivalent transverse stress, $\sigma_{2,eq}$, and the equivalent shear stress, $\tau_{12,eq}$, as functions of time based on the loading scenario given above. The two equivalent stress signals differ significantly. As already mentioned above, the equivalent transverse stress is altering between values of $\sigma_{2,eq,min} \approx -90\text{MPa}$ and $\sigma_{2,eq,max} \approx 20\text{MPa}$, whereas the equivalent shear stress is altering between values of $\tau_{12,eq,min} \approx 34.5\text{MPa}$ and $\tau_{12,eq,max} \approx 45.7\text{MPa}$. Since the portion of transverse stress, σ_2, in the original time signal (shown in Figure 4.2, left) is rather small, the equivalent shear stress signal, $\tau_{12,eq}(t)$, does not differ significantly from the shear stress component signal $\tau_{12}(t)$. It seems likely that in case the loading is dominated by shear stresses, an equivalent shear stress may lead to more realistic results, whereas the equivalent transverse stress may give more reasonable results, when the loading is dominated by transverse stressing.

Another feature, which can be observed for this loading scenario, is the frequency of the equivalent stress signals, see Figure 4.3. In case of equivalent transverse stress, the signal $\sigma_{2,eq}(\text{t})$ has the same frequency as the transverse stress signal, $\sigma_2(\text{t})$ (cf. left

Figure 4.2), while the frequency of the equivalent shear stress signal, $\tau_{12,eq}(t)$, corresponds to the frequency of the original shear stress signal, $\tau_{12}(t)$. A higher frequency means more load cycles and especially in fatigue analysis the number of load cycles is an important quantity, which is another reason why the type of equivalent stress should be chosen accordingly to the dominating stress component.

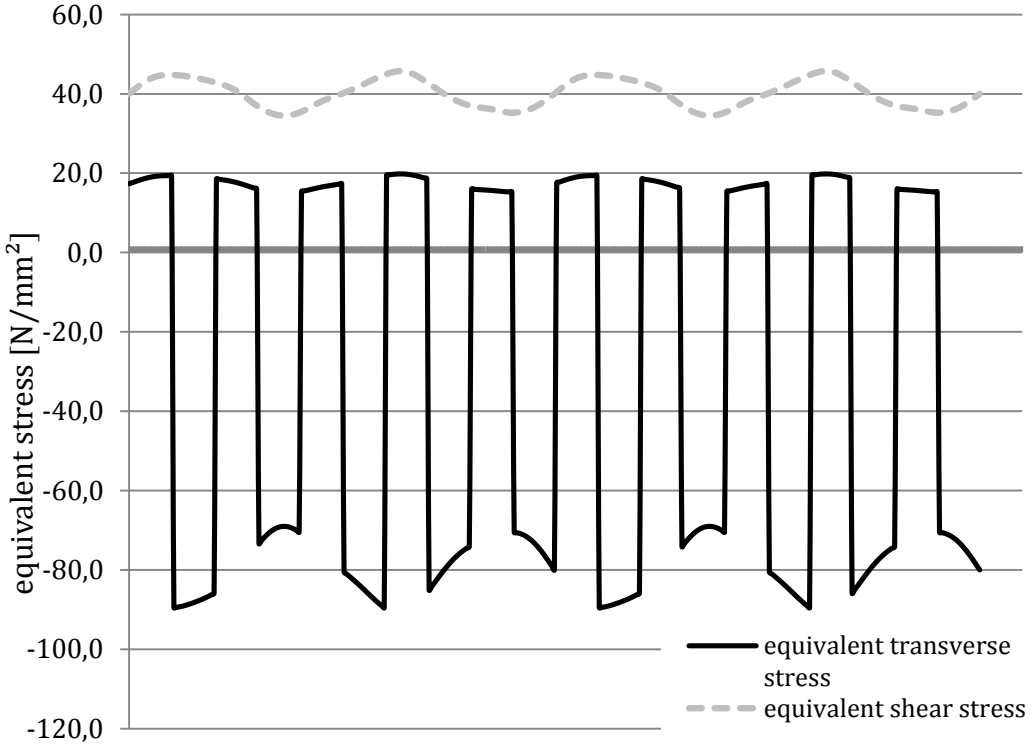

Figure 4.3: Resulting equivalent stress over time signals for the stress signal as shown in the left Figure of Figure 4.2

Since the strength in transverse compressive direction, $R_{\perp}^{-}$, is usually much higher than the transverse tensional strength, $R_{\perp}^{+}$, one may argue whether or not it is reasonable to determine an equivalent stress according to equation (4.2). The equivalent stress in compression becomes a very large value, which can also be seen in Figure 4.3. Furthermore, the fracture angle for fracture mode *C* is different than the fracture angle for fracture mode *A* and *B* (cf. subsection 2.1.4) and a stress amplitude may not contribute to failure that much. Therefore, an alternative to the equivalent transverse stress, where the equivalent stress is always determined based on the stress exertion for all fracture modes, may be formulated as follows:

If a stress state lies in the region of fracture mode A the equivalent transverse stress is determined, as it was done before, by projecting the stress state onto the transverse stress axis such that the stress exertion remains the same. In case of fracture mode B or C the equivalent stress is not determined by a transverse stress of same stress exertion, but instead the equivalent stress is set equal to the σ_2 stress component, see Figure 4.4. In order to avoid confusion between the equivalent transverse stress according to equations (4.1), (4.2), the alternative equivalent transverse stress is labelled as $\sigma_{2,\mathrm{eq}}^{*}$. It is determined by the following relations:

$$\sigma^*_{2,\mathrm{eq}} = f_{E,IFF} \cdot R^+_\perp \qquad \text{for} \quad \sigma_2 \geq 0 \tag{4.5}$$

$$\sigma^*_{2,\mathrm{eq}} = \sigma_2 \qquad \text{for} \quad \sigma_2 < 0 \tag{4.6}$$

Thus it is assumed that no interaction between shear stress, τ_{12}, and transverse stress, σ_2, takes place when $\sigma_2 < 0$. There is no real physical motivation behind this formulation, but instead this might be an alternative to the equivalent transverse stress, $\sigma_{2,eq}$. Since the equivalent stress in compression will be less for the alternative method than for the original one ($\sigma^*_{2,\mathrm{eq}} < \sigma_{2,eq}$ for $\sigma_2 < 0$), using these two methods of computing an equivalent transverse stress, gives the possibility to express the influence of compressive stress.

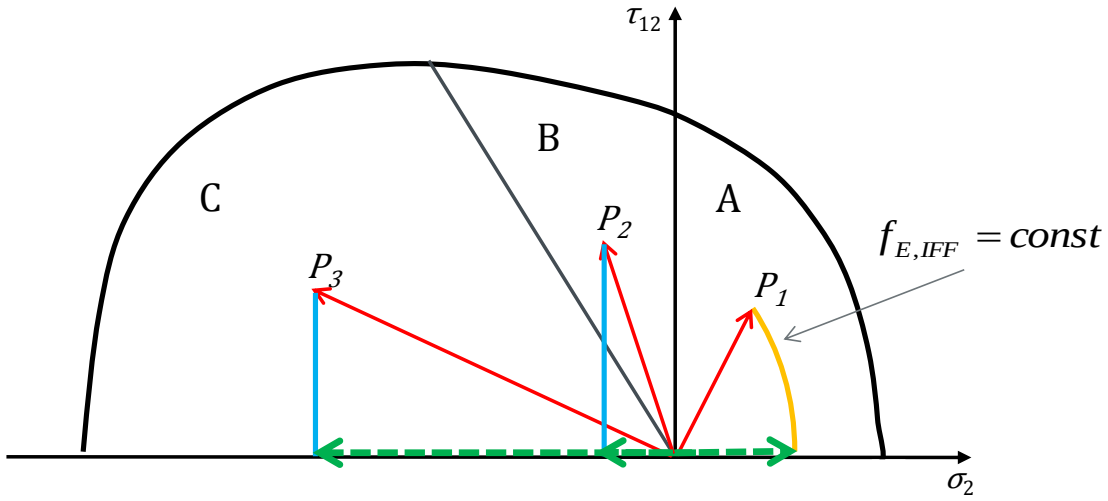

Figure 4.4: Procedure for determining the alternative equivalent transverse stress $\sigma^*_{2,eq}$ based on three stress states (P_1, P_2, P_3) for different fracture modes. The orange line is a line of constant stress exertion, whereas the blue, vertical lines are lines of constant transverse stress

Implementation into the simulation process

In the current process of fatigue analysis for composites no stress interaction is taken into account. As described in chapter 3.2 each stress component is analysed separately. A way to apply the method of equivalent stress based on the stress exertion to the simulation process is described in the following. Unfortunately, FEMFAT does not offer the possibility to control or modify fatigue analyses by using a macro programming language or the like as it is possible for most of the finite element software. That means that the user has to rely on the functions FEMFAT already offers and cannot implement own routines.

With the procedure described in the following the influence of stress interaction is not taken into account for all nodes of the structure but only for a selected node of interest. At the beginning the fatigue analysis for composites according to the concept of single stress component assessment as described in chapter 3.2 has to be carried out. The structure is analysed in this case three times for each stress component $(\sigma_1, \sigma_2 \; or \; \tau_{12})$ separately. This leads to three critical nodes, the nodes with highest

damage: One critical node with highest damage for pure σ_1-stressing, one critical node for pure σ_2-stressing and one critical node for pure τ_{12}-stressing. As already mentioned, no stress interaction has to be taken into account for damage longitudinal to the fibre direction, which would lead to fibre failure. But stress interaction plays a role for inter-fibre failure, i.e. the critical nodes for pure σ_2-stressing and pure τ_{12}-stressing show a tendency to IFF.

In order to compute an equivalent stress, the stress state at the critical node has to be known. The structure is usually subjected to a time varying stress state, which is obtained as a superposition of multiple stress states scaled with different load over time signals. The result file of the finite element analysis contains the stress values at the elements, which are averaged at the nodes in FEMFAT. Since FEFMAT uses the stress data at the nodes, one needs to obtain the nodal stresses from the element stresses in the FEA result file. This stress data for each load case can be extracted at the nodes with postprocessors, e.g. METAPOST. Table 4.1 shows the superposition of nodal stress data $(\sigma_1, \sigma_2, \tau_{12})$ for two load cases. The stress data for each load case is a result of a linear FEA and is displayed directly below the stress components in Table 4.1. The stress data is then scaled with a variable load over time signal (LTS) for each load case and then summed up over all load cases at each time step.

Table 4.1: Superposition of stress data of a node for two different load cases. The stress data is scaled with a corresponding load over time signal (LTS) and summed up over each time step. The stress values right below the stress components represent the stress values from the linear static FEA with unit loading. Units of stress data are N/mm².

	Load case 1				Load case 2				Sum over load cases		
	LTS	σ_1(t)	σ_2(t)	τ_{12}(t)	LTS	σ_1(t)	σ_2(t)	τ_{12}(t)	σ_1(t)	σ_2(t)	τ_{12}(t)
time		2	1	1,5		1	2	2	3	3	3,5
1	-10	-20	-10	-15	13	13	26	26	-7	16	11
2	-22	-44	-22	-33	3	3	6	6	-41	-16	-27
3	-20	-40	-20	-30	-10	-10	-20	-20	-50	-40	-50

The sum of stresses of each load case represents the stress state which is present at each time step, e.g. during a driving manoeuvre. The resulting transverse and shear stress over time signal are highlighted red in Table 4.1. Based on this data the fracture mode according to Puck can be determined as well as the stress exertion for each time step. Depending on the type of equivalent stress, equations (4.1) – (4.6) are used for the computation of the equivalent stress, which is depicted in Table 4.2 for equivalent transverse stress, $\sigma_{2,eq}$, alternative equivalent transverse stress, $\sigma^*_{2,\mathrm{eq}}$, and equivalent shear stress, $\tau_{12,eq}$, respectively.

Table 4.2: Illustration of the impact of stress interaction on equivalent stress values. Strength data in transverse direction for tension $R_{\perp}^{+} = 39N/mm^2$, for compression $R_{\perp}^{-} = 180N/mm^2$ and in transverse longitudinal direction $R_{\perp\parallel} = 90N/mm^2$.

t	Stress components $\sigma_2(t)$	Stress components $\tau_{12}(t)$	Fracture mode according to Puck	Stress exertion according to Puck	$\sigma_2(t)$ Equivalent stress $\sigma_{2,eq}$	$\sigma_2(t)$ Alternative equivalent stress $\sigma^*_{2,eq}$	$\tau_{12}(t)$ Equivalent stress $\tau_{12,eq}$
1	16.0	11.0	A	0.43	16.8	16.8	36.3
2	-16.0	-27.0	B	0.25	-45.2	-16.0	-22.6
3	-40.0	-50.0	C	0.44	-78.4	-40.0	-39.2

In Table 4.2 it can be seen that the absolute value of the equivalent transverse stress, $\sigma_{2,eq}$, is always larger than the single σ_2 stress component. If one compares the equivalent shear stress, $\tau_{2,eq}$, with the single τ_{12} component one can observe that for fracture mode B and fracture mode C the equivalent stress is lower than the single stress component. This implies the fact which was already stated in chapter 2.1.4 that the material can sustain higher shear stresses when it is subjected to compression. The equivalent stress is then reduced for specific constellations of shear stress and compressive transverse stresses.

In order to take multi-axial stress states into account the idea is to "feed" FEMFAT with a respective equivalent stress signal as a load over time signal. In chapter 3 it was stated that FEMFAT cannot just process a single stress component, but has to compute an FEMFAT internal equivalent stress. In this case the method of min/max principal stress is used. This equivalent stress is a FEMAT internal equivalent stress and should not be confused with the equivalent transverse, or shear stress to account for stress interaction. The principal stresses under plane stress conditions are computed as:

$$\sigma_{I,II} = \frac{\sigma_1+\sigma_2}{2} \pm \sqrt{\left(\frac{\sigma_1+\sigma_2}{2}\right)^2 + {\tau_{12}}^2} \tag{4.7}$$

FEMFAT chooses the principal stress, which has the highest absolute value, as equivalent stress. For a stress state, where all stress components are zero, except the transverse stress component, given as:

$$\begin{bmatrix} \sigma_1 & \tau_{12} \\ \tau_{12} & \sigma_2 \end{bmatrix} = \begin{bmatrix} 0 & 0 \\ 0 & 1 \end{bmatrix} \mathrm{N/mm^2} \tag{4.8}$$

the principal stresses are computed as $\sigma_I = 1N/mm^2$ and $\sigma_{II} = 0$. In this case FEMFAT would choose $\sigma_I = 1\mathrm{N/mm^2}$, since its absolute value is largest. If this stress state is scaled with a load over time signal, the FEFMAT-equivalent stress over time signal would be the same as the load over time signal (cf. Chapter 3.1.2). Based on this fact, a second fatigue analysis is carried out on a single element FE model. The stress state of the single finite element is set to a unity transverse stress state, as shown in equation (4.8). This can easily be done by editing the punch-file, which contains the stress data and is used as an import into FEMFAT. The input load signal into FEMFAT is a simple text-file, which contains one of the equivalent stress over time

signals as exemplarily shown in Table 4.2, meaning that the FEMFAT internal equivalent stress is equal to the equivalent stress determined according to Puck's stress exertion ($\sigma_{2,eq}$, $\sigma^*_{2,eq}$, or $\tau_{12,eq}$). FEMFAT applies then the rainflow counting method to the equivalent stress history in order to determine the number of cycles of each rainflow class, which is characterised by a stress amplitude and mean stress. The mean stress effects are taken into account by the corresponding constant life diagram. When the equivalent shear stress, $\tau_{12,eq}$, is used as a load over time signal, the material for transverse longitudinal direction ("shear material") has to be used in the fatigue analysis in FEMFAT. For the case of running the fatigue analysis with an equivalent transverse stress, $\sigma_{2,eq}$ or $\sigma^*_{2,eq}$, the material for transverse direction ("transverse material") needs to be used.

The procedure described above enables the fatigue analysis based on an equivalent stress (transverse or shear), which accounts for the interaction between σ_2 and τ_{12}. The change of geometry from a complex FE model to a simple one-element model has the effect that factors, which are determined by the geometry data, e.g. influence of stress gradients, cannot be taken into account since the geometry is different, which would lead to different stress gradients. Only one single finite element is considered, which has a certain stress state. Averaging this stress state at the nodes would result into the same stress state at all nodes and therefore the difference between the nodal stress states is zero, which means that the stress gradient is zero too. Nevertheless, no influence factors, which are based on the geometry, are taken into account in the fatigue analysis in FEMFAT and therefore changing the geometry does not lead to different results.

The described procedure shows how a FEMFAT user can carry out fatigue analysis and take multi-axial stress states into account by computing an equivalent stress based on the stress exertion. It is summarized in the following:

1. Carry out a fatigue analysis on a component by using the single stress component method for pure transverse stress, σ_2, and pure shear stress, τ_{12}. This will give two critical nodes: one with highest damage for pure transverse loading and one for pure shear loading.

2. Extract nodal stresses for these two nodes from FEA for each load case. Multiply stresses of each load case with corresponding load over time signal. Sum up stress components over all load cases at each time step.

3. Based on the superposed stress over time signal, determine fracture mode at each time step according to Puck's theory.

4. Compute stress exertion at each time step depending on fracture mode.

5. Determine equivalent transverse stress, equivalent shear stress and/or the alternative equivalent transverse stress by using the appropriate equations.

6. Carry out a fatigue analysis in FEMFAT on a single element FE model with a plane stress state:

$$\begin{bmatrix} \sigma_1 & \tau_{12} \\ \tau_{12} & \sigma_2 \end{bmatrix} = \begin{bmatrix} 0 & 0 \\ 0 & 1 \end{bmatrix} MPa$$

And use the max/min principal stress as method for computing FEMFAT internal equivalent stress.

7. Use the respective equivalent stress as a load over time signal.

8. Use "shear material" when using $\tau_{12,eq}$ as load signal, and use "transverse material" for $\sigma_{2,eq}$, or $\sigma^{*}_{2,eq}$, respectively.

9. Run fatigue analysis and determine "new" damage.

It should also be mentioned that some load cases exist, at least in theory, where the method of equivalent stress according to constant stress exertion leads to inappropriate results. One special case occurs when the load is altering only on a curve of constant stress exertion for pure positive shear stress or pure negative shear stress, as shown in Figure 4.5 for the case of pure positive transverse stressing. The orange line is a line of constant stress exertion. Three different stress states (P_1, P_2, P_3) have different shear stress and transverse stress components but they result into the same stress exertion. Due to the same stress exertion the equivalent shear stress would always result into the same value $\tau_{2,eq}$. According to the equivalent shear stress the structure would be loaded by a quasistatic shear stress, with constant mean stress $\tau_{2,eq,m} = \tau_{2,eq}$ and stress amplitude $\tau_{2,eq,a} = 0$, which would not lead to any fatigue damage at all, since the stressing is constant and not cyclic.

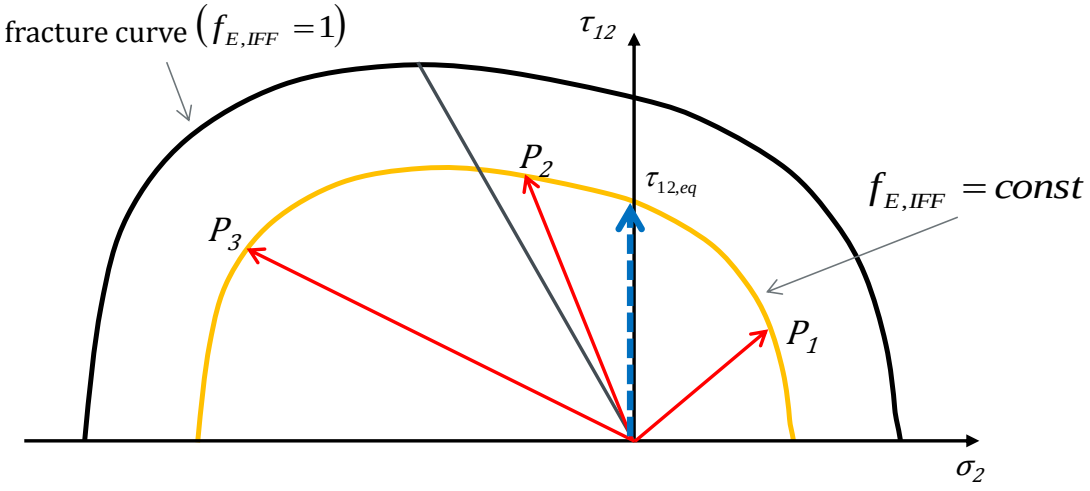

Figure 4.5: Three different stress states (P_1, P_2, P_3) with same stress exertion $f_{E,IFF}$ result into same value of equivalent shear stress $\tau_{12,eq}$

The same goes for the equivalent transverse stress, $\sigma_{2,eq}$, when the load is altering along a curve of constant stress exertion only in the compressive or only in the tensional transverse stress region. These fictional loading cases are very constructed and the chance of occurrence during the service life of a car is very small. Nevertheless, one has to be aware of this behaviour when using this method.

4.2 An a posteriori damage interaction method

A second method suggested by Hahne [2], which uses also the Puck criterion for stress interaction, is based on the VDI guideline VDI 2014. The guideline consists of three parts and deals with the design and construction of FRP components. The third part, "*Development of FRP components (fibre-reinforced plastics) Analysis"* [24], gives recommendations for the analysis of composites and also to some extend for fatigue analyses.

The main idea is that the damage mechanism for static failure and cyclic failure do not change significantly and can be assumed to be identical. Therefore, one can apply Puck's failure criteria also to fatigue analyses. The failure criteria for inter-fibre failure (IFF) under plane stress conditions can be expressed by three conditions depending on the fracture mode, as explained in chapter 2.1.4. These criteria depend on the stress state (σ_2, τ_{12}) the pitch factors and the material strength for shear and transverse stressing $(R_{\perp\parallel}, R_{\perp}^{+}, R_{\perp}^{-})$. If for example a material is subjected to pure static shear stressing, failure occurs when the maximum shear stress is equal to the transverse longitudinal material strength, $\tau_{12,max} = R_{\perp\parallel}$. In case the material is not subjected to a static load but to a cyclic loading, the maximum bearable stress is decreasing, depending on the number of repetitions. This decrease as a function of number of cycles can be expressed in S-N curves as already described in chapter 2.2.

This gives the possibility to modify the Puck failure criteria in a way that the static material strengths, are replaced by dynamic material strengths, which are obtained from S-N curves. Since S-N curves depend not only on the number of cycles to failure but also on the stress ratio R, the parameters for dynamic material strength become functions of number of load cycles, N, and stress ratio, R. Puck's failure criteria for IFF under plane stress can then be rewritten for the different fracture modes as:

Fracture mode A for $\sigma_2 \geq 0$

$$f_{E,IFF} = 1 = \sqrt{\left(1 - p_{\perp\parallel}^{+} \frac{R_{\perp}^{+}(R,N)}{R_{\perp\parallel}(R,N)}\right)^2 \left(\frac{\sigma_{2,\max}}{R_{\perp}^{+}(R,N)}\right)^2 + \left(\frac{\tau_{21,\max}}{R_{\perp\parallel}(R,N)}\right)^2} + p_{\perp\parallel}^{+} \frac{\sigma_{2,\max}}{R_{\perp\parallel}} \quad (4.9)$$

Fracture mode B for $\sigma_2 < 0$ and $0 < \left|\frac{\sigma_2}{\tau_{12}}\right| < \left|\frac{R_{\perp\perp}^{A}(R,N)}{\tau_{12,c}(R,N)}\right|$

$$f_{E,IFF} = 1 = \sqrt{\left(\frac{\tau_{21,\max}}{R_{\perp\parallel}(R,N)}\right)^2 + \left(\frac{p_{\perp\parallel}^{-}}{R_{\perp\parallel}(R,N)} \sigma_{2,\max}\right)^2} + p_{\perp\parallel}^{-} \frac{\sigma_{2,\max}}{R_{\perp\parallel}(R,N)} \quad (4.10)$$

Fracture mode C for $\sigma_2 < 0$ and $0 \leq \left|\frac{\tau_{12}}{\sigma_2}\right| \leq \left|\frac{\tau_{12,c}(R,N)}{R_{\perp\perp}^{A}(R,N)}\right|$

$$f_{E,IFF} = 1 = \left[\left(\frac{\tau_{21,\max}}{2\left(1+p_{\perp\perp}^{-}\right)R_{\perp\parallel}(R,N)}\right)^2 + \left(\frac{\sigma_{2,\max}}{R_{\perp}^{-}(R,N)}\right)^2\right] \frac{R_{\perp}^{-}(R,N)}{\left(-\sigma_{2,\max}\right)} \quad (4.11)$$

The dynamic material strengths are determined from S-N curves and therefore, it is required that one S-N curve, typically for a stress ratio $R = -1$, is available. The effect of different stress ratio, R, which is associated with the effect of mean stress, is taken into account by using constant life diagrams (CLD).

Figure 4.6 depicts the method described above. The fracture curve $(f_{E,IFF} = 1)$ for static inter-fibre failure under plane stress conditions is shrunk according to appropriate S-N curves for transverse and shear stressing. By using this method, fracture curves of constant life can be plotted in the (σ_2, τ_{12})-diagram corresponding to equations (4.9) to (4.11).

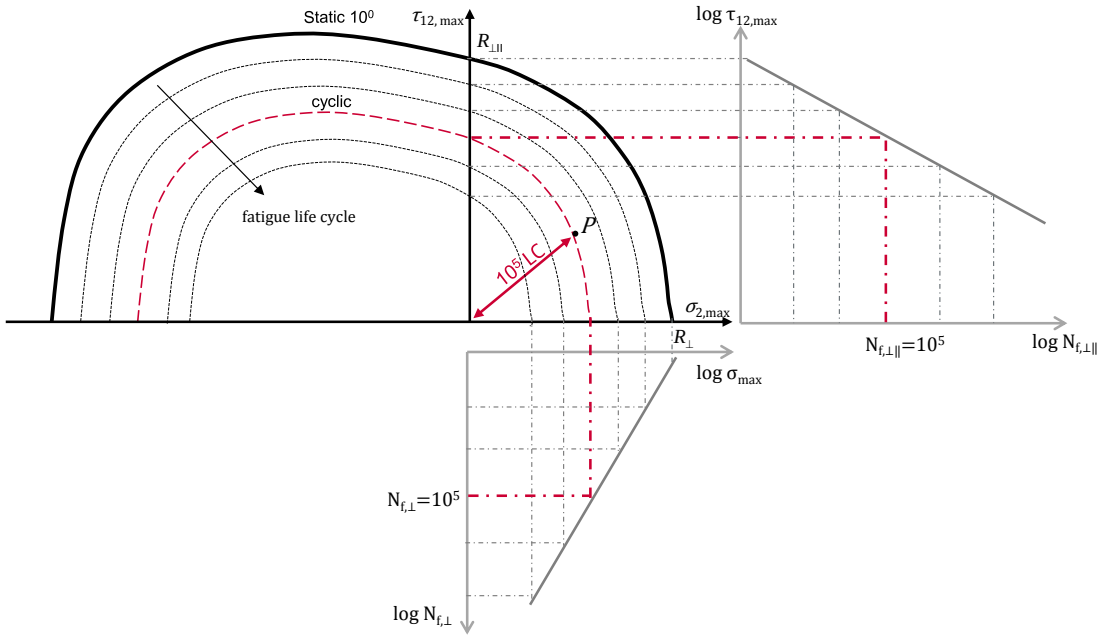

Figure 4.6: Shrinkage of Puck's failure curve for IFF under plane stress conditions according to S-N curves for cyclic shear stressing (right) and cyclic transverse stressing (bottom). Figure based on [2]

Gude et al. used this idea and compared it to multi-axial fatigue tests, where CFRP specimens where subjected to superposed shear and transverse stressings at constant stress amplitudes. The correlation between multi-axial fatigue testing and prediction by shrinkage of the failure curve according to appropriate S-N curves was good and therefore they draw the conclusion that the failure curve may be shrunk by appropriate S-N curves. [25]

For a given biaxial, in-phase, cyclic stressing with constant shear stress amplitude, τ_a, shear stress ratio, $R^{\perp\parallel}$, and constant transverse stress amplitude, σ_a, transverse stress ratio, $R^{\perp}$, the fracture curve can be shrunk as long as the decreased curve comes in contact with the maximum stress peak P (σ_{max} and τ_{max}) of the loading. This leads to the resulting number of cycles to failure. In other words, the equations for IFF have to be solved for the number of load cycles, N, which can be done iteratively. In case of fracture mode B an explicit solution exist, which reads:

$$R_{\perp\parallel}(R,N) = p_{\perp\parallel}^{-}\sigma_2 + \sqrt{\left(\tau_{12,\max}\right)^2 + \left(p_{\perp\parallel}^{-}\sigma_{2,\max}\right)^2} \tag{4.12}$$

The dynamic material strength, $R_{\perp\parallel}(R,N)$, is determined by an S-N curve, which can be formulated in a log-log-diagram as:

$$R_{\perp\parallel}(R,N) = R_{\perp\parallel}\left(N_f\right)^{\frac{-1}{k}} \tag{4.13}$$

where $R_{\perp\parallel}$ is the static material strength, N_f is the number of cycles to failure and k the inclination of the S-N curve, which depends on the stress ratio, R. Actually not only the dynamic material strength depends on the number of cycles to failure in equation (4.9) – (4.11), but also the pitch factors. In order to estimate these parameters multi-axial tests need to be carried out, but since no test data is available, it is assumed that these factors remain constant.

Implementation into the simulation process

In order to apply the method of a posteriori damage interaction, the fatigue analysis by using the method of single stress component (see Chapter 3.2) needs to be carried out in advance, which gives the two nodes with highest damage due to pure transverse stressing and due to pure shear stressing, respectively. As for the stress interaction method according to Puck's theory, only selected nodes can be analysed. In this case the procedure is described for analysing the node with the highest damage due to pure shear stressing.

An output result of the FEMFAT analysis is the rainflow matrix of the critical node, which contains the number of load cycles for a specific stress amplitude and mean stress. It also reveals the rainflow classes, which contribute mostly to the total damage. Figure 4.7 shows two rainflow matrices of a critical node as an example. In the left matrix the numbers of load cycles for each rainflow class are displayed. In the right matrix the damage in percent of the total damage is shown. One can see that in terms of number of load cycles a few classes have more than 100 load cycles and classes with low stress amplitude are repeated more often than classes with higher stress amplitude. But when it comes to contribution to the total damage, only one class contributes significantly. The other classes do not contribute at all to the total damage.

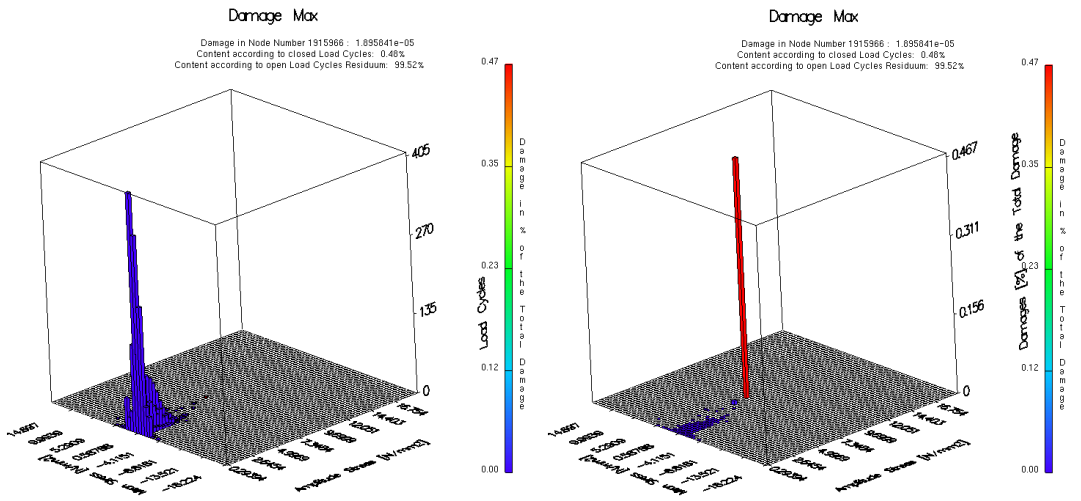

Figure 4.7: Rainflow matrices for closed load cycles. Left: Number of load cycles for each rainflow class. Right: Damage [%] of total damage

Hahne [2] suggests a method to account for stress interaction which is described in the following paragraphs. It is based on the idea that a load spectra, which consists of different rainflow classes, may be reduced to a constant amplitude loading. The shear stress amplitude, $\tau_{12,a}$, and mean shear stress, $\tau_{12,m}$, of this constant amplitude loading is determined by the rainflow class with highest partial damage. From the obtained mean and amplitude shear stress the stress ratio can be determined. In case only one or at least very few rainflow classes are dominating in terms of damage, the load spectra can be expressed fairly well by this approximation. The more rainflow classes contribute significantly to the total damage, the more uncertain becomes the approximation by a constant amplitude loading.

Since the idea is to express the total load spectra and also the total damage by one rainflow class, which is repeated in the original spectra n_i times, an equivalent number of cycles has to be determined, such that the resulting damage of the rainflow class is equal to the total damage. That means that the number of cycles for the particular rainflow class has to be increased such that the damage of this class is equal to the total damage, which can be done by using equation (4.14).

$$n_{eq} = \frac{D_{\perp\parallel}}{D_{\perp\parallel,i}^{LC}} \cdot n_i \tag{4.14}$$

where $D_{\perp\parallel}$ is the total damage due to pure shear stressing obtained from the FEMFAT analysis, n_i is the number of cycles of the rainflow class with highest damage contribution and $D_{\perp\parallel,i}^{LC}$ is the damage per load cycle of this rainflow class, which is also a FEMFAT output and expressed in a rainflow matrix. The total damage in transverse longitudinal direction, $D_{\perp\parallel}$, can then be expressed by a constant amplitude loading with mean stress $\tau_{12,m}$ and amplitude stress $\tau_{12,a}$, which is repeated n_{eq} times.

The damage in transverse direction, $D_{\perp}$, needs to be expressed by a single rainflow class as well. In order to use the stress interaction diagram it needs to be assumed that the transverse damage, $\mathrm{D}_{\perp}$, due to pure transverse stressing is caused for the same number of cycles, n_{eq}. This leads to a number of cycles to failure in transverse direction, $\mathrm{N}_{\mathrm{f},\perp}$, as:

$$\mathrm{N}_{\mathrm{f},\perp} = \frac{\mathrm{n_{eq}}}{\mathrm{D}_{\perp}} \tag{4.15}$$

By using an appropriate S-N curve and knowing the numbers of cycles to failure, $\mathrm{N}_{\mathrm{f},\perp}$, the stress amplitude can be determined. The only information missing is the stress ratio, which is needed for choosing the correct S-N curve by accounting for mean stress effects as illustrated in chapter 2.2.3. Hahne recommends two possibilities. The first one is to take the same stress ratio for transverse stressing, as for shear stressing, i.e. $R^{\perp} = R^{\perp\parallel}$. The other possibility is to determine the rainflow class which causes the highest partial damage in transverse direction and pick the stress ratio of this class. In this Thesis the first option is used.

Having determined the transverse stress amplitude, $\sigma_{2,a}$, which causes the damage in transverse direction, $D_{\perp}$, when repeated n_{eq} times and knowing the shear stress amplitude, which causes the damage in shear direction, $D_{\perp\parallel}$, when repeated n_{eq} times, one can use the stress interaction diagram to plot the stress state. To determine the

resulting number of cycles to failure, N_f, the fracture curve has to be shrunk as long as it comes in contact with the stress state. This is done by determining the fracture mode and solving the corresponding equations (4.9) – (4.11) iteratively for N_f, or by using equation (4.12) in case of fracture mode B. The lowest number of cycles to failure gives the final result.

The steps to account for stress interaction according to the method of a posterior damage interaction are listed below:

1. Carry out a fatigue analysis on a component by using the single stress component method for pure transverse stressing, σ_2, and pure shear stressing, τ_{12}. This will give two critical nodes: one with highest damage for pure transverse loading and one for pure shear loading.

   The next steps have to be carried out when the node with highest shear damage, $D_{\perp\parallel}$, is analysed. When analysing the node with highest transverse damage, $D_{\perp}$, the procedure is carried out analogous.

2. Determine rainflow class which is largest contributor to the total shear damage, $D_{\perp\parallel}$. This will give $\tau_{12,a}$, $\tau_{12,m}$ and $R^{\perp\parallel}$.

3. Assume that the total damage is caused by this rainflow class and determine the equivalent number of cycles, n_{eq}, such that the damage due to this rainflow class is equal to the total damage (equation (4.14)).

4. Extract the corresponding transverse damage $D_{\perp}$ for the node with highest shear damage, $D_{\perp\parallel}$.

5. Based on the number of load cycles determined in step 3 and the damage in transverse direction, $D_{\perp}$, compute the number of cycles to failure $N_{f,\perp}$ (equation 4.15)).

6. Determine the stress amplitude, $\sigma_{2,a}$, which leads to the number of cycle to failure, $N_{f,\perp}$, obtained in step 5. Therefore, an S-N curve needs to be constructed. Take mean stress effects into account by using the constant life diagram and assume $R^{\perp\parallel} = R^{\perp}$.

7. Having obtained the representing stress amplitudes, $\sigma_{2,a}$ and $\tau_{12,a}$, determine number of cycles to failure by shrinkage of the fracture curve according to the appropriate S-N curves. N_f has to be determined iteratively.

8. The resulting damage is then computed as: $D = \frac{n_{eq}}{N_f}$

It is possible to analyse also different nodes, than the critical nodes. In order to do that, a detailed result groups needs to be defined in FEMFAT, which contains the node-ID of interest. FEMFAT provides then also the rainflow matrices for the specified node.

4.3 Method based on Hashin's criterion

One of the first fatigue failure criterions for composites, which distinguished between fibre failure and inter-fibre failure under plane stress condition, was proposed by Hashin and Rotem in 1973 [5]. They derived the fatigue failure criterion from a static failure criterion, which is stated in equation (4.16) – (4.19).

Fibre failure:

$$\sigma_1 = R_{\parallel}^{+} \qquad \text{for} \quad \sigma_1 \geq 0 \tag{4.16}$$

$$|\sigma_1| = R_{\parallel}^{-} \qquad \text{for} \quad \sigma_1 < 0 \tag{4.17}$$

Inter-fibre failure:

$$\left(\frac{\sigma_2}{R_{\perp}^{+}}\right)^2 + \left(\frac{\tau_{12}}{R_{\perp\parallel}}\right)^2 = 1 \qquad \text{for} \quad \sigma_2 \geq 0 \tag{4.18}$$

$$\left(\frac{\sigma_2}{R_{\perp}^{-}}\right)^2 + \left(\frac{\tau_{12}}{R_{\perp\parallel}}\right)^2 = 1 \qquad \text{for} \quad \sigma_2 < 0 \tag{4.19}$$

The criterion for fibre failure depends only on the longitudinal stress, σ_1, and the respective material strength, $R_{\parallel}$. In case of inter-fibre failure Hashin and Rotem proposed an elliptic equation, which depends on the transverse stress, σ_2, and on the transverse-longitudinal stress, τ_{12}. They assumed that in case of failure due to fatigue the same criterion can be used, but instead of using the static material strength a fatigue resistance needs to be applied, which depends on the number of cycles, n, and the stress ratio, R.

A method based on this fatigue failure criterion shall be used to account for stress interaction in case of inter-fibre failure. It is of simple form and written as:

$$\left(\frac{\sigma_2}{\sigma_{2,R}}\right)^2 + \left(\frac{\tau_{12}}{\tau_{12,R}}\right)^2 = CV < 1 \tag{4.20}$$

where $\sigma_{2,R}$ and $\tau_{12,R}$ are the material fatigue resistances in transverse and transverse-longitudinal direction, respectively. They can be obtained from S-N curves in the following way. If a specimen is subjected to n cycles the fatigue resistance is the stress which would lead to failure after n cycles. CV is the computed comparison value, which needs to be smaller than one to avoid failure.

The method shall be used for analyses where a component is subjected to complex loadings with variable amplitudes and mean stresses. Since the two previously presented methods for accounting of multi-axial stress states are rather complex or require a certain degree of manual work, emphasise of this methods lies on providing a simple method, which can be applied rather quickly. The idea is to express the complex loading as two constant amplitude loadings in transverse direction and shear direction similar to the APDI method. The constant amplitude loading in transverse direction causes the total damage in transverse direction, D_2, and the constant amplitude loading in shear direction causes the total damage in shear direction, D_{12}. The two cyclic loadings have a certain number of repetitions, which do not

necessarily have to be identical. These numbers of cycles are required to determine the fatigue resistances, which can be derived from suitable S-N curves. In order to do this the stress ratio of the constant amplitude loading needs to be known and the constant life diagram is used to account for mean stress effects.

Implementation into the simulation process

When analysing the influence of stress interaction with the use of the approach based on Hashin's criterion, the fatigue analysis according to the single stress component method has to be carried out before. As described in the previous subsections, this will lead to two critical nodes, one node with highest damage when subjected to pure shear stressing and one node with highest damage when subjected to pure transverse stress. Similar to the a posteriori damage interaction method it is made use of the rainflow matrices, which are a FEMFAT output for the critical node. Due to the fact that both the rainflow matrices for pure transverse stressing and pure shear stressing for the node of interest are required, the fatigue analysis has to be run twice: The first time to determine the critical node e.g. due to transverse stressing and the second time to determine the respective damage for pure shear stressing at this node. The second analysis can be carried out only for the node of interest by defining a detailed result group in FEMFAT. This reduces the computational time significantly.

The first step is to determine the damage equivalent constant amplitude loadings. It shall be defined that the rainflow class, which contributes mostly to the damage defines the stress amplitude and the mean stress of the constant amplitude loading. FEMFAT outputs the damage contribution of all rainflow classes and therefore, this quantity is easy to obtain. Since it is seldom that one rainflow class deals 100% of the total damage, its number of cycles needs to be increased such that the damage of the rainflow class is equal to the total damage, which can be done according to equation (4.21):

$$n_{eq} = \mathrm{n_i} \cdot SF \cdot \frac{D_{total}}{D_i} \tag{4.21}$$

where D_{total} is the total damage, D_i is the partial damage due to the rainflow class, n_i is the number of cycles of the particular rainflow class and SF is the scaling factor of the driving manoeuvre. It is basically a factor which scales the number of repetitions and is going to be explained in more detail in the next chapter.

The rainflow class is defined by the mean stress and the stress amplitude, which allows the computation of the stress ratio R. Knowing the stress ratio enables the determination of the S-N curve from the constant life diagram. Hence, the S-N curve can be used to establish the fatigue resistance for n_{eq} cycle. In a last step equation (4.20) is used to compute the comparison value and evaluate whether failure occurs or not.

The necessary steps are summarized in the following:

1. Carry out a fatigue analysis on a component by using the single stress component method for pure transverse stress, σ_2, and pure shear stress, τ_{12}.

This will give two critical nodes: one with highest damage for pure transverse loading and one for pure shear loading.

2. In case of analysing the critical node due to pure transverse stressing. Rerun fatigue analysis for the critical node when subjected to pure shear stressing to obtain the required rainflow matrices for shear loading and vice versa.

3. From the rainflow classes obtained as a FEMFAT output pick rainflow class with highest damage due to pure shear stressing and due to pure shear stressing.

4. Determine the stress ratios, *R*, of the two rainflow classes.

5. Determine the equivalent number of cycles for the two rainflow classes according to equation (4.21).

6. Use the stress ratio and the constant life diagram to compute the slopes of the two S-N curve for the two stressings.

7. Determine the fatigue resistance, $\sigma_{2,R}$ and $\tau_{12,R}$, for the number of cycles determined in step 5.

8. Use equation (4.20) to compute the comparison value, CV, and evaluate failure.

One advantage by using this method is that this method is an easy-to-use method. Not more material data is needed than the data used for the fatigue analysis. The manual work load which is required for the post processing of the results of the fatigue analysis is rather small compared to the work load of the previously presented methods.

Three methods to account for stress interaction in fatigue simulation for composite were described in this chapter. They are applied to the fatigue analysis of a complete vehicle in the following chapter.

5 Application to complete vehicle simulation

In this chapter fatigue analyses are carried out on the CFRP cross member of the trimmed body model, which was already introduced in chapter 3. In the first section of this chapter the results of the fatigue analysis according to the single stress component method are presented. Based on these results, the three multi-axial fatigue models for composite material, which were described in chapter 4, are applied. The results are compared and discussed at the end of this chapter.

5.1 Single stress component method

When carrying out a fatigue analysis of composite component by using the single stress component method, each layer of the composite and each stress component have to be analysed separately. The material of the cross member was defined as an 8-ply composite, which means it has to be analysed 24 times (8 layers, 3 stress components) instead of just one analysis for the original case when the material was metal. Furthermore, the trimmed body is subjected to five different driving manoeuvres, which are represented by different load over time signals. That means that the number of analyses is increased to 120, (5x24). The results, i.e. the damage of each driving manoeuvre, are multiplied with a scaling factor. It weights the manoeuvres with respect to their occurrence during the service life of the car, such that the total service life is represented by the driving manoeuvres. Table 5.1 shows the scaling factors for the different driving manoeuvres. The driving manoeuvre braking represents a strong braking on asphalt. R4u7 is referred to round four and round seven on the testing track EVP (cf. section 3.1.2). The testing track was divided into four parts (Pt), where part 1 and part 2 do not contain high lateral accelerations.

Table 5.1: Driving Manoeuvres and their respective scaling factor, SF

Braking	R4u7	R1u2	R4u7-Pt1	R4u7-Pt2
33271	3096	3096	1459	4380

The total damage, D_{total}, caused by the different driving manoeuvres is obtained according to equation (5.1). The sum of the partial damages, D_i, of the driving manoeuvres, which are multiplied by the scaling factors, SF, gives the total damage.

$$\mathrm{D_{total}} = \sum \mathrm{D_i} \cdot \mathrm{SF_i} \tag{5.1}$$

At first the FEA has to be carried out to obtain the stress distribution over the cross member for each load case. Therefore the complete trimmed body needs to be considered in the stress analysis. When it comes to the fatigue analysis of the cross member it is sufficient to analyse only the cross member and not the whole trimmed body model. The fatigue analysis does only depend on the stress state in each finite element and it does not take any boundary conditions of the FEA into account.

Figure 5.1 shows the total damage plotted over the cross member for layer 101 when subjected to pure transverse stressing, i.e. the sum of the partial damages for the

different driving manoeuvres multiplied with the respective scaling factors. The maximum damage is located in the area surrounded by the red circle and it is of magnitude $D_{total} = 8.3 \cdot 10^{-2}$. A damage less than one implies that no failure occurs, but it needs to be mentioned, that the thickness of the cross member was increased and the material was simply replaced by a composite with quasi-isotropic layup in order to demonstrate the simulation process. It is therefore not a real case and the results can only be used for comparison and critical areas can be highlighted.

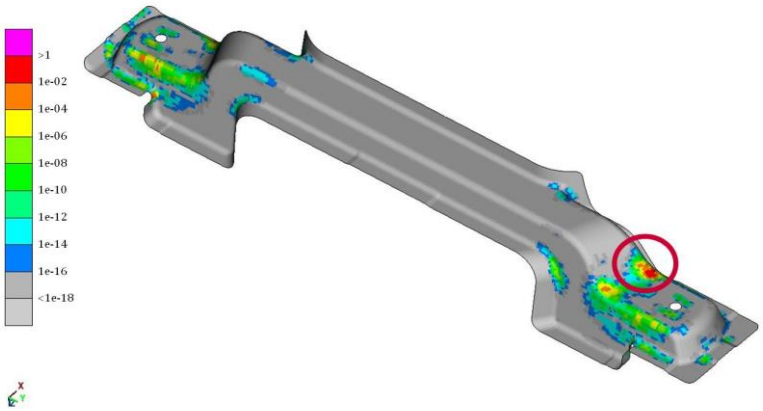

Figure 5.1: Total damage due to transverse stressing plotted for layer 101 as a superposition of five partial damage plots due to driving manoeuvres scaled with corresponding scaling factors.

The highest damage under transverse stressing occurs in layer 108, which is shown in Figure 5.2. The maximum damage is $D_{\perp,total} = 2355$, but it has to be mentioned that it occurs in a region, where the cross member is connected to other components via rigid body elements (RBEs), as shown in Figure 5.3. At that specific node the movement is constrained such that it cannot move independently, which might result into numerical singularities. An evaluation of fatigue results at these nodes is not recommended.

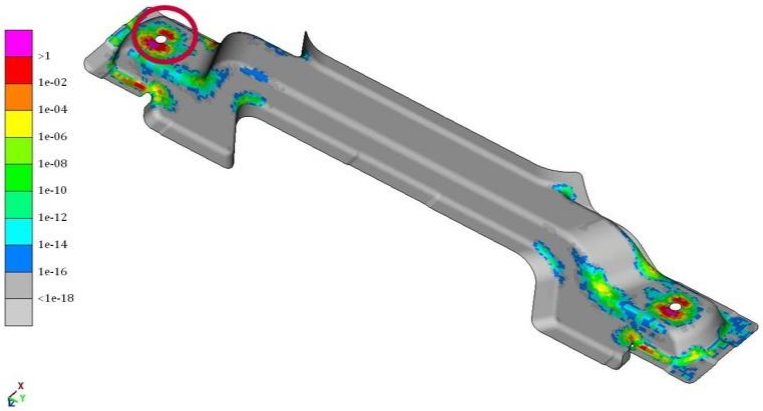

Figure 5.2: Total damage due to transverse stressing plotted for layer 108 as a superposition of five partial damage plots due to driving manoeuvres scaled with corresponding scaling factors.

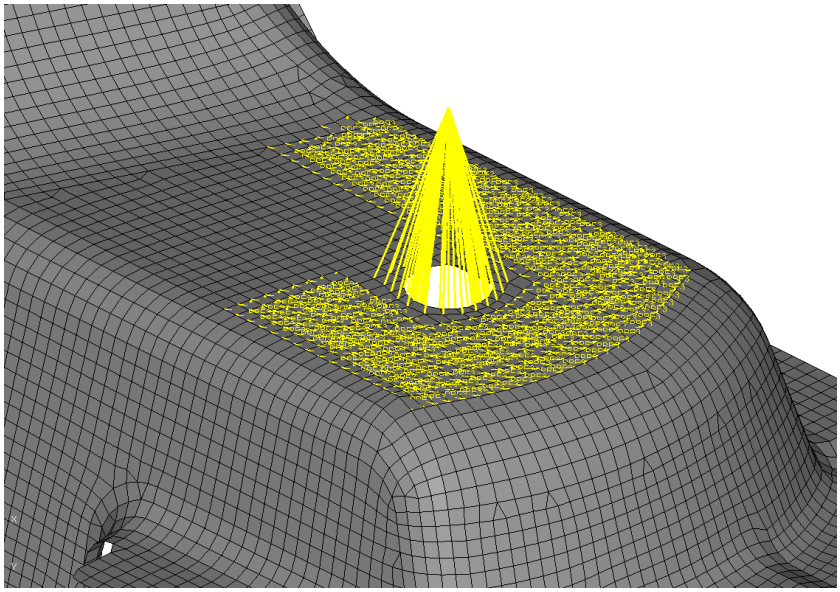

Figure 5.3: Connection to the car body represented by RBEs [3]

Figure 5.4 shows the damage distribution due to shear stressing. In case of pure shear stressing the maximum total damage in layer 101 is $D_{\perp\parallel,total} = 1.1 \cdot 10^{-3}$. The red circle in Figure 5.4 indicates the area where the highest damage occurs. As for the damage plots due to transverse stressing the area in the middle of the cross member does not suffer any significant fatigue damage at all and the damage is mostly located along the blunted edges of the cross member.

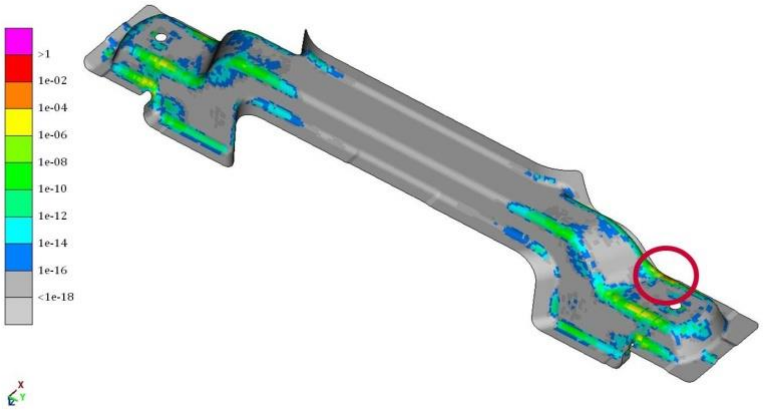

Figure 5.4: Total damage due to shear stressing plotted for layer 101 as a superposition of five partial damage plots due to driving manoeuvres scaled with corresponding scaling factors.

Scope of this Thesis is to apply different methods to account for stress interaction, which is mainly relevant for transverse and shear stressing, but plays a minor role for stressing in longitudinal fibre direction. Nevertheless, for the sake of completeness the damage plot due to pure longitudinal stressing in layer 101 is shown in Figure 5.5. Since the material strength in fibre direction is very high, the damage is rather low and the maximum total damage in layer 101 is only $D_{\parallel,total} = 1.5 \cdot 10^{-7}$.

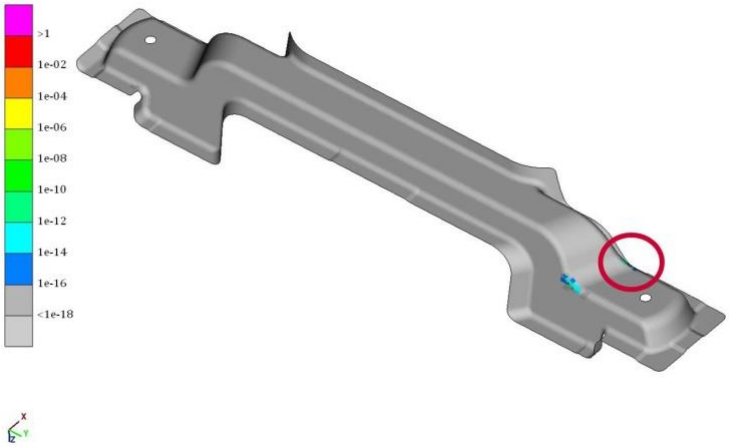

Figure 5.5: Total damage due to longitudinal stressing plotted for layer 101 as a linear superposition of five partial damage plots due to driving manoeuvres scaled with corresponding scaling factors.

The damage plots of all layers for the different types of stressing are shown in Appendix A1, A2 and A3, respectively.

The maximum total damage in each layer and the corresponding nodal identification number for the case of pure shear stressing and pure transverse stressing, respectively, are listed in Table 5.2. Nodes, of which the local stress is influenced by the

connection as shown in Figure 5.3, are not taken into account. The highest total damage, which is the maximum of the total damages over all layers, is highlighted in red and the corresponding node-ID is highlighted in green. For both pure shear and transverse stressing the maximum damage occurs in layer 101, but at different nodes: Namely, node 1917998 for pure shear stressing and node 1915966 for transverse stressing.

Table 5.2: Maximum total damage due to pure shear and pure transverse stressing in each Layer. The maximum damage over all layers is highlighted red and the corresponding node-ID is highlighted green

	Pure shear stressing			Pure transverse stressing	
Layer ID	Node- ID	Damage $D_{\perp\parallel}$		Node-ID	Damage $D_{\perp}$
101	1917998	1,13E-03		1915966	8,30E-02
102	1917249	4,71E-05		940754	1,82E-03
103	1918238	6,20E-07		941740	3,20E-02
104	1918277	4,00E-07		941010	2,30E-04
105	1918276	4,40E-07		941978	1,23E-05
106	1918276	1,35E-07		940732	1,51E-02
107	1918311	5,63E-07		940723	3,36E-02
108	1918311	4,06E-05		940677	5,32E-02

The total damage of these two critical nodes are examined in more detail in the following. Table 5.3 shows the damage due to pure transverse stressing for the critical node (node-ID: 1915966) and layer 101 for each driving manoeuvre. The product of the partial damage for each driving manoeuvre and the respective scaling factor adds up to the total damage of $D_{\perp,total} = 8.3 \cdot 10^{-2}$. It is noticeable that the damage of the driving manoeuvre R4u7-Pt2 is significantly higher than the other manoeuvres. The difference in percent between the total damage, $D_{\perp,total}$, and the partial damage due to manoeuvre R4u7-Pt2, $D_{\perp,R4u7-Pt2}$, is only 0.006%, which means that nearly all damage is caused by the driving manoeuvre R4u7-Pt2.

Table 5.3: Damage, $D_{\perp}$, for critical node due to pure transverse stressing for different driving manoeuvres. Node-ID: 1915966; Layer-ID: 101

	Damage $D_{\perp}$ for different driving manoeuvre						
Manoeuvre	Braking	R4u7	R1u2	R4u7-Pt1	R4u7-Pt2		Sum damage
Scaling factor (SF)	33271	3096	3096	1459	4380		
Partial damage	5,79E-22	1,58E-09	1,02E-12	5,15E-13	1,90E-05	=	1,90E-05
Damage · SF	1,93E-17	4,89E-06	3,17E-09	7,51E-10	8,30E-02	=	**8,30E-02**

The same can be observed when comparing the damage of the driving manoeuvres for the case that the cross member is subjected to pure shear stressing, as shown in Table 5.4. The total damage, $D_{\perp\parallel,total}$, is dominated by the driving manoeuvre R4u7-Pt2. The relative difference between the total damage and the damage due to manoeuvre R4u7-Pt2 is 0.38%.

Table 5.4: Damage, $D_{\perp\parallel}$, for critical node due to pure shear stressing for different driving manoeuvres. Node-ID: 1917998; Layer ID: 101

	Damage $D_{\perp\parallel}$ for different driving manoeuvre						
Manoeuvre	Braking	R4u7	R1u2	R4u7_Pt1	R4u7_Pt2		Sum damage
Scaling factor (SF)	33271	3096	3096	1459	4380		
Partial damage	2,38E-15	5,16E-10	1,90E-11	1,79E-09	2,57E-07	=	2,60E-07
Damage · SF	7,90E-11	1,60E-06	5,89E-08	2,61E-06	1,13E-03	=	**1,13E-03**

Nearly all damage is caused by the driving manoeuvre R4u7-Pt2. The other driving manoeuvres do not contribute significantly to the total damage. Therefore, only manoeuvre R4u7-Pt2 is taken into account and the other manoeuvres are neglected in the following. The stress interaction methods described in chapter 4 are applied to the two critical nodes for pure transverse and pure shear stressing in the next sections.

5.2 Stress interaction according to Puck's theory

When applying the method of stress interaction according to Puck's theory the stress data at the node of interest has to be read for each load case and scaled by the corresponding load over time signal. The resulting stress states over time are summed up at each time step, which leads to the effective stress state as a result of the driving manoeuvre. Only the driving manoeuvre R4u7-Pt2 is considered, since it causes nearly all damage. The whole driving manoeuvre last almost 100 seconds and the forces are gathered with a frequency of 313Hz, which leads to a total number of 30849 time steps. Figure 5.6 shows the stress states varying over time in a σ_2, τ_{12}-diagram for the node 1917998.

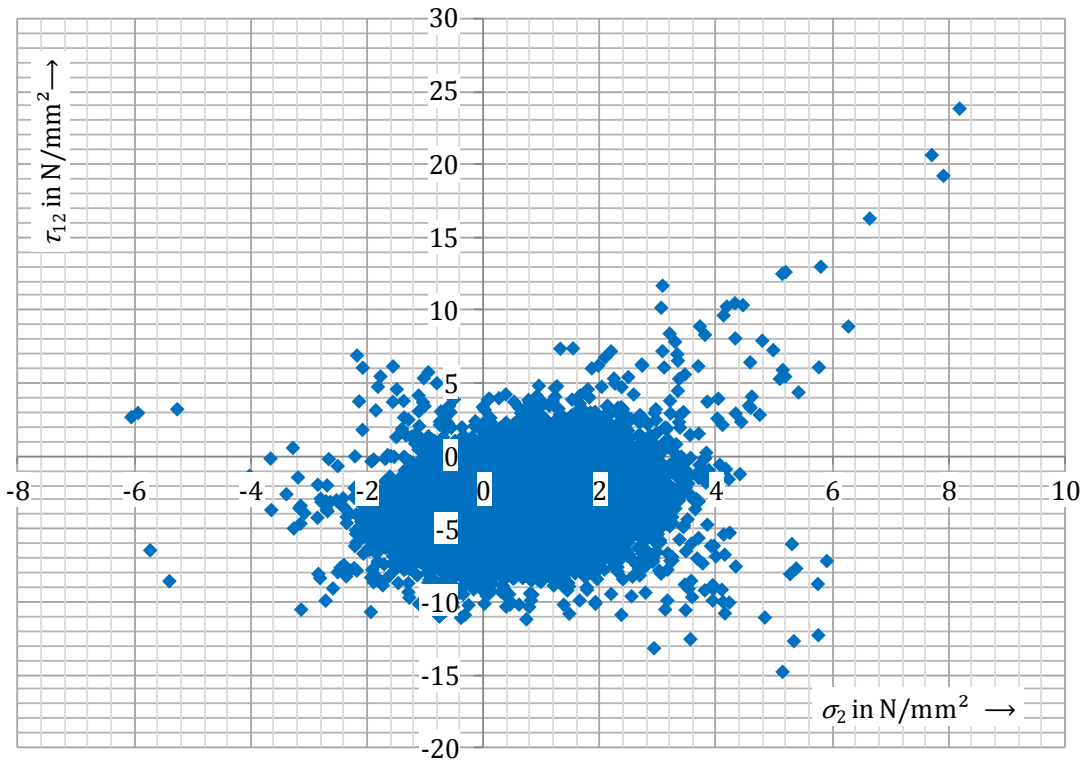

Figure 5.6: Stress states plotted in the stress interaction diagram at each time step for node 1917998 (node with highest damage due to pure shear stressing) when subjected to the driving manoeuvre R4u7-Pt2

The maximum shear stress is approximately $\tau_{12,max} \approx 24N/mm^2$. At this point in time the node is also subjected to the largest transverse stress, which is $\sigma_{2,max} \approx 8N/mm^2$. The Figure gives the possibility to estimate the degree of multi-axiality and whether the stressing is dominated by shear or transverse stressing. In this case the shear stress is dominating, but the material strength, which differs for the shear and transverse direction, has to be kept in mind. Therefore, it is sometimes useful to normalize the axes by its respective material strengths. The material strength in transverse tensional direction is $R_{\perp}^{+} = 39N/mm^2$, whereas the material strength in transverse longitudinal direction is $R_{\perp\parallel} = 90N/mm^2$. That means that the maximum transverse stress is approximately 20% of the material strength, $R_{\perp}^{+}$, and the maximum shear stress 27% of $R_{\perp\parallel}$. Based on this stress plot the fracture mode and the stress exertion according to Puck's criterion for static failure can be determined for each stress state. Most of the stress states lie in the region of fracture mode *A*, namely 26080. Fracture mode *B* appears in 4578 of the cases and fracture mode *C* is only 191 times present. This information is then used to compute an equivalent stress.

Three possibilities of computing an equivalent stress were proposed by Hahne [2]. It was suggested to use the equivalent shear stress method, when the loading is dominated by shear stresses. Figure 5.7 compares the equivalent shear stress, $\tau_{12,eq}$, with the single shear stress component, τ_{12}. The difference between the two curves is due to the transverse stress, σ_2, which is taken into account in the equivalent stress, $\tau_{12,eq}$. The maximum of the equivalent stress is $\tau_{12,eq} \approx 32N/mm^2$, whereas the maximum of the shear stress is $\tau_{12} \approx 24MPa$. This increase in stress leads to a shortened fatigue life, or in other words to a higher damage.

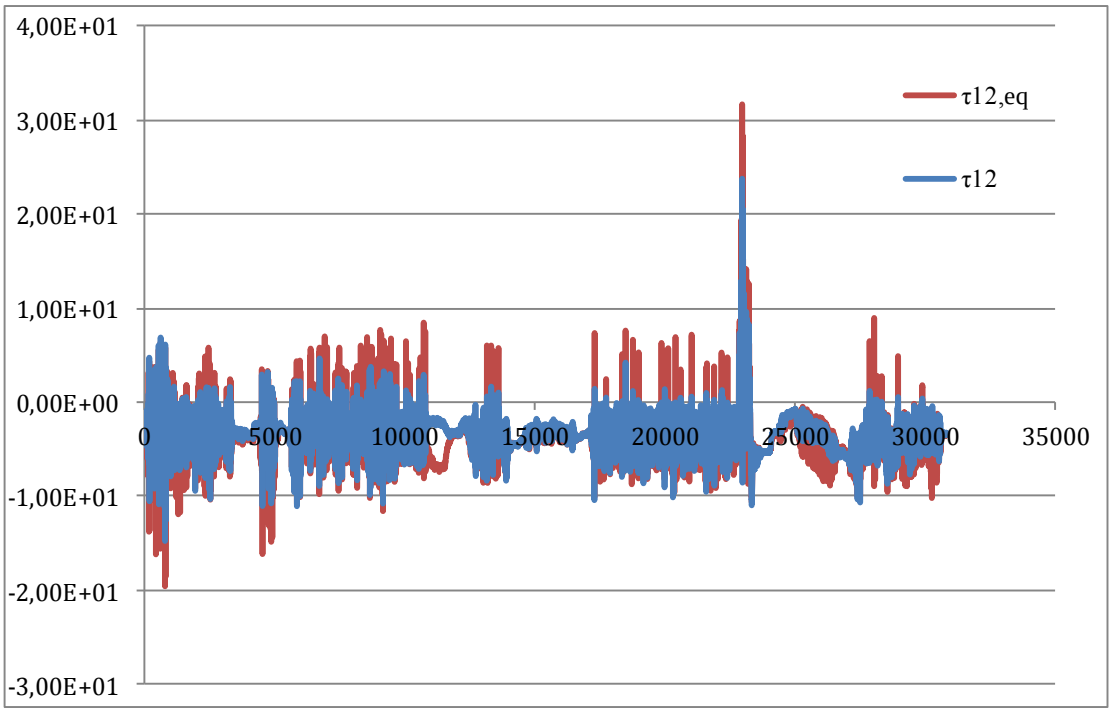

Figure 5.7: Comparison of the shear stress over time signal, τ_{12} (blue), and the equivalent shear stress over time signal, $\tau_{12,eq}$ (red,) for node 1917998

A comparison between the equivalent shear stress, $\tau_{12,eq}$, and the equivalent transverse stress, $\sigma_{2,eq}$, is not meaningful, since they are evaluated for different material properties. When the equivalent transverse stress over time signal is used for the fatigue assessment the material in transverse direction is used and vice versa.

The different stress over time signals, equivalent stresses as well as single stress components, are applied to a single finite element model, as described in section 4.1. The resulting damages are given in Table 5.5, where the scaling factor for the driving manoeuvre is already considered.

Table 5.5: Comparison of total damage due to driving manoeuvre R4u7-Pt2 for node 1917998 according to the method of single stress component and to the method of equivalent stress according to Puck's theory

Single stress component method		Equivalent stress according to Puck's theory		
τ_{12}	σ_2	$\tau_{12,eq}$	$\sigma_{2,eq}$	$\sigma^*_{2,eq}$
$1.02 \cdot 10^{-3}$	$1.65 \cdot 10^{-5}$	$1.96 \cdot 10^{-2}$	$7.95 \cdot 10^{-3}$	$2.39 \cdot 10^{-3}$

According to the single stress component method the damage due to pure shear stressing is $D_{\perp\parallel} = 1.02 \cdot 10^{-3}$ and for pure transverse stressing $D_{\perp} = 1.65 \cdot 10^{-5}$. The damage in transverse stressing is lower since the loading was dominated by shear stressing as shown in Figure 5.6. If fatigue assessment is carried out by using an equivalent stress the resulting damage is higher than the damages computed according to the single stress component method. The highest damage is computed for the case of equivalent shear stress, $\tau_{12,eq}$. The damage, $D_{\perp\parallel,eq}$, is nearly 20 times higher than

the damage due to pure shear stressing, $D_{\perp\parallel}$. An equivalent transverse stress gives slightly less damage. The factor between damage due to $\tau_{12,eq}$ and damage due to $\sigma_{2,eq}$ is around 2.5, which is rather small in fatigue analysis. When using the alternative transverse stress the resulting damage, $D^*_{\perp,eq}$, is only twice as high as the damage due to pure shear stressing, $D_{\perp\parallel}$.

The damage due to pure shear stressing, when applied to a single finite element, is slightly lower than the damage determined by FEFMAT, when the whole cross member is analysed $D_{\perp\parallel} = 1.02 \cdot 10^{-3}$ versus $D_{\perp\parallel} = 1.13 \cdot 10^{-3}$. The difference is approximately 10%, but actually they should be the same, since they are both based on the same stress signal, i.e. the pure shear component, τ_{12}. To investigate the reason for this behaviour a comparison of the FEFMAT internal equivalent stress is conducted. Figure 5.8 shows the FEMFAT internal equivalent stress for the critical node 1917998, when subjected to pure shear stressing in the analysis of the cross member. In Figure 5.9 the FEFMAT internal equivalent stress for the single finite element subjected under pure shear stress is displayed. No difference between the two equivalent stresses is visible at a first glance, but when comparing the maximum values of both equivalent stress histories a small difference can be observed. The maximum of the FEFMAT internal equivalent stress in the analysis of the cross member is $\sigma_{eq} = 23.86 N/mm^2$, whereas the maximum value for the analysis of the single finite element is $\sigma_{eq} = 23.80 N/mm^2$. The difference is small but leads to different result in the fatigue analysis.

One reason for this behaviour may be explained by the change of the geometry. FEMFAT averages the element stress at the nodes and transforms the stress data into the global coordinate system. In the stress tensor of the element coordinate system only one element of the stress tensor was unequal zero, the transverse stress component σ_2. The stress transformation into the global coordinate system leads to the fact, that depending on the transformation, all elements are non-zero. Until now the difference in damage is rather low and this phenomenon is neglected, but further research should be carried out to find the reason for this behaviour.

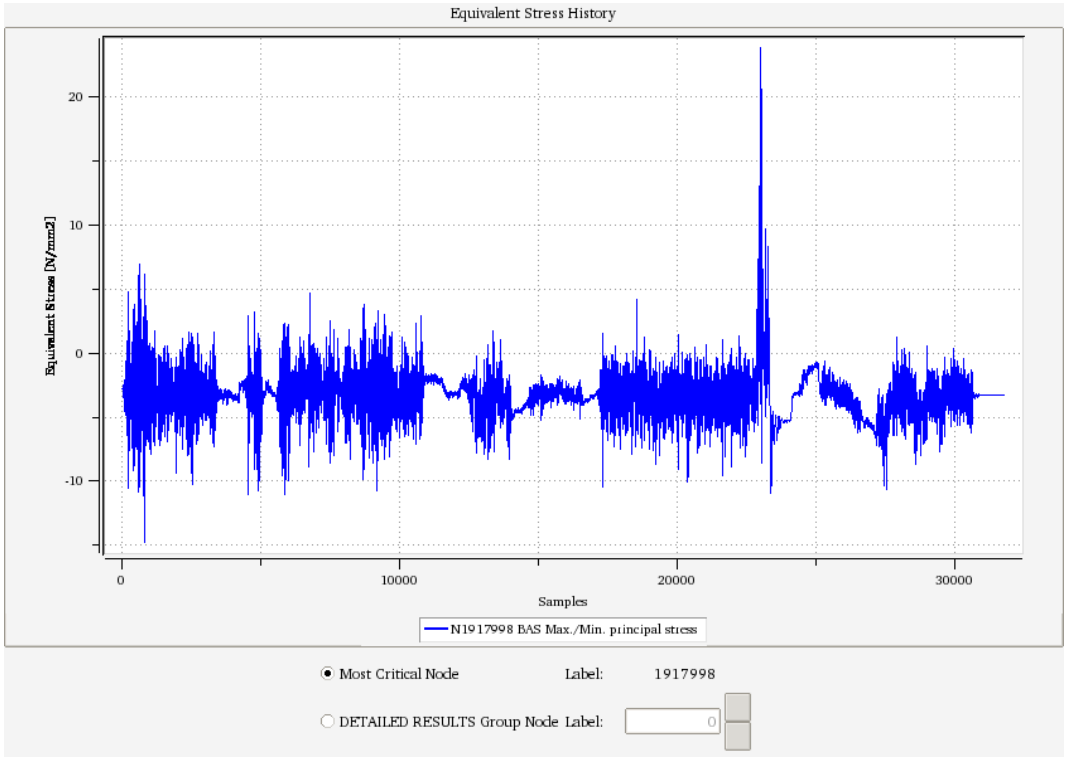

Figure 5.8: FEMFAT internal equivalent stress for the analysis of the cross member according to the single stress component method for pure shear stressing.

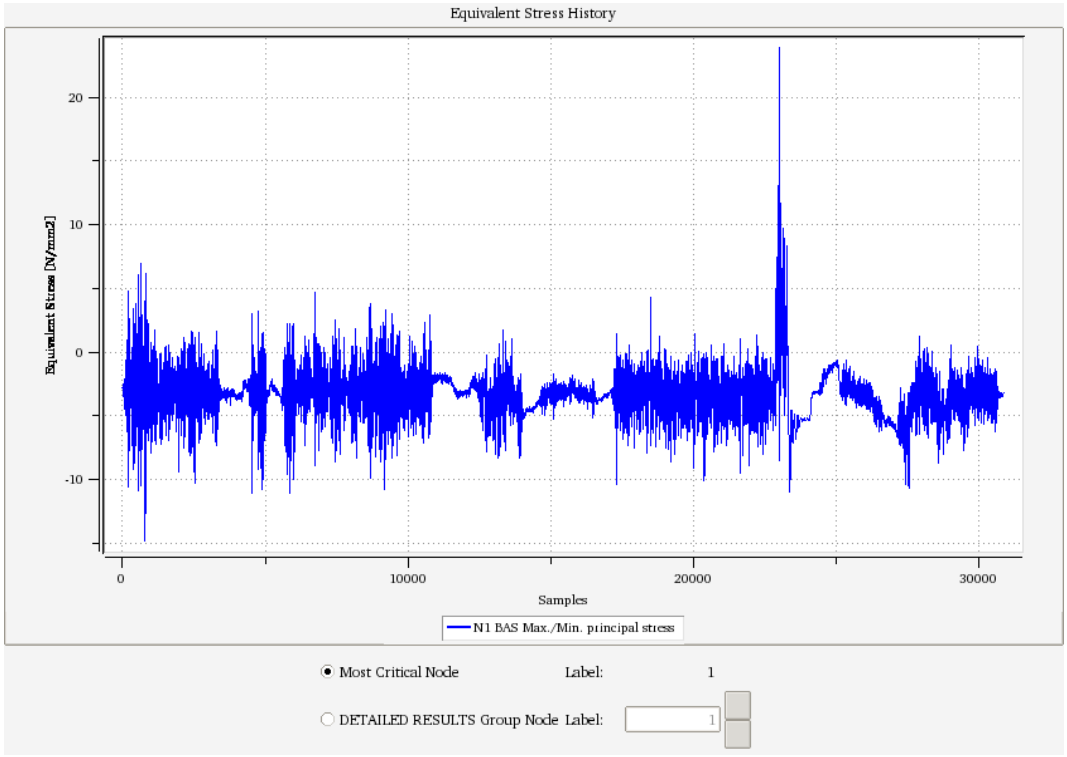

Figure 5.9: FEMFAT internal equivalent stress for the analysis of the single finite element according to the single stress component method for pure shear stressing

The same procedure can be carried out for node 1915966, the node with highest damage when subjected to pure transverse stressing. As for the node with highest shear damage, $D_{\perp\parallel,total}$, the varying stress states over time are plotted in a σ_2, τ_{12}-diagram in Figure 5.10 to get an idea of the loading. The transverse stress is dominating for this case, which is not surprising since the node with highest damage in transverse direction is analysed. The maximum transverse stress in tension is $\sigma_{2,max}^{+} \approx 19N/mm^2$ and $\sigma_{2,max}^{-} \approx -8N/mm^2$ in compression. The shear stress is bounded by the values $\tau_{12} \approx 5N/mm^2$ and $\tau_{12} \approx -8N/mm^2$. Again fracture mode *A* occurs most often, 20951 times, followed by fracture mode *B* (6145 times) and mode *C* (3753 times).

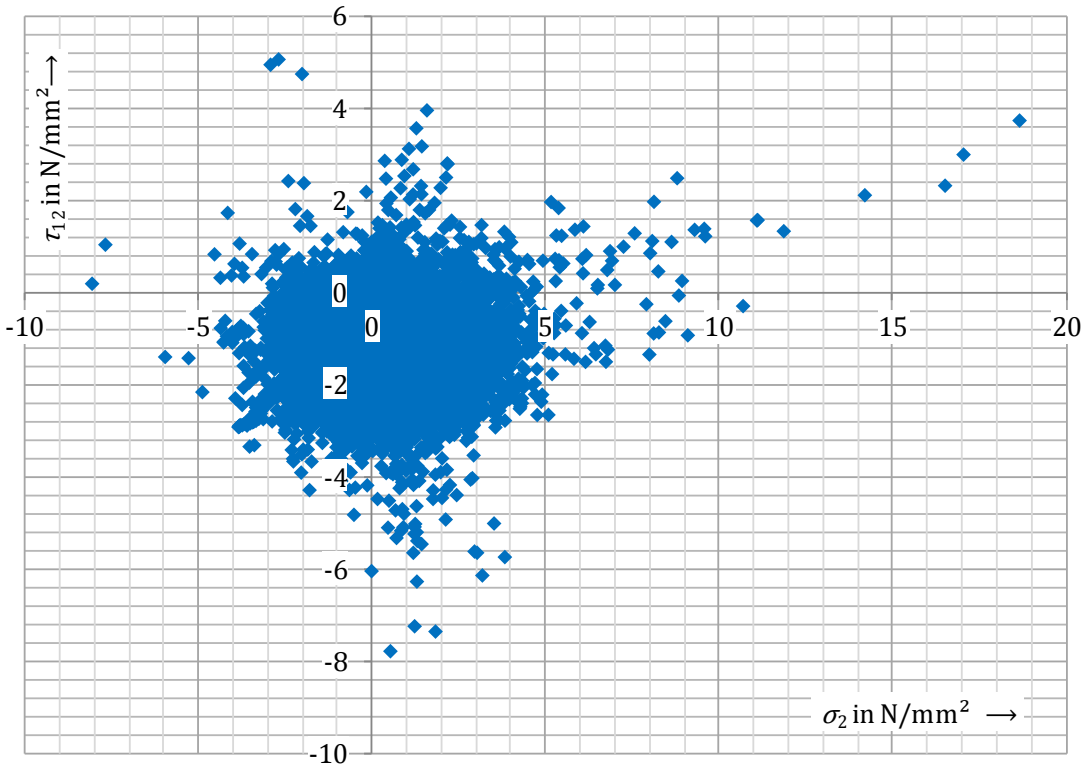

Figure 5.10: Stress states plotted in the stress interaction diagram at each time step for node 1915966 (node with highest damage due to pure transverse stressing) when subjected to the driving manoeuvre R4u7-Pt2

When comparing the transverse stress, σ_2, with the equivalent transverse stress, $\sigma_{2,eq}$, as shown in Figure 5.9, it can be seen that the differences between the two stress histories are minor in tension and only noticeable in compression. The influence of shear stress on the maximum transverse stress peak is very low. The maximum transverse stress is $\sigma_{2,eq,max} = 18.65N/mm^2$, whereas the maximum equivalent transverse stress is $\sigma_{2,eq,max} = 18.74N/mm^2$. The fatigue life in transverse direction is more sensitive to tensional stress than to compressive stress. Since the difference between the two stress histories is rather small in tension, it can be expected, that the damage due to the two different histories is also rather small.

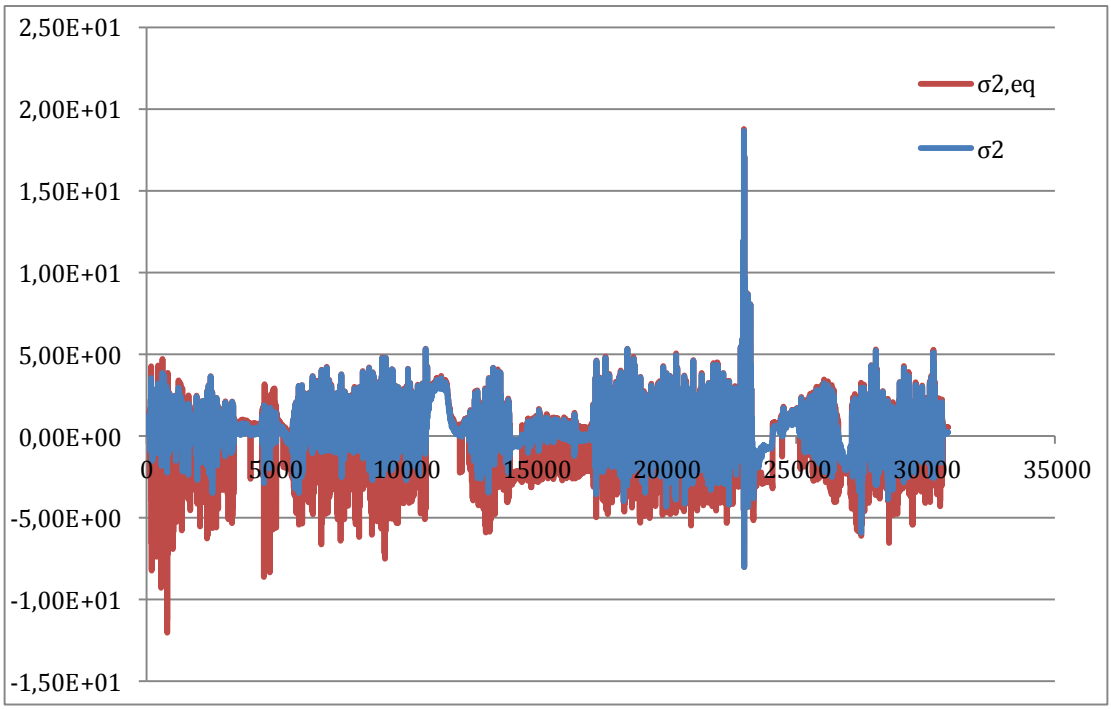

Figure 5.11: Comparison of the shear stress over time signal, σ_{12} (blue), and the equivalent shear stress over time signal, $\sigma_{12,eq}$ (red,) for node 1915966

Table 5.6 compares the total damage for the single stress component method and the damage due to an equivalent stress, when the scaling factors are taken into account. As expected, the damage due to equivalent transverse stress, $D_{\perp,eq} = 1.28 \cdot 10^{-1}$, is only slightly higher than the damage due to pure transverse stressing, $D_{\perp} = 9.04 \cdot 10^{-2}$. The difference between the transverse damage, $D_{\perp}$, and the damage due to the alternative equivalent stress, $D^{*}_{\perp,eq}$ is even less. The alternative equivalent stress is generated equally to the single stress component for compressive stresses. The only difference is in tension, where the alternative equivalent stress is computed by an equivalent stress exertion, instead of using the transverse stress component (cf. chapter 4.1). The highest damage is computed when the equivalent shear stress component, $\tau_{12,eq}$, is used, which is $D_{\perp\parallel,eq} = 6.61 \cdot 10^{-1}$ and thus approximately five times higher than the damage due to the equivalent transverse stress, $D_{\perp,eq}$.

Table 5.6: Comparison of total damage due to driving manoeuvre R4u7-Pt2 for node 1915966 according to the method of single stress component and to the method of equivalent stress according to Puck's theory

Single stress component method		Equivalent stress according to Puck's theory		
τ_{12}	σ_2	$\tau_{12,eq}$	$\sigma_{2,eq}$	$\sigma^{*}_{2,eq}$
$2.42 \cdot 10^{-11}$	$9.04 \cdot 10^{-2}$	$6.61 \cdot 10^{-1}$	$1.28 \cdot 10^{-1}$	$9.50 \cdot 10^{-2}$

Again there is a difference in damage when carrying out the fatigue analysis for the single stress component method on a single finite element model and on the cross member. The damage due to pure transverse stressing when analysing the whole cross member is $D_{\perp} = 8.30 \cdot 10^{-2}$ (see Table 5.3). If the transverse stress is applied to the single element model, the damage is slightly increased to $D_{\perp} = 9.04 \cdot 10^{-2}$, which is less than 10%.

5.3 An a posteriori damage interaction method

According to the a posteriori damage interaction method as described in chapter 4.2 a complex load spectrum is reduced to a damage equivalent constant amplitude loading in transverse and shear direction. Again the two critical nodes for pure shear stressing (node ID: 1917998) and pure transverse stressing (node ID: 1915966) are analysed. At first the critical node due to pure shear stressing is analysed. The rainflow matrices for the loading spectra in terms of number of cycles are displayed in Figure 5.12, which are resulting from the fatigue analysis of the cross member by using the single stress component method. The left rainflow matrix depicts the number of closed load cycles, whereas the right rainflow matrix shows the number of residua. The colour of the bars illustrates the contribution to the total damage, where red means high damage contribution and blue low contribution.

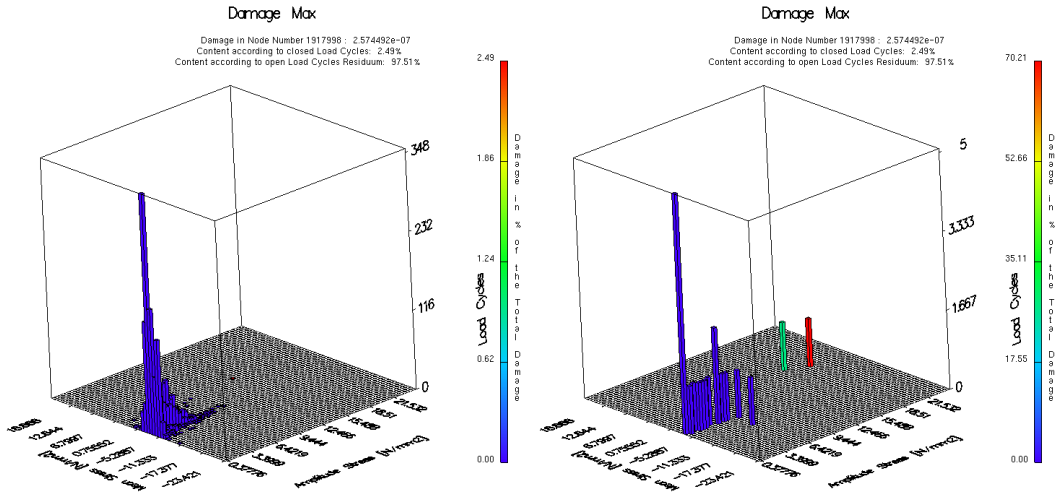

Figure 5.12: Rainflow matrices for node 1917998 of the analysis of the cross member according to the single stress component method (pure shear stressing). Left: closed load cycles. Right: residua

The header of the rainflow matrix gives information how much damage is caused by closed load cycles and how much damage is caused by residua. In this case 97.5% of the total damage is caused by residua and only 2.5% is caused by closed load cycles. Hahne [2] suggested that the class with highest damage determines the mean and amplitude stress of the equivalent constant amplitude loading. In this case the rainflow class with highest damage is a residuum and has an amplitude stress of $\tau_a = 19.6 N/mm^2$ and a mean stress of $\tau_m = 4.5 N/mm^2$, which leads to a shear

stress ratio of $R^{\perp\parallel} = -0.625$. This rainflow class causes 70.2% of the total damage and is repeated one time, but since it is a residuum and the FEFMAT analysis was run with a residuum factor of 0.5 the actual number of cycles is $n = 0.5$. The next step is to determine the equivalent number of cycles, n_{eq}, such that this rainflow class causes 100% of the total damage. This can be obtained by using equation (4.23) or by simple calculation of percentage. In this case the equivalent number of cycles is $\mathrm{n}_{eq} = 0.71$. Based on this number of cycles an equivalent transverse loading with stress amplitude $\sigma_{eq,a}$, and mean stress $\sigma_{eq,m}$, needs to be determined, which causes the complete transverse damage, $D_{\perp}$. In this case the damage due to pure transverse stressing is $D_{\perp} = 3.69 \cdot 10^{-10}$. Knowing the damage and the equivalent number of cycles, n_{eq}, the number of cycles to failure can be computed as $N_f = \frac{\mathrm{n}_{eq}}{D_{\perp}} = 1.9 \cdot 10^{9}$. The stress ratio of the constant amplitude loading in transverse direction should be per definition equal to the stress ratio of the constant amplitude loading in shear direction, i.e. $R^{\perp\parallel} = R^{\perp}$. By using the constant life diagram for transverse direction and the S-N curve, the stress amplitude can be computed. The resulting stress amplitude is $\sigma_{eq,a} = 7.5 N/mm^2$, which leads to a mean stress of $\sigma_{eq,m} = 1.7 N/mm^2$. The equivalent transverse stress, σ_{eq}, and the equivalent shear stress, τ_{eq}, can be plotted in a σ, τ −diagram as shown in Figure 5.13. It is assumed that the transverse stress and the shear stress amplitude are acting in-phase.

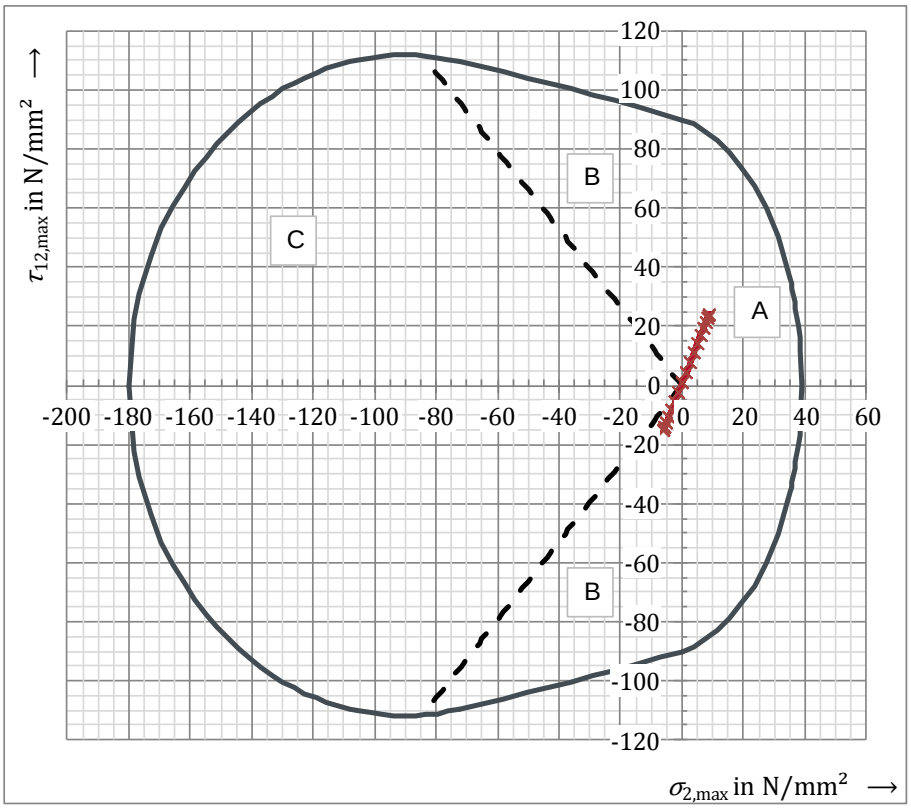

Figure 5.13: Equivalent constant stress amplitude signal (red) plotted in the interaction diagram for static inter-fibre failure for node 1917998. The black dashed line indicates the border from failure mode B to mode C.

When shrinking the failure curve, the cross member would fail in failure mode *A* and therefore, the equation for fracture mode *A* (cf. equation (4.9)) needs to be solved for the number of cycles to failure as described in chapter 4.2. It has to be kept in mind that the equation uses the stress maxima $\sigma_{2.max}$ and $\tau_{12.max}$, i.e. the sum of amplitude and mean stress. This results into $N_f = 1.18 \cdot 10^5$, which leads to a damage of $D = \frac{n_{eq}}{N_f} = 6.04 \cdot 10^{-6}$ and when multiplied with the scaling factor for driving manoeuvre R4u7-Pt2 the resulting damage is $D = 2.65 \cdot 10^{-2}$.

The same procedure can be carried out for the critical node due to pure transverse stressing. The rainflow matrices in Figure 5.14 show the number of load cases of each rainflow class and also their partial damage in per cent of the total damage. Nearly all damage is caused by residua, namely 99.5% and only 0.5% of the total damage is due to closed load cycles. The rainflow class with highest partial damage contributes with 45.8%. Its stress amplitude is $\sigma_{eq,a} = 13.5N/mm^2$ and the mean stress is of magnitude $\sigma_{eq,m} = 5.3N/mm^2$, which means that the stress ratio is $R^{\perp} = -0.44$. The rainflow class with highest damage contribution is repeated one time and since it is a residuum it is considered as half a cycle, $n = 0.5$. This leads to an equivalent number of cycles $n_{eq} = 1.1$.

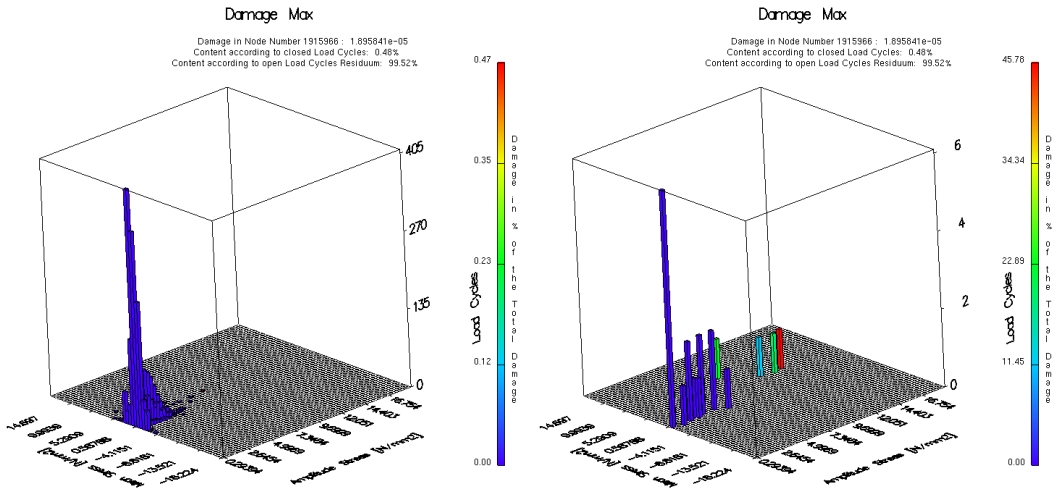

Figure 5.14: Rainflow matrices for node 1915966 of the analysis of the cross member according to the single stress component method (pure transverse stressing). Left: closed load cycles. Right: residua.

Knowing the damage in shear direction and the equivalent number of cycles, the total numbers of cycles to failure can be computed as $N_f = \frac{n_{eq}}{D_{\perp\parallel}} = 2.3 \cdot 10^{14}$. The number of cycles to failure is below the knee point of the S-N curve ($N_e = 10^7$) and therefore the rule of Miner modified has to be applied. Using the CLD for shear stressing as well as the stress ratio $R^{\perp\parallel} = R^{\perp} = -0.44$ an appropriate S-N curve can be determined, which can then be used together with the number of cycles to failure, N_f, to determine the shear stress amplitude as $\tau_{eq,a} = 8.1N/mm^2$ and a corresponding mean stress as $\tau_{eq,m} = 3.2N/mm^2$. Figure 5.15 shows the constant amplitude loadings, σ_{eq} and τ_{eq} when plotted in a σ, τ −diagram. It is assumed that both

loadings are in-phase. The Figure displays also the fracture curve for static failure and the regions of different fracture modes. The equivalent loading lies mostly within the region of fracture mode *A*, but also in the area of fracture mode *C*. Solving the equation for fracture mode *A* for N_f gives the number of failure $N_f = 9.9 \cdot 10^3$, which corresponds to a damage of $D_{eq} = \frac{n_{eq}}{N_f} = 1.10 \cdot 10^{-4}$. The driving manoeuvre R4u7-Pt2 is repeated 4380 times and therefore the resulting damage is $D = 4.83 \cdot 10^{-1}$ and is fairly close to one, which means that failure almost occurs in that case.

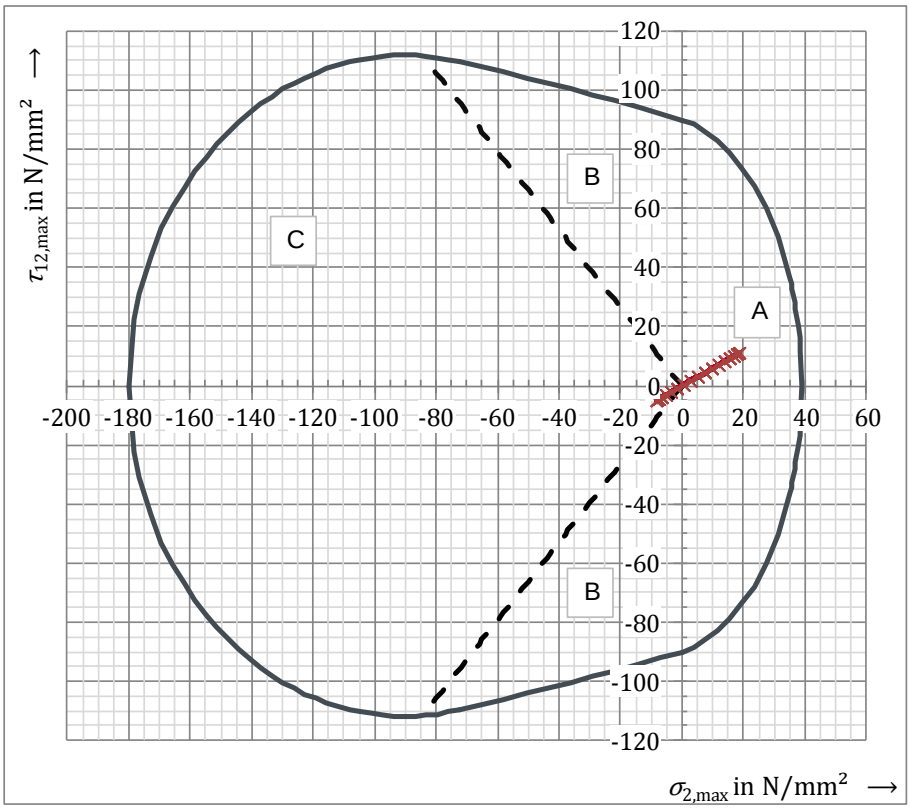

Figure 5.15: Equivalent constant stress amplitude signal (red) plotted in the interaction diagram for static inter-fibre failure for node 1915966. The black dashed line indicates the border from failure mode B to mode C.

One feature of the APDI shall be briefly discussed in the following. It is assumed, that the equivalent transverse stress and shear stress are acting in-phase. This assumption is quiet substantial, when it comes to determination of the final damage as illustrated in Figure 5.16. The Figure on the left shows the constant amplitude stressing when both, shear stress and transverse stress, are acting in-phase. On the other hand, the Figure to the right depicts the loading, when transverse stress and shear stress are acting 180° out-of-phase.

If the fracture curve was shrunk for increasing number of cycles, the fracture curve would first come into contact with the maximum stress peak in the left Figure, which results in a damage of $D_{eq} = 2.65 \cdot 10^{-2}$. In case of an out-of-phase loading failure would occur in mode *B* and the total damage would be of magnitude $D_{eq} = 5.78 \cdot 10^{-4}$, which is significantly lower. It is not possible to obtain any information about the phase of the loadings from the rainflow matrices. Therefore, it

is essential to visualize the loading in a $\sigma - \tau$-diagram in order to draw conclusions whether or not the assumption of in-phase loading leads to highest damage or if different phase angles may exist, which lead to more conservative results compared to the results of in-phase loading.

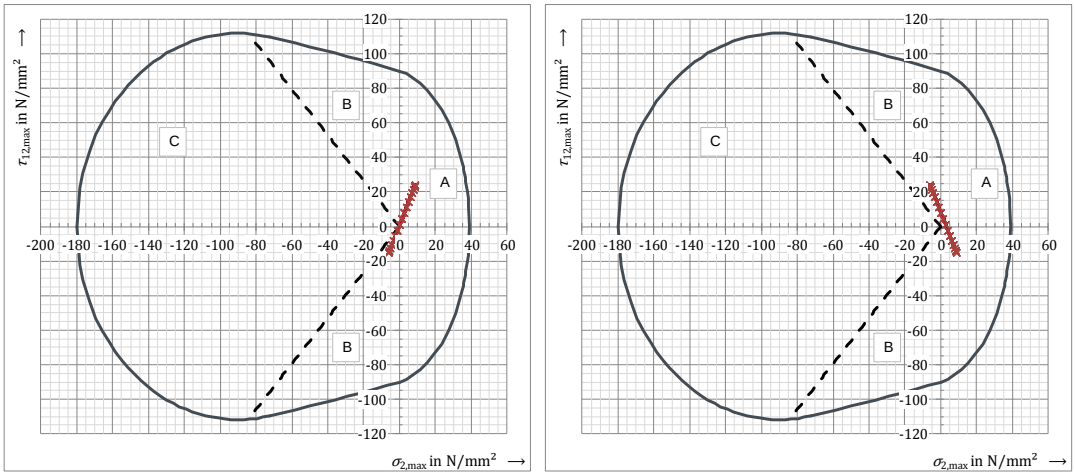

Figure 5.16: Equivalent constant stress amplitude signal (red) according to the a posteriori damage interaction method for node 1917998. Left: When assuming that equivalent transverse stress and shear stress are in-phase. Right: When assuming that equivalent transverse stress and shear stress are 180° out-of-phase.

5.4 Method based on Hashin's criterion

In the approach based on Hashin's failure criterion the load spectrum is reduced to a single constant transverse stress amplitude and shear stress amplitude loading. The mean stress and stress amplitude of these constant amplitude loadings are determined by the rainflow classes, which lead to the highest partial damage. Quiet many rainflow classes are present during the driving manoeuvre, but only few of them contribute significantly to the total damage. The critical node due to pure shear stressing, namely node 1917998, is analysed first.

From the rainflow matrix as shown in Figure 5.12 the rainflow classes with highest partial damage can be determined. It causes 70.2% of the total damage. Its mean stress is $\tau_m = 4.5MPa$ and its amplitude stress is $\tau_a = 19.6MPa$, which leads to a stress ratio of $R = -0.63$. The class is a residuum and is acting $n_i = 0.5$ times. When taking the scaling factor of $SF = 4380$ into account and the fact, that the class causes 70.2% of the total damage, an equivalent number of cycles according to equation (4.21) can be determined to be $n_{eq} = 3120$. Using the determined stress ratio and the constant life diagram for shear stressing an S-N curve can be determined. Its slope parameter is equal to $k = 11.2$. The equivalent number of cycles, n_{eq}, leads to a fatigue resistance of $\tau_{12,R} = 35.6MPa$.

Similar to the computation of an equivalent constant amplitude load in transverse-longitudinal direction, one can compute a constant amplitude load in transverse direction. The rainflow class with highest damage in transverse direction is of stress

amplitude $\sigma_{2,a} = 7.0MPa$ and mean stress $\sigma_{2,m} = 1.3MPa$, which leads to a stress ratio of $R = -0.69$. The damage contribution of this rainflow class is 41.1% and it is repeated 0.5 times. Therefore, the equivalent number of load cycles is $n_{eq} = 5334$ resulting in a fatigue resistance of $\sigma_{2,R} = 19.9MPa$. All relevant values of the constant amplitude stressings are summarized in Table 5.7.

Table 5.7: Parameters of constant amplitude loading for analysis of node 1917998 (node with highest damage due to pure shear stressing)

Type	Amplitude	Mean	R	k_i	n_{eq}	Resistance
τ	19.6	4.5	-0.63	11.2	3120	35.6
σ	7.0	1.3	-0.69	12.9	5334	19.9

Using the computed fatigue resistance and the stress amplitudes as shown in Table 5.7 the comparison value can be computed according to equation (4.20), which is $CV = 0.48$ and hence smaller than one. Failure does therefore not occur. Accounting for multiple repetitions of a driving manoeuvre cannot be done by multiplying the comparison value by a scaling factor, since CV does not scale linearly with the number of repetition. Hence it needs to be considered in n_{eq}.

The same procedure can be applied to the node which shows highest damage due to pure transverse stressing, node 1915966. Table 5.8 shows the relevant quantities which lead to a comparison value of $CV = 0.85$, which is lower, but very close to one.

Table 5.8: Parameters of constant amplitude loading for analysis of node 1915966 (node with highest damage due to pure shear stressing)

Type	Amplitude	Mean	R	k_i	n_{eq}	Resistance
τ	6.5	-1.2	-1.47	11.0	2894	36.6
σ	13.5	5.3	-0.44	13.5	4782	14.9

The results of the fatigue simulation by using the concept of single stress component as well as by applying the three models for accounting for multi-axial stressings are summarized and discussed in the following subchapter.

5.5 Summary

The results of the fatigue analysis by using the single stress component method (SSCM) and by applying the three multi-axial fatigue models for composites are given in Table 5.9 for node 1917998. First of all, it can be seen that the resulting damage is always higher when stress interaction is taken into account.

When using the method of equivalent stress according to constant stress exertion, it was suggested that the equivalent stress is used in accordance with the dominating stress component, i.e. in the case of node 1917998 failure should be evaluated according to the equivalent damage $D_{\perp\parallel,eq}$. The damage is almost 20 times higher than the damage due to pure shear stressing, $D_{\perp\parallel}$. Furthermore, it is surprisingly close to the damage determined by the a posteriori damage interaction (APDI) method, D_{eq}, which is only slightly higher.

The fatigue assessment based on Hashin's approach (MBHA) gives highest value, but CV is not a damage and it cannot directly compared to the damages, since it does not scale linearly with number of repetitions. Instead, the increase of number of cycles reduces the fatigue resistance according to the slope of the equivalent S-N curve, which leads to an increase of CV.

Table 5.9: Comparison of the total fatigue damage for node 1917998, the node with highest damage when subjected to pure shear stressing

SSCM		Equivalent stress according to constant stress exertion			APDI	MBHA
$D_{\perp\parallel}$	$D_{\perp}$	$D_{\perp\parallel,eq}$	$D_{\perp,eq}$	$D^{*}_{\perp,eq}$	D_{eq}	CV
$1.13 \cdot 10^{-3}$	$1.62 \cdot 10^{-5}$	$1.96 \cdot 10^{-2}$	$7.95 \cdot 10^{-3}$	$2.39 \cdot 10^{-3}$	$2.65 \cdot 10^{-2}$	$2.80 \cdot 10^{-1}$

Table 5.10 summarizes the results of the fatigue assessment when analysing node 1915966, the node with highest damage when subjected to pure transverse stress. Accounting for stress interaction leads to higher damages, than by using the single stress component method, where no stress interaction is taken in account. In case of evaluating the fatigue life by using the equivalent stress according to constant stress exertion the equivalent transverse damage, $D_{\perp,eq}$, should be used, since the loading is dominated by transverse stresses. The difference between $D_{\perp,eq}$ and the damage due to pure transverse stressing, $D_{\perp}$, is rather small. The reason for this is the fact, that the shear stressing at this node is very low, which can be seen by the damage due to pure shear, $D_{\perp\parallel}$, and therefore the shear stress does not influence the equivalent damage, $D_{\perp,eq}$, much. The APDI method gives 5-6 times higher damage than the pure transverse stress method and is three times higher than $D_{\perp,eq}$.

Table 5.10: Comparison of the fatigue damage for node 1915966, the node with highest damage when subjected to pure transverse stressing

SSCM		Equivalent stress according to constant stress exertion			APDI	MBHA
$D_{\perp\parallel}$	$D_{\perp}$	$D_{\perp\parallel,eq}$	$D_{\perp,eq}$	$D^{*}_{\perp,eq}$	D_{eq}	CV
$2.10 \cdot 10^{-11}$	$8.30 \cdot 10^{-2}$	$6.61 \cdot 10^{-1}$	$1.28 \cdot 10^{-1}$	$9.50 \cdot 10^{-2}$	$4.83 \cdot 10^{-1}$	$3.46 \cdot 10^{-1}$

It needs to be kept in mind, that only two nodes of the cross member were analysed with respect to stress interaction. There is the possibility that nodes exist which were not critical when using the single stress component method, but would possess the highest damage when stress interaction is taken into account. The APDI method and the MBHA require an a priori fatigue analysis according to the SSCM. The method of equivalent stress according to constant stress exertion does not necessarily require a fatigue analysis. On the other hand the effort for carrying out this method is larger compared to the other two methods.

Does failure occur, or does the component withstand the loading? This question cannot be answered exactly. From a numerical point of view, failure does not occur, since the damage or the comparison value, *CV*, is always lower than one. Experimental results would be beneficial to estimate which method predicts the fatigue life best or if all methods over- or underpredict the fatigue life.

In the last chapter of this Thesis conclusions, which are drawn from the results of this investigation, are presented and recommendation how these methods can be applied to the simulation process at AUDI are given. Finally a brief outlook is given where improvement is required and next possible steps for the continuation of this work are suggested.

6 Conclusions and Future Work

In the current simulation processes at AUDI AG the software FEMFAT is used to evaluate the fatigue life of components. FEMFAT does not support the analysis of endless fibre composites and therefore a work-around is made, where each stress component is analysed separately. This allows accounting for the anisotropic material behaviour of composites by using different material properties for longitudinal and transverse fibre direction as well as for transverse longitudinal shear direction. On the other hand, analysing each stress component separately is a major drawback, since it is contradictory to the failure theory of composites, i.e. the multi-axiality of the stress state needs to be taken into account for the case of inter-fibre failure in order to obtain reliable results.

Aim of this Thesis was to improve the simulation process in terms of validity by applying three methods of stress interaction to a fatigue analysis of a composite component. Two methods are based on Puck's failure criteria, where the first method is applied a priori by computing an equivalent stress at every time step on the basis of constant stress exertion. The second method is applied a posteriori, which means that the fatigue analysis is conducted by analysing each stress component separately. These results are then used to account for stress interaction. The third method, which is also carried out a posteriori, uses an elliptical equation for accounting for multi-axial stress states and was proposed by Hashin in its original form.

The obtained results of the analyses showed, that taking stress interaction into account always led to higher damage results in the investigations within this Thesis. Due to the fact that the a priori method of computing an equivalent stress takes stress interaction at every time step into account, it may be assumed, that the results of this method represent the physical behaviour of composites best. Therefore, this method should be preferred. Depending on the degree of multi-axiality the resulting damage was up to 20 times higher than the damage determined by the single stress component method. This is a quiet substantial number, which underlines the importance of accounting for stress interaction in multi-axial fatigue analysis.

The a posteriori damage interaction (APDI) method carries out the stress interaction at the end of the fatigue analysis. It can be understood as an interaction between the damages in shear and transverse direction. Based on the results of the fatigue analysis it computes an equivalent constant amplitude loading. This loading is determined by the rainflow class, which causes the highest partial damage. This assumption becomes the better the higher the damage contribution of the specific rainflow class is and may be inaccurate when the damage is dominated by many rainflow classes. Furthermore, it was shown that the assumption of in-phase loading between the damage equivalent shear stress and the damage equivalent transverse stress has a major influence on the resulting damage.

When comparing the manual and computational effort between the method based on Hashin's approach and the APDI method, one could notice that the APDI method required higher effort. Compared to the whole work load of carrying out the fatigue analysis, the difference was rather small. Since the APDI method is based on Puck's failure criterion and it computes a damage, which can be more easily compared, it is

suggested to use the APDI method as a preferred method for an a posteriori assessment.

In general the manual effort to carry out the fatigue analysis by analysing each layer and each stress component separately is high and therefore, automation of the process to some extent would be beneficial. By taking stress interaction into account the simulation results can be used to point out critical regions of the component more reliable than before, but whether the computed damage is conservative or non-conservative and which of the three methods give most accurate results cannot exactly be answered. Therefore, experimental results of specimens subjected to shear and transverse stressing are required in order to validate the different models. These tests could be carried out on filament wound tubular specimens, with fibre orientation in circumferential direction, subjected to tension and torsion.

7 References

[1] European Commission. *Road transport: Reducing CO2 emissions from vehicles,* http://ec.europa.eu/clima/policies/transport/vehicles/index_en.htm. web page of the European commission, last updated 2012-07-30, last access 2013-09-23

[2] Hahne, C.: *Leichtbau mit Faser-Kunststoff-Verbunden / beanspruchungsgerechte Festigkeitsbewertung von Fahrzeugstrukturen unter Betriebs- und Sonderlasten*. (Lightweight Design with fibre-reinfoced Polymers / Load-oriented Strength Assessment of Vehicle Structures under operating and special Loads. In German). PhD Thesis. Technical University Darmstadt. 2014 (not yet published).

[3] Kloska, T.: *Simulation Faserverbundleichtbau – rechnerische Festigkeitsbewertung der Langzeitqualität von CFK*. (Simulation Lightweight Design – Computational Fatigue Assessment of CFRP. In German). Diploma Thesis. Rheinisch-Westfaelische Technische Hochschule Aachen. 2012.

[4] Puck, A.: *Festigkeitsanalysen von Faser-Matrix-Laminaten.* (Strength Analysis of Fibre Matrix Laminates. In German). Hanser. München, Wien. 1996.

[5] Hashin, Z., Rotem A.: *A Fatigue Failure Criterion for Fiber Reinforced Materials.* In: Journal of Composite Mechanics. 7 (1973), pp. 448-464.

[6] Agarwal, B. D., Broutman, L. J., Chandrashekara, K.: *Analysis and Performance of Fiber Composites*. 3rd edition. John Wiley & Sons Inc. Hoboken. 2006.

[7] Knops, M.: *Analysis of Failure in Fibre Polymer Laminates: the Theory of Alfred Puck*. Springer. Berlin, Heidelberg, New York. 2008.

[8] Schürmann H.: *Konstruieren mit Faser-Kunststoff-Verbunden*. (Design with fibre-reinforced ploymers. In German). Springer. 2nd edition. Berlin, Heidelberg. 2007.

[9] Jenkin, C. F.: *Report on materials of construction used in aircraft and aircraft engines*. HM Stationery Office. London. 1920.

[10] Tsai, S. W., Azzi, V. D.: *Anisotropic Strength of Composites*. In: Experimental Mechanics. 5.9 (1965), pp. 283-288.

[11] Tsai, S. W., Wu, E. M.: *A General Theory of Strength for Anisotropic Materials*. In: Journal of Composite Materials. 5 (1971), pp. 58-80.

[12] Hashin, Z. *Fatigue Failure Criteria for Unidirectional Fiber Composites*. In: Journal of Applied Mechanics, Transactions ASME. 48 (1981), pp. 846-852.

[13] Hinton, M J., Kadddour, A. S., Soden, P D., eds. *Failure criteria in fibre reinforced polymer composites: the world-wide failure exercise*. Elsvier. Oxford, 2004.

[14] Puck A., Kopp J., Knops M.: *Guidelines for the determination of the parameters in Puck's action plane strength criterion*. In: Composites Science and Technology; 62.3 (2002), pp. 371-378.

[15] Dowling N. E.: M*echanical Behaviour of Materials Engineering Methods for Deformation, Fracture , and Fatigue.* Pearson. 4th edition. Harlow. 2012.

[16] Haibach E.: *Betriebsfestigkeit - Verfahren und Daten zur Bauteilberechnung*. (Fatigue Strength - Methods and Data for Fatigue Design of Components. In German). Springer. 3rd edition. Berlin, Heidelberg. 2006.

[17] Post, N. L., Case, S. W., Lesko, J. J.: *Modeling the variable amplitude fatigue of composite materials: A review and evaluation of the state of the art for spectrum loading*. In: International Journal of Fatigue. 30 (2008), pp. 2064-2086.

[18] Harris, B. ed.: *Fatigue in composites: science and technology of the fatigue response of fibre-reinforced plastics*. Woodhead Publishing. Cambridge. 2003.

[19] Nijssen R. P. L.: *Fatigue life prediction and strength degradation of wind turbine rotor blade composites.* Delft University. 2007.

[20] Hahne C., Knaust U., Schürmann H.: *Zur Festigkeitsbewertung von CFK-Strukturen unter PKW-Betriebslasten.* (Fatigue Evalauation of CFRP Structures under Complex Car Loads. In German). Deutscher Verband für Materialforschung und –prüfung e.V. conference paper. Herzogenaurach. 2013.

[21] Presentation of EVP. AUDI Internal document.

[22] Engineering Center Steyr GmbH. *Benutzerhandbuch FEMFAT 5.0 – Max.* (User Manual FEMFAT 5.0 – Max. In German). St. Valentin. 2012.

[23] Engineering Center Steyr GmbH. *Benutzerhandbuch FEMFAT 5.0 – Basic.* (User Manual FEMFAT 5.0 –Basic. In German). St. Valentin. 2011.

[24] Verein Deutscher Ingenieure: *Development of FRP components (fibre-reinforced plastics) Analysis*. Guideline 2014 Paper 3. Düsseldorf. 2006.

[25] Gude M., Hufenbach W., Koch I.: *Fatigue failure criteria and degradation rules for composites under multiaxial loadings.* Mechanics of Composite Materials. 42.5 (2006), pp. 443-450.

Appendix

A1: DAMAGE PLOTS DUE TO PURE TRANSVERSE STRESSING

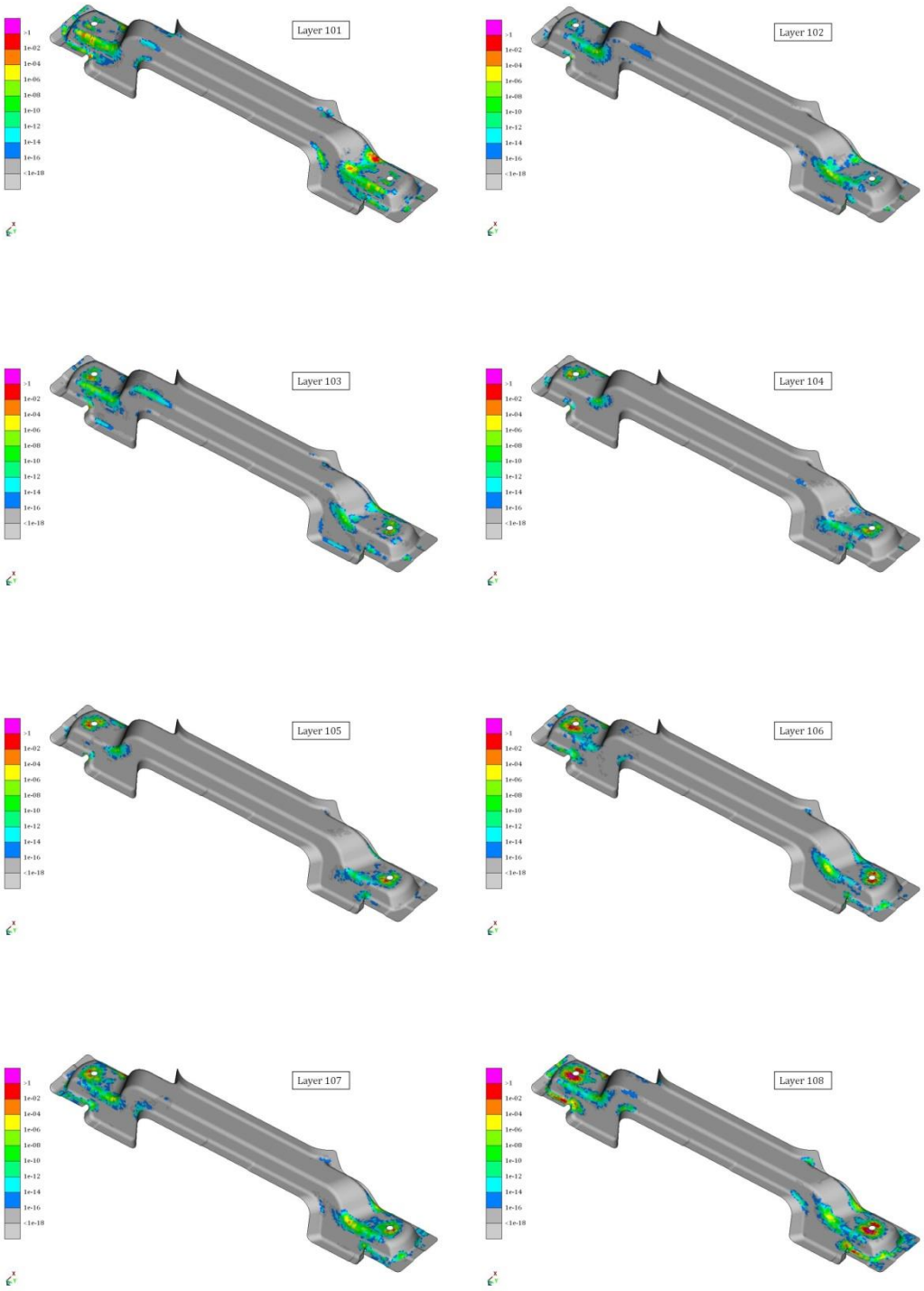

A2: DAMAGE PLOTS DUE TO PURE SHEAR STRESSING

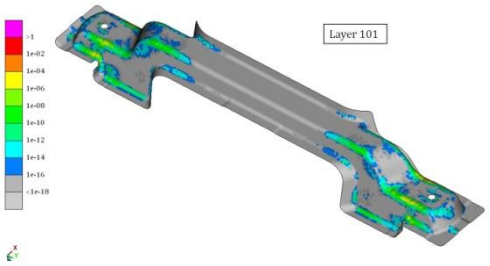

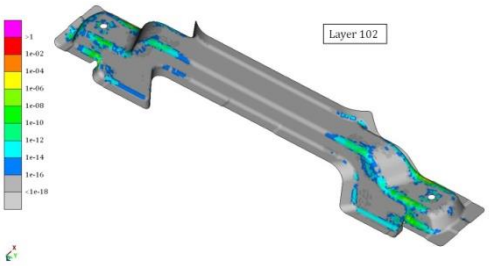

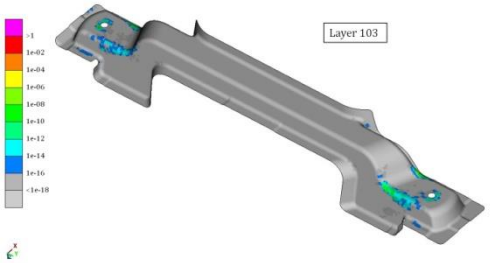

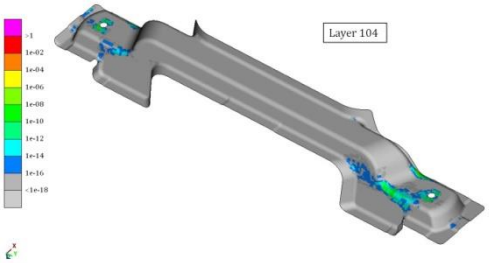

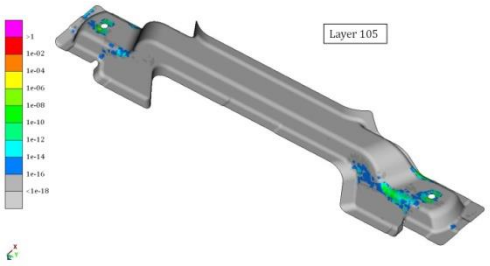

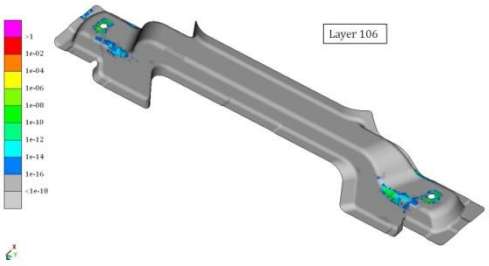

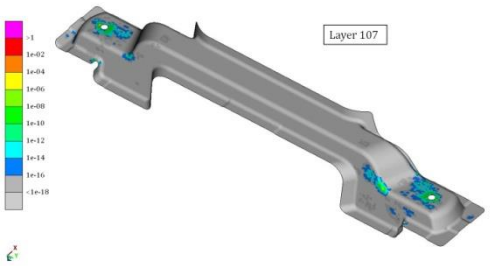

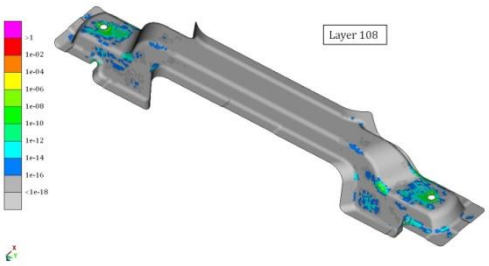

A3: DAMAGE PLOTS DUE TO PURE LONGITUDINAL STRESSING

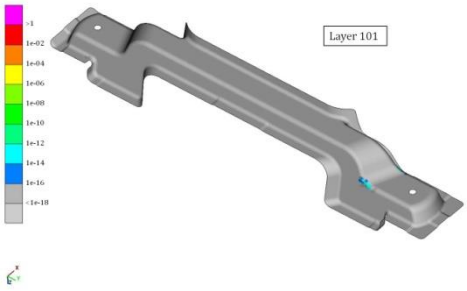

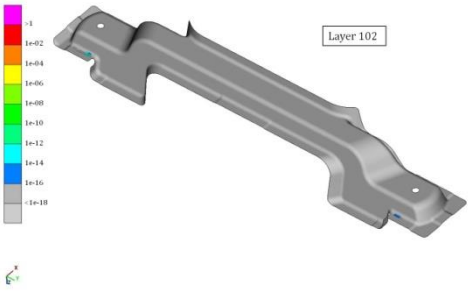

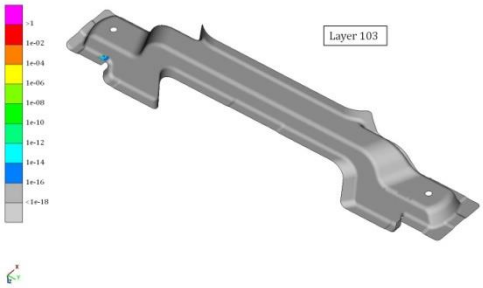

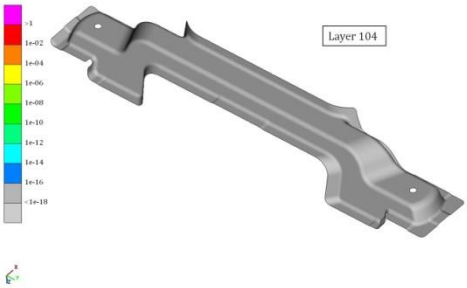

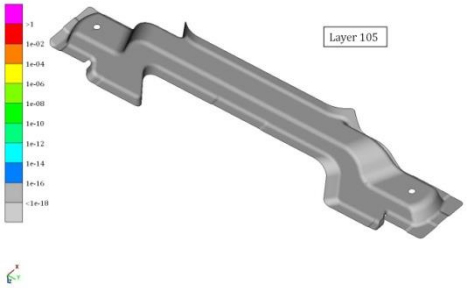

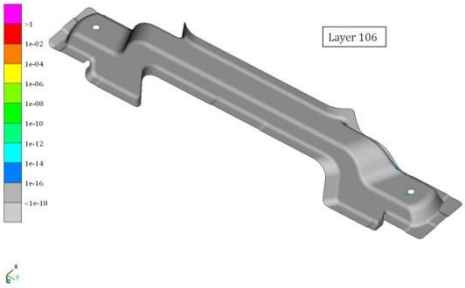

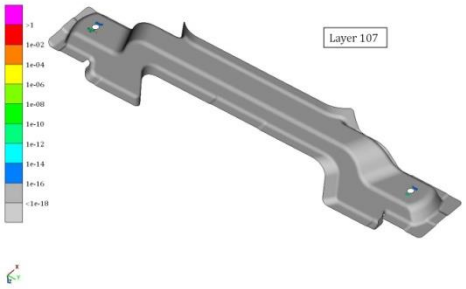

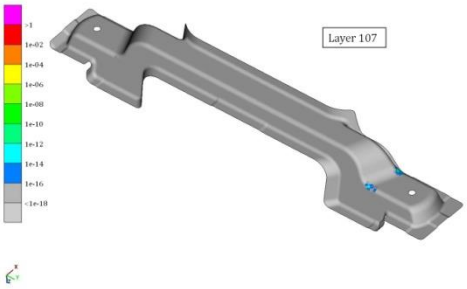

A4: MATERIAL DATA FOR CFRP

Parameter	Value	Units
E_1	134450	N/mm²
E_2	8640	N/mm²
E_3	8640	N/mm²
G_{12}	5800	N/mm²
G_{13}	5800	N/mm²
G_{23}	3085	N/mm²
ν_{12}	0.3	
ν_{13}	0.3	
ν_{23}	0.4	
R_{11}^{-}	1000	N/mm²
R_{11}^{+}	1500	N/mm²
R_{12}	90	N/mm²
R_{13}	90	N/mm²
R_{22}^{+}	180	N/mm²
R_{22}^{-}	39	N/mm²
R_{23}	72.49	N/mm²
R_{33}^{+}	180	N/mm²
R_{33}^{-}	39	N/mm²